Syngas fermentation: from bubbleless to bubbled bioreactors

Perdigão Elisiário, M.

DOI
10.4233/uuid:7820255d-165d-4397-8640-a2001a639065

Publication date
2025

Document Version
Final published version

Citation (APA)
Perdigão Elisiário, M. (2025). *Syngas fermentation: from bubbleless to bubbled bioreactors*. [Dissertation (TU Delft), Delft University of Technology]. https://doi.org/10.4233/uuid:7820255d-165d-4397-8640-a2001a639065

Important note
To cite this publication, please use the final published version (if applicable).
Please check the document version above.

SYNGAS FERMENTATION

FROM BUBBLELESS TO BUBBLED BIOREACTORS

MARINA PERDIGÃO ELISIÁRIO

Syngas Fermentation:

From Bubbleless to Bubbled Bioreactors

Syngas Fermentation:
From Bubbleless to Bubbled Bioreactors

Dissertation

for the purpose of obtaining the degree of doctor
at Delft University of Technology
by the authority of the Rector Magnificus Prof. dr. ir. T.H.J.J. van der Hagen,
Chair of the Board for Doctorates
to be defended publicly on
Friday, 20 June 2025 at 10:00 o'clock

by

Marina PERDIGÃO ELISIÁRIO

Master of Science in Life Science and Technology,
Technical University of Delft, The Netherlands,

Born in Beja, Portugal

This dissertation has been approved by the promotors.

Composition of the doctoral committee:

Rector Magnificus	Chairperson
Dr. ir. A. J. J. Straathof	Delft University of Technology, promotor
Prof. dr. ir. H. J. Noorman	Delft University of Technology, promotor
Dr. H. de Wever	VITO, non-independent member

Independent members:

Prof. dr. ir. M. C. M. van Loosdrecht	Delft University of Technology
Prof. dr. ir. C. A. Ramirez Ramirez	Delft University of Technology
Prof. dr. ir. J. van der Schaaf	Eindhoven University of Technology
Prof. dr. ir. R. Weusthuis	Wageningen University
Dr. ir R. Kleerebezem	Delft University of Technology, reserve member

This work is part of the MicroSynC research programme (project number P16-10/6) and is (partly) financed by the Netherlands Organization for Scientific Research (NWO).

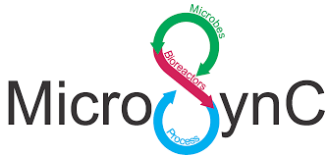

Printed by Proefschriftspecialist:

Cover illustration and design: David Calderón Franco & Marina Perdigão Elisiário

ISBN: 978-94-6384-807-7

An electronic version of this dissertation is available at http://repository.tudelft.nl

Para os meus avós

"Da minha aldeia vejo quanto da terra se pode ver do Universo...
Por isso a minha aldeia é tão grande como outra terra qualquer,
Porque eu sou do tamanho do que vejo
E não do tamanho da minha altura..."

Alberto Caeiro (Fernando Pessoa)

Contents

Summary

Syngas fermentation has emerged as a promising technology for the transition towards sustainable and environmentally friendly energy sources. This transition is crucial to mitigate greenhouse gas emissions and combat climate change. This technology employs anaerobic bacteria, known as acetogens, to convert carbon monoxide (CO), hydrogen (H_2), and carbon dioxide (CO_2) into biofuels and valuable chemicals, such as ethanol and acetic acid, through the Wood-Ljungdahl pathway. This ancient microbial pathway allows for the fixation of CO and CO_2 using H_2 as an energy source, offering a versatile and flexible approach to biotechnological solutions aimed at facilitating the energy transition.

Despite its potential, syngas fermentation faces challenges, particularly the slow gas-to-liquid mass transfer that can limit its efficiency and productivity. Efficient gas-to-liquid mass transfer is critical in syngas fermentation processes as it ensures optimal substrate utilization, which is linked to product formation. Industrial-scale syngas fermentation typically employs bubbled bioreactors like gas-lift or bubble column reactors, which provide a large surface area for gas-liquid contact. However, non-standard designs, including bubbleless bioreactors, may offer superior performance at an industrial scale. Additionally, the properties and composition of the fermentation broth influence mass transfer efficiency.

Volumetric productivity, or the product formation rate, is one of the key process performance indicators in syngas fermentation, often targeted for optimization. Microbial metabolism, specifically growth rate, can constrain volumetric productivity. Biomass retention strategies, such as biofilm-based bioreactors, could enhance process performance. Understanding the interplay between mass transfer rates, growth rates, and co-product concentrations is essential to optimize continuous syngas fermentation processes.

This thesis aims to provide a comprehensive understanding of the role of gas-to-liquid mass transfer in syngas fermentation processes, and the impact of syngas fermentation broth characteristics on mass transfer efficiency. The research covers both experimental studies in standard bubbled bioreactor configurations (bubble column and CSTR) and computational studies on novel membrane bioreactors for syngas permeation and fermentation.

Chapter 2 explores hollow fibre membrane (HFM) bioreactors as a solution to mass transfer limitations in syngas fermentation. It establishes the state-of-the-art of HFM bioreactors, reviewing their potential to enhance gas-to-liquid mass transfer and cell retention. Various membrane materials, module types, and flow configurations are

discussed, emphasizing the importance of optimizing these parameters to improve reactor performance.

Chapter 3 presents a computational model developed to optimize syngas fermentation in HFM bioreactors, incorporating hydrodynamics, mass transfer, and microbial kinetics. The model allows for systematic study and optimization of process variables, using CO fermentation to ethanol as a case study. Parametric analysis identifies hydraulic retention time as a critical parameter affecting ethanol concentration and productivity trade-offs. Future model improvements should focus on experimental validation of key assumptions and parameters.

Chapter 4 investigates the influence of ethanol on mass transfer in syngas fermentation broths. The addition of ethanol significantly increases the volumetric mass transfer coefficient (K_La) by inhibiting bubble coalescence, leading to smaller bubbles and higher mass transfer rates. The dynamic nature of K_La is highlighted, emphasizing the need for more realistic mass transfer models for fermentations.

Chapter 5 examines the impact of acetic acid concentration, growth rate, and mass transfer rate on metabolic shifts, product titres, and production rates in CO fermentation by *Clostridium autoethanogenum*. High undissociated acetic acid concentrations shift metabolism towards ethanol production. These findings have significant implications for process optimization by targeting optimal acetic acid concentration.

Chapter 6 reflects upon the feasibility and expected performance of HFM bioreactors for syngas fermentation processes and how they compare with the current bubbled bioreactors implemented in industry. Furthermore, we explore potential applications of HFM reactors for *in-situ* product removal, and product and biomass recycling process design options for productivity enhancement in syngas fermentation processes. The economic feasibility of HFM bioreactors for syngas fermentation remains a significant challenge despite their potential to surpass gas-to-liquid mass transfer performance compared to traditional bubbled reactors. A techno-economic analysis has revealed that HFM bioreactors are prohibitively expensive, primarily due to the high capital investment costs associated with the extensive number of reactor units required. This setup leads to high operational expenses, including maintenance and depreciation, making HFM bioreactors less economically attractive despite their operational efficiency in terms of utility usage. In comparison, Bubble Column (BC) reactors emerge as the more economically viable option for industrial syngas fermentation. BC reactors achieve higher biomass concentrations and volumetric productivities, leading to significantly lower capital investment costs, offering a more efficient economy of scale for BC configurations.

Furthermore, sufficiently high K_La values are predicted for industrial bubbled bioreactors during syngas fermentation to ethanol since ethanol stabilizes smaller bubbles, increases gas hold-up, and enhances mass transfer rates. Consequently, BC reactors offer a favourable balance between productivity and cost, currently making them the preferred choice for industrial applications.

Future developments in the syngas fermentation field should focus on optimizing the interplay between broth components and mass transfer characteristics to enhance process efficiency. Developing accurate predictive models and investigating scalability is crucial for translating laboratory successes to commercial applications. Additionally, understanding microbial kinetics and their relation to dissolved gases and product concentrations will drive further optimization. Advancements in these areas are essential for improving syngas fermentation processes, facilitating industrial defossilization, and promoting sustainable biotechnological production.

Sammenvatting

Syngasfermentatie is een opkomende en veelbelovende technologie die een rol kan spelen in de transitie naar duurzame en milieuvriendelijke energiebronnen, die noodzakelijk is om de uitstoot van broeikasgassen te verminderen en klimaatverandering tegen te gaan. Deze technologie maakt gebruik van anaerobe bacteriën, ook wel bekend als acetogenen, die koolmonoxide (CO), waterstof (H_2) en kooldioxide (CO_2) om kunnen zetten in biobrandstoffen en waardevolle chemicaliën, zoals ethanol en azijnzuur, via de Wood-Ljungdahl route. Deze oeroude microbiële route maakt de fixatie van CO en CO_2 mogelijk met H_2 als energiebron en biedt daarmee veelzijdige en flexibele mogelijkheden voor verscheidene biotechnologische oplossingen in de energietransitie.

Ondanks het grote potentieel kent syngasfermentatie verschillende uitdagingen. Deze zijn met name gericht op de trage gas-vloeistof stofoverdracht, wat de efficiëntie en productiviteit limiteert. Efficiënte gas-vloeistof massaoverdracht is cruciaal voor syngasfermentatieprocessen omdat het zorgt voor een verbeterd substraatgebruik, wat gekoppeld is aan productvorming. Voor syngasfermentatie op industriële schaal wordt meestal gebruik gemaakt van bioreactoren met bellen, zoals gaslift- of bellenkolomreactoren, die een groot oppervlak hebben voor gas-vloeistofcontact. Niet-standaard reactorconfiguraties, waaronder bellenloze bioreactoren, kunnen echter mogelijk superieure stofoverdrachtsprestaties leveren op industriële schaal. Daarnaast beïnvloeden de eigenschappen en samenstelling van het fermentatiebeslag de efficiëntie van de stofoverdracht.

De volumetrische productiviteit, of de productvormingssnelheid, is een van de kritieke procesprestatie-indicatoren in syngasfermentatie en wordt derhalve vaak geoptimaliseerd. Bovendien kan het trage microbiële metabolisme, resulterend in een lage groeisnelheid, de volumetrische productiviteit beperken. Strategieën om biomassa vast te houden, zoals bioreactoren met een biofilm, kunnen de procesprestaties verbeteren. Inzicht in de wisselwerking tussen de stofoverdrachtssnelheid, groeisnelheid en bijproductconcentraties is essentieel voor het optimaliseren van continue syngasfermentatieprocessen.

Dit proefschrift heeft als doel een uitgebreid begrip te geven van de rol van gas-vloeistof stofoverdracht in syngasfermentatieprocessen en de invloed van de eigenschappen van syngasfermentatie beslagen op de efficiëntie van de stofoverdracht. Het onderzoek omvat zowel experimentele studies in standaard bioreactorconfiguraties met bellen (bellenkolom en CSTR) als computationele studies naar nieuwe membraanbioreactoren voor syngaspermeatie en -fermentatie.

Hoofdstuk 2 onderzoekt holle vezelmembraanbioreactoren (HFMR) als oplossing voor stofoverdrachtlimitaties in syngasfermentaties. De huidige stand van deze technologie wordt beschreven en er wordt gekeken naar het potentieel van HFMR om de gas-vloeistof stofoverdracht en de celretentie in syngasfermentaties te verbeteren. Verschillende membraanmaterialen, moduletypes en stromingsconfiguraties worden besproken, waarbij wordt benadrukt hoe belangrijk het is om deze parameters te optimaliseren om de reactorprestaties te verbeteren.

Hoofdstuk 3 presenteert een mathematisch model dat is ontwikkeld om syngasfermentatie in HFMR te optimaliseren, waarbij hydrodynamica, stofoverdracht en microbiële kinetiek zijn geïntegreerd. Met het model kunnen procesvariabelen systematisch worden bestudeerd en geoptimaliseerd, waarbij CO-fermentatie tot ethanol als casestudy wordt gebruikt. Een parametrische analyse identificeert de hydraulische retentietijd als een kritieke parameter die zowel de ethanolconcentratie en productiviteit beïnvloedt. Toekomstige modelverbeteringen moeten zich richten op experimentele validatie van belangrijke aannames en parameters.

Hoofdstuk 4 onderzoekt de invloed van ethanol op de stofoverdracht in syngasfermentatiebeslag. De toevoeging van ethanol verhoogt de volumetrische stofoverdrachtscoëfficiënt (K_La) aanzienlijk door het samenvoegen van bellen te verminderen, wat leidt tot kleinere bellen en een hogere stofoverdracht. De dynamische aard van de K_La wordt besproken, samen met de beperkingen van de huidige modellen om K_La te voorspellen.

Hoofdstuk 5 onderzoekt de invloed van de azijnzuurconcentratie, de groeisnelheid en de stofoverdrachtssnelheid op metabole veranderingen, productconcentraties en productiesnelheden in CO fermentatie door *Clostridium autoethanogenum*. Hoge azijnzuurconcentraties leiden tot metabole veranderingen in de richting van ethanolproductie. Deze bevindingen hebben belangrijke implicaties voor procesoptimalisatie door te focussen op de optimale azijnzuurconcentratie.

Hoofdstuk 6 gaat in op de haalbaarheid en verwachte prestaties van HFMR voor syngasfermentatieprocessen en hoe deze zich verhouden tot de huidige bellen-gebaseerde bioreactoren die in de industrie worden toegepast. Verder onderzoeken we de mogelijke toepassingen van HFMR voor *in-situ* productverwijdering en de opties voor product- en biomassaretentie die beiden moeten zorgen voor een productiviteitsverhoging in syngasfermentatieprocessen. De economische haalbaarheid van HFMR voor syngasfermentatie blijft een belangrijke uitdaging. Dit is ondanks hun potentieel voor verbeterde gas-vloeistof stofoverdracht in vergelijking met traditionele reactoren met bellen. Een techno-economische analyse

heeft aangetoond dat HFMR buitengewoon duur zijn, met name door de hogere investeringskosten voor het grote aantal benodigde reactoren. Deze opzet leidt tot hoge operationele kosten, inclusief onderhoud en afschrijving, waardoor HFMR economisch minder aantrekkelijk worden ondanks hun hoge operationele efficiëntie. In plaats daarvan komen bellenkolomreactoren naar voren als economisch meest haalbare optie voor industriële syngasfermentatie. Bellenkolomreactoren bereiken hogere biomassaconcentraties en volumetrische productiviteiten, wat leidt tot aanzienlijk lagere investeringskosten en mede door de efficiëntere schaalvoordelen die bellenkolomreactoren bieden. Bovendien worden voldoende hoge $K_L a$ -waarden voorspeld voor industriële bioreactoren met bellen tijdens de fermentatie van syngas tot ethanol, omdat ethanol de kleinere bellen stabiliseert, de gasfractie vergroot en daardoor de stofoverdracht verbetert. Bijgevolg bieden bellenkolomreactoren een voordelige balans tussen productiviteit en kosten, waardoor ze momenteel de voorkeur genieten voor industriële toepassingen van syngasfermentatie.

Toekomstige ontwikkelingen op het gebied van syngasfermentatie moeten zich richten op het optimaliseren van de wisselwerking tussen de componenten in fermentatiebeslagen en stofoverdrachtskarakteristieken om de procesefficiëntie te verbeteren. Het ontwikkelen van nauwkeurige voorspellende modellen en het onderzoeken van de schaalbaarheid is cruciaal voor het vertalen van laboratoriumsuccessen naar commerciële toepassingen. Daarnaast zal een beter begrip van de microbiële kinetiek en hun relatie tot opgeloste gassen en productconcentraties bijdragen aan verdere optimalisatie. Vooruitgang op deze gebieden is essentieel voor het verbeteren van syngasfermentatieprocessen, voor industriële defossilisering en het bevorderen van een duurzame biotechnologische industrie.

Nomenclature

Abbreviations

Abbreviation	Meaning
BC	Bubble Column
EPS	Extracellular Polymeric Substances
ISPR	*In-situ* Product Removal
HFM	Hollow Fibre Membrane
HFM-BCR	Hollow Fibre Membrane Bubble Column Reactor
HRT	Hydraulic Retention Time
KPI	Key Performance Indicator
NPV	Net Present Value
PDMS	Polydimethylsiloxane
PMP	Polymethylpentene
PP	Polypropylene
PTMSP	Poly(1-trimethylsilyl-1-propyne)
PVDF	Polyvinylidene fluoride
STR	Stirred Tank Reactor

Mathematical symbols

Symbols	Meaning	Unit
a	Specific surface area	m^{-1}
A	Surface area	m^2
A_m	Membrane surface area	m
C	Dissolved gas concentration	$mol.m^{-3}$
c	Concentration	$mol.L^{-1}$ or $g.L^{-1}$
D	Diffusion Coefficient	$m^2.s^{-1}$
d	Diameter	m
d_{32}	Sauter mean bubble diameter	m
d_b	Bubble diameter	m
d_{eq}	Equivalent bubble diameter	m
d_i	Inner Diameter of hollow fibre membrane	m
d_{lm}	Logarithmic mean diameter of hollow fibre membrane	m
d_o	Outer diameter hollow fibre membrane	m
e	Eccentricity	-
H	Dimensionless gas-water Henry coefficient	$mol.m^{-3}_{gas}.(mol.m^{-3}_{liquid})^{-1}$
I	Ionic strength	$mol.L^{-1}$
k	Volume specific mass transfer coefficient	$m.s^{-1}$
K_L	Overall Mass Transfer Coefficient, based on liquid side	$m.s^{-1}$
k_L	Liquid-side mass transfer coefficient	$m.s^{-1}$
K_La	Overall volumetric mass transfer coefficient, based on liquid side	s^{-1}
k_La	volumetric mass transfer coefficient, based on liquid side	s^{-1}
L	Length of hollow fibre membrane	m
M	Molecular weight	$kg.mol^{-1}$
P	Permeability	$m^2.s^{-1}$
P	Power	W
Q	Volumetric flow through the membrane module	$m^3.s^{-1}$
R	Ideal Gas Constant	$J.mol^{-1}.K^{-1}$
r	Radius	m
S	Solubility coefficient or Gas-membrane partition coefficient	$mol.m^{-3}_{membrane}.(mol.m^{-3}_{gas})^{-1}$
Sh	Sherwood number	(dimensionless)
T	Temperature	K
t	Sampling time	s
$u_{G,s}$	Superficial gas velocity	$m.s^{-1}$
V	Volume	m^3
v	Velocity	$m.s^{-1}$
z	Ionic charge	-
δ	Membrane thickness	m
ΔC	Concentration difference	$mol.m^{-3}$
ε	Porosity	-
τ	Tortuosity	-

Sub- and superscripts

Symbol	Meaning
*	Saturated
0	Initial
a	Semi-major axis
Ac	Acetate
b	Bubble
c	Semi-minor axis
d	Dense layer
D	Dispersion
eff	Effective
EtOH	Ethanol
g	In the gas phase
G	Gas
k	Knudsen (diffusivity)
l	In the liquid phase
L	Liquid
L,out	Liquid outlet of membrane module
lm	Logarithmic mean
m	In the membrane or microporous layer
M	Membrane module
p	Pore
prot	Protein
R	Reservoir
x	Biomass

Chapter 1

Introduction

1. Introduction

As the world deals with the urgent need to transition towards a more sustainable and environmentally friendly economy, the quest for renewable and clean energy sources is becoming increasingly important. Currently, war and conflict in gas and energy-supplying countries often lead to significant disruptions in global energy markets and prices thereby emphasising the urgency for diversified and clean energy sources. Environmental concerns, particularly the escalating impacts of climate change such as rising global temperatures and increased frequency of extreme weather events, keep propelling the necessity for an energy transition. This transition from fossil fuels to cleaner, renewable sources is crucial to mitigate greenhouse gas emissions and stabilize the planet's climate system. The global economy is, therefore, witnessing a paradigm shift towards sustainability, particularly in industrial sectors, which are traditionally major contributors to environmental degradation.

1.1. Syngas fermentation as a technology at the forefront of energy transition

An emerging technology that stands at the forefront of this transition is syngas fermentation. Syngas fermentation revolves around the ability of certain anaerobic bacteria - known as acetogens - to convert carbon monoxide (CO), hydrogen (H_2), and carbon dioxide (CO_2) into biofuels and other valuable chemicals (1). This microbial pathway, often referred to as the Wood-Ljungdahl pathway, is believed to be one of the earliest forms of microbial metabolism on Earth, dating back approximately 3.8 billion years (2). The bacteria in question are able to fix CO and CO_2 via this pathway, using H_2 as well, an energy source. This biochemical mechanism involves two parallel branches - the carbonyl branch and the methyl branch - which ultimately converge in the formation of acetyl-CoA, a precursor for a wide array of bioproducts (3, 4). Syngas fermentation, therefore, provides a promising, sustainable avenue for the utilization of waste gases and contributes significantly to biotechnological solutions aimed at facilitating the energetic transition (5). The technology's inherent flexibility allows to produce different end products based on the needs of the market, including biofuels such as ethanol, butanol, and even long-chain hydrocarbons (6). Consequently, syngas fermentation, while harnessing an ancient microbial pathway, it rises as one solution to modern critical environmental challenges. It not only alleviates dependency on fossil fuels but also offers a renewable strategy for carbon capture and sequestration, thus embodying a powerful tool in the quest for a sustainable future and the fight against climate change. It is considered a versatile and flexible technology not only because of the product diversity but also due to the wide range of resources from which syngas can be derived. This includes coal gasification, steam reforming of natural gas,

and gasification of biomass or waste (7). Each syngas source provides a distinct syngas composition, presenting unique challenges for the fermentation process (8). As such, understanding the dynamics of these different syngas types is critical to optimizing fermentation and subsequently, product yield (9). In the broader context of transitioning to a sustainable energy landscape, it is essential that fossil carbon remains underground, and gas fermentation is progressively applied to recycle above-ground carbon sources. This approach will play a crucial role in mitigating the impacts of climate change by enabling the recycling of carbon through renewable processes.

Despite the potential benefits, however, the implementation of syngas fermentation technology is not without its challenges. One of the most prominent issues encountered in deploying this technology on a commercial scale is the slow gas-to-liquid mass transfer (10 - 13). Mass transfer is a critical factor that influences the overall performance of syngas fermentation, as it refers to the transport of gases from the bulk phase to the cell, where the biochemical reactions occur. Slow mass transfer can limit volumetric productivity, which is an important measure of process performance. At higher mass transfer rates, volumetric productivity can become limited by microbial metabolism and kinetics (product selectivity, substrate and product inhibition).

1.2. Mass transfer role in syngas fermentation

In syngas fermentation mass transfer refers to the transport of the gaseous substrates to the liquid bulk, where they can be metabolized by the microorganism. Therefore, gas-to-liquid mass transfer plays an integral role in the overall efficiency and productivity of syngas fermentation, as it directly influences substrate availability to the microorganism. In case of insufficient mass transfer (i.e. the mass transfer rate is lower than the maximum substrate consumption rate by the microorganism), the reaction rate is limited by the mass transfer rate. Therefore, effective mass transfer rate also ensures optimal substrate utilization (syngas conversion). This impacts productivity, as the substrate uptake is metabolically linked to product formation.

In syngas fermentation processes, especially those involving high cell densities, the gas-liquid mass transfer rate can act as a bottleneck, limiting the overall rate of fermentation. Therefore, a thorough understanding of mass transfer mechanisms becomes very relevant. The rate at which mass is transferred in syngas fermentation, is governed by a small driving force: the difference ΔC between equilibrium at the G/L interface and the local dissolved concentration. This is a consequence of the poor aqueous solubility of gaseous substrates like CO and H_2, coupled with relatively

low absolute pressures and even lower partial pressures of these substrates (due to the presence of CO_2 and occasionally N_2). To counterbalance these factors, it is crucial to ensure that the volume-specific interfacial area a between the gas and liquid medium is high, leading to an increased value of the volumetric mass transfer coefficient, known as K_La, in which K_L is the mass transfer coefficient (4). The dominant operational factors are the energy input to the bioreactor, related to the superficial gas velocity and the pressure gradient, and liquid properties ensuring inhibition of gas bubble coalescence. Therefore, overcoming the challenges posed by mass transfer limitations should be achieved by making appropriate choices in terms of the bioreactor design and operational conditions, aimed at maximizing the concentration gradient ΔC, the mass transfer coefficient K_L, and/or the interfacial area a. In bubbled bioreactors, K_L could in theory be increased by high local turbulence but there are limited practical ways to influence it. In membrane bioreactors for gas permeation, K_L is also influenced by membrane permeabilities and thickness (14, 15).

Industrial-scale syngas fermentation typically employs bubbled bioreactors: gas-lift or bubble column reactors (16). These work by injecting gas at the bottom of the reactor into the liquid phase, creating bubbles which disperse, rise, mix the liquid, and provide a large surface area for gas-liquid contact (17). These are well studied designs and typically used industrially due to their simplicity, relative low energy consumption and operating costs and sufficient gas-to liquid mass transfer. Nevertheless, thoughtful design and operation are needed to achieve optimal performance and economic efficiency. Furthermore, it becomes relevant to investigate non-standard bioreactor designs for syngas that could potentially outperform these configurations at industrial scale, including bubbleless bioreactors.

The properties and composition of the fermentation broth are another fundamental aspect of the process which also significantly influence the mass transfer in syngas fermentation (18 - 20). For instance, the viscosity and density of the broth play key roles in determining the gas-liquid mass transfer coefficient. A high viscosity broth can impede the movement of gas bubbles, reducing the mass transfer rate. Similarly, the presence biomass or other fermentation products (organic acids, alcohols, etc.) with surfactant activity, can affect interfacial area available for mass transfer and interfere with the bubble size distribution (21). Furthermore, temperature of the broth can influence the solubility of the syngas components, thereby affecting their transfer from the gas phase to the liquid phase. Therefore, knowledge of these dynamics and properties interdependence as well as careful design, monitoring and control of broth properties are crucial for efficient mass transfer during syngas fermentation.

Since mass transfer plays such a vital role in the syngas fermentation process (affecting its efficiency, reaction rate, and productivity) understanding and optimizing mass transfer can greatly enhance the effectiveness of syngas fermentation, making it a primary area of focus in the design and operation of syngas fermentation processes.

1.3. Productivity in Syngas fermentation

The volumetric productivity (product formation rate, often expressed as mol/m^3h or kg/m^3h) of syngas fermentation processes is a process key performance indicator (KPI) as it impacts its economic feasibility while it is influenced by process design. However, syngas fermentation volumetric productivities are frequently low and, therefore, often a target of research, development and optimization by industry and academia (22). The volumetric productivity can be limited by the microbial metabolism, specifically by the microbial growth rate. A slow growth rate leads to low biomass concentrations, which results in low productivities and low syngas conversion rates. In the absence of mass transfer limitation, a too high concentration of dissolved carbon monoxide could result in substrate inhibition of microbial growth. Biomass retention strategies can counteract this by increasing biomass concentrations and improve process performance. Strategies such biofilm-based bioreactors, or operational units coupling biomass concentration and recirculation could be used (23, 24). Research and development on new bioreactor designs integrating such strategies are a promising route to improve process performance. However, in the scenario of high biomass concentration, mass transfer could again become insufficient and result in very low and unfavourable dissolved gaseous substrate concentrations. The dissolved CO (and or H_2) concentration is a pivotal variable in the process outcome, and it is influenced by a combination of operational and microbial traits. Therefore, syngas fermentation processes should be carried on a constrained operational window where biomass concentration, mass transfer rate and dissolved gas concentration are balanced for optimal productivity.

1.4. Research goals and thesis structure

This thesis aims at providing a comprehensive understanding of the role of gas-to-liquid mass transfer in syngas fermentation processes performance (including volumetric productivity), both for standard bubbled bioreactors and non-standard bubbleless bioreactor configurations; and reversely the impact of syngas fermentation broth characteristics on gas-to-liquid mass transfer efficiency.

The research covers computational studies on novel bioreactor configurations, namely membrane bioreactors for syngas permeation and fermentation. The research on membrane bioreactors for syngas fermentation is driven by their

promising potential on enhancement of gas-to-liquid mass transfer efficiency, cell retention and volumetric productivity (11). Furthermore, it also explores syngas fermentation experiments on standard bioreactor configurations, namely stirred tank reactors and bubble columns, to understand performance of industrial bioreactor configurations and guide future optimization.

With those goals in mind, we will attempt to answer the following research questions:

i. Which membrane bioreactor configuration is most suitable/promising for improvement of syngas fermentation volumetric productivity?
ii. Which operational conditions for such a syngas fermentation membrane bioreactor maximize volumetric productivity?
iii. What is the influence of syngas fermentation broth properties on gas-to-liquid mass transfer rate?
iv. What is the influence of mass transfer rates, growth rates and co-products concentrations on performance (titres and volumetric productivities) of continuous syngas fermentation?

To begin, we explore the potential of Hollow Fibre Membrane (HFM) bioreactors as a solution to mass transfer limitations in syngas fermentation. In **Chapter 2** we establish the state-of-the-art of HFM bioreactors in syngas fermentation technology, exploring and reviewing the potential of this configuration to enhance gas-to-liquid mass transfer and cell retention in syngas fermentation. Here we discuss and compare mass transfer phenomena in various membrane materials and module types, and flow configurations used for syngas permeation and fermentation.

In **Chapter 3**, we present a computational model developed to optimize the performance of syngas fermentation in HFM bioreactors. Here we investigate the influence of process variables on key performance indicators, such as ethanol productivity, ethanol concentration, and CO conversion, providing valuable insights for systematic study and optimization.

In **Chapter 4**, we aim to better understand the behaviour of mass transfer in the fermentation broth of conventional industrial gas bubble reactors. We explore the influence of ethanol and other syngas fermentation broth components on mass transfer in gas fermentations. We highlight the complex interactions between different compounds and their impact on mass transfer characteristics, emphasizing the need for more realistic mass transfer models for fermentations.

Lastly, in **Chapter 5** we aim to understand the impact of mass transfer and other fermentation variables on the metabolism of acetogenic bacteria. Here, we

investigate the individual impact of acetic acid concentration, growth rate, and mass transfer rate on metabolic shifts, product titres, and production rates in CO fermentation by *C. autoethanogenum*. This Chapter provides insights into the factors governing shifts in CO metabolism and sheds light on the role of acetic acid inhibition in driving metabolic shifts towards ethanol production.

In **Chapter 6**, we reflect upon the feasibility and expected performance of HFM bioreactors for syngas fermentation processes and how they compare with the current bubbled bioreactors implemented in industry. Furthermore, we explore potential applications of HFM bioreactors for *in-situ* product removal, and product and biomass recycling process design options for productivity enhancement in syngas fermentation processes.

The thesis establishes a comprehensive framework for systematically exploring the critical aspects of gas-to-liquid mass transfer in syngas fermentation and the operation of bubbleless and bubbled bioreactors, paving the way for further research and development in this field.

Chapter 2

Membrane bioreactors for syngas permeation and fermentation

This chapter has been published as:

Marina P. Elisiário, Heleen De Wever, Wouter Van Hecke, Henk Noorman & Adrie J. J. Straathof (2022) Membrane bioreactors for syngas permeation and fermentation, *Critical Reviews in Biotechnology*, 42:6, 856-872,

Abstract

Syngas fermentation to biofuels and chemicals is an emerging technology in the biobased economy. Mass transfer is usually limiting the syngas fermentation rate, due to the low aqueous solubilities of the gaseous substrates. Membrane bioreactors, as efficient gas-liquid contactors, are a promising configuration for overcoming this gas to liquid mass transfer limitation, so that sufficient productivity can be achieved. We summarize published performances of these reactors. Moreover, we highlight numerous parameters settings that need to be selected for the enhancement of membrane bioreactors performance. To enable this selection, we relate mass transfer and other performance indicators to type of membrane material, module, and flow configuration. Hollow fibre modules with dense or asymmetric membranes on which biofilm might form seem suitable. A model-based approach is advocated to optimize their performance.

2. Membrane bioreactors for syngas permeation and fermentation

2.1. Introduction

Microbial conversion of syngas

Syngas fermentation is a process in which acetogenic microorganisms anaerobically convert mixtures of CO, H_2 and CO_2 into organic products. When consuming CO, these fermentations co-produce CO_2. Acetogens use the acetyl-CoA pathway, also referred to as the Wood–Ljungdahl pathway, for reductive synthesis of acetyl-CoA from CO_2, CO and H_2, energy conservation for growth, and assimilation of carbon from CO and CO_2 into biomass (3) – Figure 2.1. Acetyl-CoA is converted to different metabolic end products (carboxylic acids and respective alcohols), depending on the microbial metabolism.

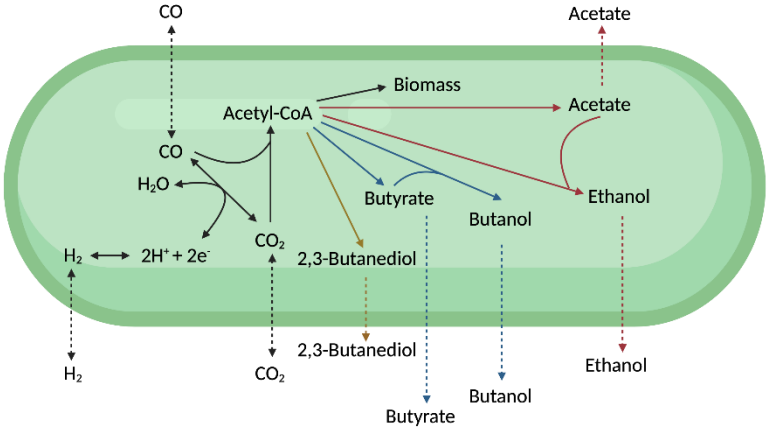

Figure 2.1 Schematic representation of the simplified Wood-Ljungdahl pathway of acetogens and their (native) metabolic end products (3, 25). Acetogenic microorganisms are able to produce different combinations of the depicted organic products, depending on their metabolism.

Syngas is obtained from several industrial processes that convert fossil carbon sources, by gasification of biomass or organic waste material, and by electrolysis of water and CO_2 to H_2 and CO. If the used syngas is renewable, syngas fermentation may contribute to sustainable chemical production in a circular, biobased economy.

Mixtures of CO, CO2 and H2 are useful as substrate for gas fermentation due the Gibbs energy content of CO and H2. Using solely CO2 as substrate is less straightforward because its activation would require another source of energy such as light or electricity (26).

Several companies have operated pilot and demonstration plants for fermentative conversion of syngas to ethanol. LanzaTech is operating the production of bioethanol from syngas at commercial scale (27). Other alcohols (2,3-butanediol, 1-butanol, 1-hexanol) and carboxylic acids (acetate, butyrate, hexanoate) are examples of potential products (1, 4, 6). For a general overview and description of syngas fermentation technology, we refer to the aforementioned papers.

As compared to carbohydrate fermentations (28), the main bottlenecks currently restricting syngas fermentation to valuable products are low extent and rate of substrate conversion (CO and H_2), and limited product titers and range. Metabolic and microbial engineering can be applied to improve microbial performance while process engineering can improve reaction conditions and provide smart product recovery strategies.

Mass Transfer

The gas–liquid mass transfer rate is usually limiting the overall syngas fermentation rate, particularly in case of a high cell density process (11). Therefore, understanding this mass transfer is essential. The syngas mass transfer rate ($K_La.\Delta C$) includes a small driving force because of the low aqueous solubility of the gaseous substrates CO and H_2, relatively low absolute pressures and low partial pressures due to the presence of CO_2 and sometimes N_2. This needs to be compensated by a high efficiency of contacting with the liquid medium (4), hence a high value of the volumetric mass transfer coefficient, K_La. Thus, mass transfer limitations can be addressed by selection of bioreactor and operational conditions to achieve a higher concentration gradient ΔC, mass transfer coefficient K_L, and/or interfacial area a (29, 30).

Membrane bioreactors as options for syngas conversion

Several bioreactor types have been studied for syngas fermentation. Mechanically mixed reactors such as stirred tank reactors (STRs) can achieve high volumetric power inputs by agitation, which even at low superficial gas velocities can provide reasonable gas–liquid mass transfer rates besides good liquid mixing. In STRs, higher impeller energy reduces the size of gas bubbles and thereby increases the interfacial area for mass transfer. However, costs associated with the excessive power input for very large reactors restricts economic feasibility for commercial syngas fermentation processes (31). Additionally, locally high energy dissipation rates near the agitators and/or bursting gas bubbles at the surface can potentially damage sensitive microorganisms (32).

Non-agitated reactor systems have also been investigated as suitable configurations for syngas fermentation, using much less energy than STRs (24). In trickle bed reactors, the liquid film contacting the gas phase is very thin and therefore the liquid

resistance to mass transfer is diminished (30). Monolithic biofilm reactors may achieve very high mass transfer, but could be prone to clogging by biofilms (33). Bubble columns and gas lift reactors can achieve high mass transfer rates at low operational and maintenance costs at industrial scale, but undesirable bubble coalescence may occur, especially in tall reactors.

Asimakopoulos *et al.* (23) recently reviewed different bioreactor configurations suitable for continuous syngas fermentation to added value products and compared their performance in terms of high productivity rates and high product concentrations. The authors conclude that the evolution and research on syngas fermentation platforms is oriented towards packed bed reactor and membrane modules combined with biofilm formation. Thus, membrane-based bioreactors have been reported as promising configuration for syngas conversion. Membranes can fulfill many applications but here we will review gas-liquid contacting applications and biofilm technology. Membrane processes have been claimed to offer several advantages such as low energy consumption, enabling continuous operations, being simple to operate and scale up, and have inherent properties of high selectivity and high surface-area-per-unit-volume (34, 35). Membrane contactors have the potential of controlling the extent of contact between syngas and fermentation broth without having to cope with flooding or foaming phenomena (36). These claimed advantages should compensate for the cost of membrane modules. Membrane processes scale up linearly, except the auxiliary equipment (transfer pump, piping, etc.) (37). Thus, economic comparison with other processes will be scale-dependent, and, besides, requires optimization of the processes that are compared.

Syngas fermentation using membrane bioreactor technology has not yet been optimized. This review aims to guide the optimization work required to achieve the full potential of this technology. Therefore, we will review the syngas mass transfer, membrane types, and membrane module and reactor configurations (including biofilm formation) used for syngas fermentation and relate these with process performance indicators.

2.2. Membrane (gas-liquid) contactors for syngas permeation: Theory and Principles

Syngas fermentation using a membrane contactor can be described by different physical and biological mechanisms (38):

i. Bulk mixing of the gas entering the membrane module.
ii. Gas boundary layer transport.
iii. Transport through the membrane.

iv. Transfer from the membrane, dissolution and diffusion into biofilm (if present).
v. Diffusion through and consumption within the biofilm (if present).
vi. Boundary layer transport through the liquid phase.
vii. Mixing in the bulk liquid.
viii. Consumption by suspended cells.

The membrane provides a large and fixed interfacial area between gas and liquid phase for facilitating mass transfer. This area is independent of gas and liquid flow rates, and gas to liquid mass transfer can be achieved without spending energy on keeping one phase dispersed within the other (15, 39). The chemical potential difference between substrate in gas and liquid phase is the driving force for diffusive transport across the membrane. This may be expressed as concentration difference (ΔC).

The microorganisms can be attached as biofilm on the liquid side of the membrane surface or suspended in the liquid, where the minor nutrients are provided such as ammonia, metal trace elements or vitamins (38). If the membrane provides physical support for biofilm attachment, it enables cell retention (40).

Although the applied transmembrane pressure difference is limited by the membrane material, using elevated pressures on either side is possible, leading to increased syngas solubility and hence an increase in the achievable mass transfer driving force, that is, the CO, H_2 and CO_2 concentration gradients (ΔC).

2.3. Membrane material types used for syngas permeation

Different membrane materials have distinct functionalities, performances and costs. For example, the gas mass transfer depends on the membrane bulk structure. Therefore, selecting an appropriate membrane is essential. Membranes for gas-liquid contacting can be classified with respect to their bulk structure: symmetric (microporous or dense) or asymmetric (integral or composite). The role and properties of different membrane material types is reviewed here. This includes mass transfer models such as summarized in Table 2.1 and Table 2.2.

Microporous membranes

A microporous membrane consists of a polymer matrix (e.g., polypropylene, PP, and polyvinylidene fluoride, PVDF) with a rigid, highly voided structure and with randomly distributed and interconnected pores (41). Before extensive research had been conducted, “microporous” was used for membranes with pore diameters between 0.01 and 1 μm (42). Nowadays, use of such terminology in literature can

create confusion, because the current IUPAC definition classifies materials according to their pore size as microporous (< 2 nm), mesoporous (2-50 nm) or macroporous (> 50 nm). Microporous membranes are frequently used in gas transfer applications because of their high gas permeability. The membrane pores are intentionally filled with gas since gas diffusivity is much larger than liquid diffusivity. The substrates therefore diffuse through the membrane by gaseous diffusion. A drawback of microporous membranes is their low operational transmembrane pressure (TMP).

Table 2.1 Expressions of local mass transfer coefficients.

Mass Transfer Coefficient	Expression	*Eq.*
Liquid	$k_l = Sh_l \frac{D_l}{d}$	2.1
Gas	$k_g = Sh_g \frac{D_g}{d}$	2.2
Microporous membrane	$k_m^m = \frac{D\varepsilon}{\delta\tau_m}$	2.3
Dense membrane	$k_m^d = \frac{P}{\delta} = \frac{S_m D_m}{\delta}$	2.4

Table 2.2 Expressions of overall mass transfer coefficients (based on the liquid side), for gas-liquid membrane contacting applications (14).

Membrane material	Flat sheet geometry	*Eq.*	Hollow fibre geometry [a]	*Eq.*
Microporous	$\frac{1}{K_L} = \frac{1}{k_g H} + \frac{1}{k_m^m H} + \frac{1}{k_l}$	2.5	$\frac{1}{K_L} = \frac{d_o}{k_g H d_i} + \frac{d_o}{k_m^m H d_{lm}^m} + \frac{1}{k_l}$	2.6
Dense	$\frac{1}{K_L} = \frac{1}{k_g H} + \frac{1}{k_m^d H} + \frac{1}{k_l}$	2.7	$\frac{1}{K_L} = \frac{d_o}{k_g H d_i} + \frac{d_o}{k_m^d H d_{lm}^d} + \frac{1}{k_l}$	2.8
Integral asymmetric/ Microporous-dense composite	$\frac{1}{K_L} = \frac{1}{k_g H} + \frac{1}{k_m^m H} + \frac{1}{k_m^d H} + \frac{1}{k_l}$	2.9	$\frac{1}{K_L} = \frac{d_o}{k_g H d_i} + \frac{d_o}{k_m^m H d_{lm}^m} + \frac{d_o}{k_m^d H d_{lm}^d} + \frac{1}{k_l}$ [b]	2.10

In the presence of a biofilm layer on the membrane, an extra mass transfer resistance term is included in the equation.
[a] Liquid at lumen and gas at shell side
[b] Dense layer in contact with liquid

Above a certain maximum critical pressure difference between feed (gas stream) and permeate (liquid side), called the bubble point pressure, bubbles are formed at the liquid side. This critical pressure difference depends on the gas-liquid interfacial tension, the contact angle between the liquid and polymer surface and the diameter of the pore. On the other hand, pressures below a minimum critical difference cause water to fill the membrane pores (15), which significantly increases the mass

transfer resistance through the membrane. To ensure that the gas-liquid interface is immobilized at the liquid side membrane interface, microporous membranes must be operated under a carefully controlled pressure difference between feed and permeate. High pressures of gaseous substrates can still be used when the liquid on the permeate side of the fibres is also pressurized (41).

The concentration profile of a gas species through a microporous membrane is shown in Figure 2.2A.

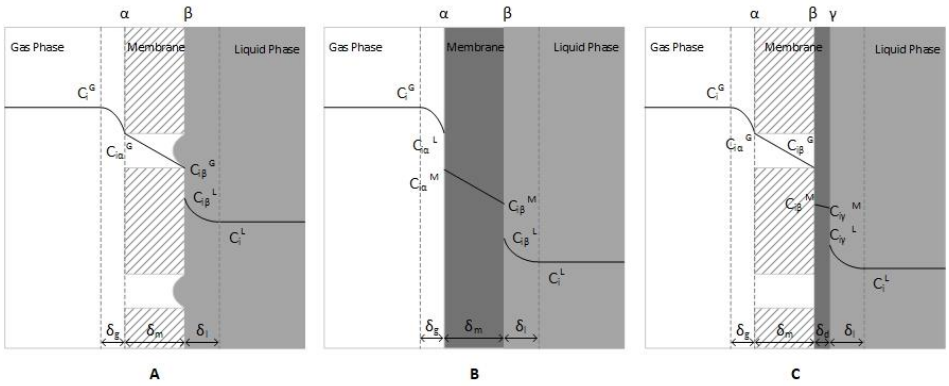

Figure 2.2 Concentration profile of compound i when moving from gas to liquid phase through a: hydrophobic microporous membrane (A), dense membrane (B) and integral asymmetric/ composite membrane (C). C_i^G: concentration of *i* in the gas phase, C_i^L: concentration of *i* in the liquid phase, C_i^M: concentration of *i* in the membrane phase, δ_g: thickness of gas boundary layer; δ_l: thickness of liquid boundary layer; δ_m: thickness of membrane boundary layer, α: gas-membrane interface, β: membrane-liquid interface, γ: microporous-dense layers interface.

The overall mass transfer resistance based on the liquid phase for a gas-filled microporous membrane is the sum of four resistances in series: for gas phase, microporous membrane, biofilm (if applicable), and liquid phase – equations 2.5 and 2.6.

Gas and liquid local mass transfer coefficients depend on the feed flow velocity and module geometry and dimensions as these determine the thickness of the mass transfer boundary layer; and on the viscosity and the density as these influence the substrate diffusion coefficients. Each local mass transfer coefficient can be estimated using semi-empirical correlations. For k_g and k_l, expressions based on Sherwood number have been reported – equations 2.1 and 2.2 (43, 44).

The gas transport through microporous membranes depends on the pore size range and it can be governed by molecular diffusion or Knudsen (free molecule) diffusion. The effective diffusion coefficient is therefore a function of bulk diffusion and

Knudsen diffusion coefficients – equation 2.11, with the latter depending on the pore diameter of the membrane, molecular mass of the gas and temperature – equation 2.12 (45).

$$\frac{1}{D_{eff}} = \frac{1}{D_g} + \frac{1}{D_k} \qquad 2.11$$

$$D_k = \frac{d_p}{3}\sqrt{\frac{8RT}{\pi M}} \qquad 2.12$$

Thus, when the pores are large enough, the interaction with the membrane material can be neglected and the diffusion coefficient in the microporous membrane equals the diffusion coefficient in gas (15). It has been suggested that deposition of proteins and cell debris and the presence of surfactants may cause the pore walls to become hydrophilic such that the pores fill with liquid, thereby rendering microporous membranes unsuitable for long-term operation (46).

Dense membranes

Dense or non-porous membranes usually consist of polymers such as silicone, structured by non-continuous passages in the polymer chain matrix (41). Diffusion occurs in the free volume between the polymer chains (47) and is described by the solution-diffusion model. The concentration profile of a gas species in case of a dense membrane is shown in Figure 2.2B.

Like for microporous membranes, for dense membranes the overall mass transfer resistance based on the liquid phase is the sum of each local resistance term – equations 2.7 and 2.8. However, the mass transfer coefficient inside the dense membrane depends on the gas species permeability in the dense membrane and its thickness – equation 2.4. The permeability of the gas molecules is controlled by two major parameters: diffusion coefficient and solubility coefficient in the dense membrane (also referred to as gas-membrane partition coefficient).

High gas permeabilities can be achieved in rubbery dense membranes, such as silicones, given their large free volume, due to the flexibility of the siloxane linkages in the polymer (48). Due to this, syngas compounds (CO, H_2, CO_2, N_2) are more soluble (two to seven times) in polydimethylsiloxane (PDMS) membrane than in water, although the respective diffusivities are three to four orders of magnitude lower. Dense glassy polymers with high free volume, such as poly(trimethylsilyl)propyne (PTMSP), polymethylpentene (PMP) and Teflon™ AF (a commercial polymer consisting of perfluorinated dioxolane) (49) have intrinsically very high gas permeabilities, showing therefore great potential for the permeation of syngas. Merkel *et al.* (50) reported extraordinarily high CO, H_2 and CO_2

permeabilities in a PTMSP dense membrane. Although this is the most permeable polymer known, it is also highly susceptible to fast physical aging, a limitation for long-term operations.

Dense membranes can operate at high transmembrane pressures, up to 3×10^5 Pa in silicone membranes for example (46). As a result, a large chemical potential gradient can easily be maintained, causing increased mass transfer rate (51).

On the other hand, dense membranes, such as silicone membranes, are traditionally thicker (100 to 400 μm) than microporous membranes (52). Together with their non-porous nature, this should lead to a higher membrane resistance to mass transfer. Nevertheless, nowadays the manufacturing of PDMS hollow fibres as thin as 20 μm has been reported.

Silicone membranes also offer high resistance to chemical and mechanical stress and, in contrast to microporous membranes, they are not susceptible to pore clogging (biofouling) or liquid entry in the pores (46).

Asymmetric membranes

Asymmetric membranes consist of an ultra-thin dense layer supported by a porous structure. In integral asymmetric membranes, the dense skin layer and the porous support are formed from the same material, while composite asymmetric membranes consist of two or more layers from different materials that can be optimized independently (53). The dense thin top-layer selectively permeates compounds while the microporous layer provides mechanical strength. In either case, the liquid is in contact with the dense layer (14). Gaseous species diffuse through the microporous layer, subsequently solubilize and diffuse through the dense layer, and then enter the liquid at the wetted dense surface (54). The concentration profile of a gas species in case of a asymmetric membrane is shown in Figure 2.2C.

Multi-layer composite membranes contain additional layers of different materials besides a microporous support layer, each with a designated function (54).

Asymmetric membranes combine the advantages of symmetric dense and porous membranes, since the porous layer offers support, the ultra-thin dense skin layer provides high permselectivity, and neither layer shows high mass transfer resistance. Moreover, they can function at higher pressure without biofouling and wetting of pores.

For syngas fermentation, where rate of permeation is more important than permselectivity, the best candidates seem to be asymmetric membranes that offer

high permeability for syngas compounds, a suitable support for microbial growth, and include a dense layer with sufficient mechanical stability, such as PDMS or PMP do. Further research should focus on novel composite membranes with thin dense non-porous layers able to operate under high transmembrane pressure drops without a decline in the permeation rates (55).

2.4. Membrane module configurations for syngas fermentation

The membrane geometry, flat or tube-shaped, defines the membrane module configuration to be integrated in a bioreactor.

Flat membranes modules are mainly used for laboratory tests, because they are easier to build, and sheet replacement is simple and fast. Usually, a single flat sheet is located between two plates that are equipped with the inlets/outlets of both phases. For large interfacial areas, flat membranes are used in plate-and-frame or in spiral wound modules (14).

In tube-shaped configurations, many membrane tubes or fibres are packed into bundles and potted into tubesheets to form a module. Depending on tube diameter, this can be a tubular (>10 mm), capillary (0.5 – 10 mm) or hollow fibre (<0.5 mm) module. The membranes divide a module into a lumen-side, which is the space enclosed by the membranes, and a shell-side which is the space between the outer surface of the membranes and the housing (56).

The choice of the module configuration for syngas permeation in a bioreactor should balance several factors such as surface area per unit of liquid volume, membrane manufacturing cost, suitability for high pressure operation, and fouling control. To guarantee an efficient performance, the module should maximize the mass transfer, reduce and control the fouling, work with low pressure drops, and have a constant performance over its whole length (14).

For industrial syngas fermentation, the membrane should be packed in an efficient and economical way for maximizing interfacial area per volume unit.

Regarding this aspect, hollow fibre membrane (HFM) modules outcompete other configurations. Furthermore, they entail the lowest membrane manufacturing costs - Table 2.3. This explains why HFM modules are the preferred and most common modules for gas-liquid membrane contacting applications. Consequently, the performance of membrane contactors for syngas fermentation has almost exclusively been studied for HFM modules.

Table 2.3 Design parameters for membrane module selection (41).

Parameter	Plate and Frame	Spiral wound	Tubular	Capillary fibres	Hollow fibres
Manufacturing cost ($/m²)	50-200	5-50	50-200	5-50	2-10
Concentration polarization/fouling control	Good	Moderate	Very good	Good	Poor
Permeate-side pressure drop	Low	Moderate	Low	Moderate	High
Suitability for pressured operation	Marginal	Yes	Marginal	No	Yes
Limitation to specific types of membrane material	No	No	No	Yes	Yes
Area per volume (m²/m³)	200 - 600	800-1000	-	-	2000-5000

2.5. Hollow Fibre Membrane Bioreactors for syngas fermentation

While the mass transfer coefficient within HFMs depends only on the material, as indicated in equations 2.3 and 2.4, the mass transfer on the shell and lumen sides of an HFM module depend on flow conditions and fibre or module geometries. For this reason, significant efforts have been addressed to the improvement of the HFM material properties, but also to optimization of packing density, fibre length and diameters, operative flowrates, pressures and concentrations, fluid physical properties, pressure drops, and breakthrough pressure (14).

In HFM modules, non-uniform flow at the shell side of the hollow fibre can occur due to channeling, bypassing, mixing, entry region phenomena (caused by fibre deformation), non-uniform fibre distribution, polydispersity of fibre diameters or presence of stagnant zones (14). Since this maldistribution of flow leads to reduction of mass transfer efficiency, much research is dedicated to improve the module design in terms of higher mass transfer coefficients at the shell side. Stanojević *et al.* (39) reviewed membrane contactor designs and operation, including different innovative types of modules for HFM contactors. One of the main strategies includes modification of the standard geometry to promote flow perpendicular to the fibres, for example, using woven hollow fibre wound helically around a central core, using woven hollow fibre wound mounted diagonally in a rectangular box or introduction of baffles in the module (44).

Published lab-scale syngas fermentation studies use commercial membrane modules or custom-built prototypes Table 2.4 and Table 2.5. These will be discussed subsequently.

Table 2.4 Different HFM reactor configurations studied for syngas mass transfer, respective characteristics and maximum K_La reported (29, 30, 32, 40, 57- 62).

Membrane Fiber Properties			Configuration			Operational settings						
Material	Porous size (µm)	ID/OD (µm)	HFM reactor	Gas feed location	Gas supply	A_m/V_L [d] (m^{-1})	TMP (kPa)	Gas composition	Gas flow rate ($mL.min^{-1}$)	Liquid recirculation rate ($mL.min^{-1}$)	Stirring speed reservoir (rpm)	K_La (h^{-1})	Reference
PS	NR	500/660	Stand-alone	Lumen	Open-end	4366	0.7-4.8	Air	1000-2000	80	NA	50	(Orgill et al. 2013)
PES	NR	1100/1300	Stand-alone	Lumen	Open-end	2271	0.7-4.8	Air	1000-2000	40	NA	20	
PP	NR	480/630	Stand-alone	Lumen	Open-end	4361	0.7-4.8	Air	1000-2000	80	NA	240	
FPS	NR	200/280	Stand-alone	Lumen	Open-end	9,198	0.7-4.8	Air	1000-2000	80	NA	50	
PDMS	Non-porous	200/300	Stand-alone	Lumen	Open-end	10000	0.7-4.8	Air	1000-2000	400	NA	1062	
PDMS	Non-porous	200/300	Stand-alone	Lumen	Open-end	10000	NA	20% O_2, 80% Ar	4.6	200	NA	484[b]	(Orgill et al. 2019)
								100% CO	5.0	184	NA	420	
								100% H_2	5.0	181	NA	840	
PVDF	0.1	700/1200	Internal	Lumen	Closed-end	63	37.2	99.99% CO	NA	NA	NA	155	(Yasin et al. 2014)
CHF	NA	NR	Internal	Lumen	Closed-end	200	241	99.99% CO	NA	500	NA	1	(Munasinghe and Khanal 2010)
PVDF	0.1	700/1200	Internal	Lumen	Closed-end	29	36.5	99.99% CO	NA	NA	NA	69	(Jang et al. 2018)
PP	0.2	330/630	Coupled to external STR reservoir	Lumen	Open-end	253	0	CO_2	128	385	500	24	(Ferreira et al. 1998)
PP	0.04	220/300	Coupled to external STR reservoir	Lumen	Open-end [a]	175	103.4	99.5% CO	5000	1000	200	1096[c]	(Shen et al. 2014)
PP	0.2	376/426	Coupled to external STR reservoir	Lumen	Open-end	56	114.5	50.0% CO, 30% H2, 20% CO2	140	670	90	385[c]	(Lee et al. 2012)
CHF	NR	200/240	Coupled to external reservoir	Shell	Closed-end	200	206.8	99.99% CO	NA	1500	NA	946[c]	(Munasinghe and Khanal 2012)
PVDF	0.2	800/1400	Coupled to external reservoir	Lumen	Closed-end	2250	203	NR	NA	1500	NA	1	(Zhao et al. 2013)

A_m/V_L: Ratio of membrane surface area per total liquid working volume (including external reservoir); ID/OD: Inner diameter/ Outer diameter; PDMS: polydimethylsiloxane; PS: polystyrene; PES: polyethersulfone; PP: polypropylene; FPS: Fresenius polysulfone; PE: polyethylene; PU: polyurethane; PVDF: polyvinylidene fluoride; CHF: composite hollow fiber; NA: Not applicable; NR: Not reported

[a] Open-end fiber configuration with consecutive gas feed to the headspace of external STR.

[b] Value measured for O_2.

[c] $a=A_m/V_m$: membrane surface area per liquid volume in HFM module.

[d] Value measured for CO.

Table 2.5 HFM bioreactor configurations for syngas fermentation and respective operational conditions. (40, 58, 59, 62 - 70).

Entry	HFM bioreactor configuration	Gas feed side/ Gas supply configuration	Syngas feed composition	Liquid Working Volume (L)	A_m/V_L (m^{-1})	Microorganisms	Temp. (°C)	pH	Duration of fermentation (d)
1	HFM-BCR	Lumen/ Closed	80% CO, 20% CO_2	0.4	27.5	*Eubacterium limosum* KIST612	37	7 [e]	3
2	HFM-BCR [a]	Lumen/ Closed	80% CO, 20% CO_2	2	29	*C. autoethanogenum* DSM10061	37	4-6	≃ 8.3
3	Stand-alone [b]	Lumen/ Open	40% N_2, 25% CO, 20% CO_2, and 15% H_2.	1.5	306.7	*Clostridium ljungdahlii* DSM13258`	37	5.0-6.0	7
4	Stand-alone [b]	Lumen/ Closed	40% CO_2, 60% H_2	0.24	458.3	Mixed culture from methane production reactor (mesophilic)	35	6.0	80
5	Stand-alone [b]	Lumen/ Closed	40% CO_2, 60% H_2	0.32	875.0	Mixed culture from methane production reactor (mesophilic)	35	4.5- 4.8	26
6	Stand-alone [b]	Lumen/ Closed	60% CO, 40% H_2	0.32	71.9	Mixed culture from digester treating starch wastewater (mesophilic)	35	4.5	108
7	Stand-alone [b]	Lumen/ Closed	40% CO, 60% H_2	0.39	256.4	Mixed culture from anaerobic digester (mesophilic)	35	6	165
8	Stand-alone [b]	Lumen/ Closed	40% CO_2, 60% H_2	0.32	71.9	Anaerobic sludge from a full-scale biogas producing reactor	55	6	120
9	Coupled to external STR [b]	Lumen/ Open	20% CO, 5% H_2, 15% CO_2, 60% N_2	8	175	*Clostridium carboxidivorans* P7	37	4.5–5.5	NR
10	Coupled to external STR [b]	Shell/ Open	40% CO, 30% H_2, 30% CO_2	≃ 3	31	*Clostridium ragsdalei* ATCC	37	5.9	20
11	Stand-alone [b]	Lumen/ Closed	60% CO, 40% H_2	0.32	71.9	Mixed culture from digester treating starch wastewater (mesophilic)	35	4.5	27
12	Stand-alone [b]	Lumen/ Closed	40% CO, 60% H_2	0.39	615.4	Mixed culture from anaerobic digester (mesophilic)	55	6.5	60
13	Stand-alone [b]	Lumen/ Closed	40% CO_2, 60% H_2	0.32	71.9	Anaerobic sludge from a full-scale biogas producing reactor	55	6	40
14	Stand-alone [b]	Lumen/ Closed	40% CO_2 60% H_2	0.32	875.0	Mixed culture from methane production reactor (mesophilic)	35	4.5-4.8	134
15	Coupled to external reservoir	Lumen/ Closed	Varying CO:N_2 ratio	0.16	5.6	*Carboxydothermus hydrogenoformans* DSM6008	70	6.9-7.8	126
16	Submerged in STR	Lumen/ Closed	100% CO	0.4	282.5	Mixed culture from digested sewage sludge	55	7.2	131

A_m/V_L – Membrane surface area per reactor working volume.

NA – Not Applicable

NR – Not Reported

[a] With gas recirculation; [b] With liquid recirculation; [c] Initial pH; pH was not controlled; [d] Only trace amounts of butyrate produced; [e] Product titers for HRT of 8.33 days;

[f] Average productivity, calculated from available data; [g] Productivity calculated from available data (volumetric CO removal rate and CO conversion efficiency).

[g] Productivity reported in $mL.L^{-1}.day^{-1}$ (at the operational temperature and pressure).

Table 2.5 (Continued)

Entry	Liquid operation mode	HRT (day)	Liquid recirculation velocity (mL.min^{-1})	Products	Product Titers (g.L^{-1})	Productivity (g.L^{-1}.day^{-1})	Syngas utilization efficiency (%)	Biofilm formation	Reference
1	Batch	NA	NA	Acetate	1.96	0.65 [f]	NR	no	(Yasin et al., 2014)
2	Batch	NA	NA	Ethanol Acetate	2.73, 1.53	1.18	NR	no	(Jang et al., 2018)
`3	Batch	NA	120	Ethanol Acetate	1.09 0.71	NR	CO - 14%	yes	(Anggraini et al., 2019)
4	Batch	NA	500	Acetate Butyrate Hexanoate Octanoate	7.4 1.8 0.98 0.42	0.19 0.06 0.03 0.02	H_2 - 100%	yes	(Zhang, Ding, Zhang, et al., 2013)
5	Batch	NA	500	Acetate Butyrate	12.5 0.1	0.59 NR	H_2 - 100%	yes	(Zhang, Ding, Shen, et al., 2013)
6	Sequential batch	NA	NR	Ethanol	16.9	NR	NR	yes	(H.-J. Wang et al., 2018)
7	Sequential batch	NA	NR	Acetate Butyrate Hexanoate Octanoate	4.22 1.35 0.88 0.52	NR NR NR NR	CO > 95% H_2 > 95%	yes	(N. Shen et al., 2018)
8	Sequential batch	NA	NR	Acetate Butyrate	42.0 0.6	2.0 NR	NR	yes	(Y.-Q. Wang et al., 2017)
9	Continuous	1.04	200	Ethanol Acetic acid	23.93 [c] ≃ 8 [c]	3.44 ≃ 2.8	CO ≃ 81 % H_2 ≃ 74%	yes	(Y. Shen et al., 2014)
10	Continuous	5	500	Ethanol	15.0	NR	NR	yes	(Tsai et al., 2012)
11	Continuous	9	NR	Ethanol Acetate	4.2 1.0	0.47 0.11	NR	yes	(H.-J. Wang et al., 2018)
12	Continuous	1.5	NR	Acetate	24.6	16.4	CO > 95% H_2 > 95%	yes	(N. Shen et al., 2018)
13	Continuous	1	NR	Acetate Butyrate	10.5 NR [d]	10.5 NR	NR	yes	(Y.-Q. Wang et al., 2017)
14	Continuous	9	500	Acetate, Butyrate	3.6 0.02	0.4 NR	H_2 - 100%	yes	(Zhang, Ding, Shen, et al., 2013)
15	Continuous	≃ 16	1500	Hydrogen	NR	6.06 [g]	CO - 69.3%	yes	(Zhao et al., 2013)
16	Continuous	10	NA	Methane	NR	1.992 [h]	NR	yes	(Luo et al., 2013)

2.5.1 Flow configurations and patterns

The distinct flow configurations in HFM reactors and their respective advantages are summarized in Table 2.6.

Table 2.6 Summary of flow configurations in a hollow fibre membrane reactor and respective advantages.

Selection item	Option		Advantages
Gas supply configuration	Open-end		- High gas velocities in membrane lumen - High average gas fluxes and transfer rates - No water condensation - No gas back diffusion
	Closed-end		- 100 % Gas transfer
Gas feed location	Shell-side feed		None
	Lumen-side feed		- Low susceptibility of blockage by biofilm growth.
Flow pattern	Axial Flow	Co-current	- Higher feed velocities
		Counter-current	
	Cross Flow	Radial flow distribution	- Uniform shell-side flow distribution - Avoids flow channelling, bypassing and dead zones - Higher mass transfer coefficient
		Helically wound bundle	
		Flow diverters and baffles	
		"U" shape closed-end bundle	

For syngas fermentation, the gas feed can enter an HFM module from the shell or lumen side. In lumen/ tube-side feed (also known as inside-out) configuration, the gas that is supplied to the lumen of the HFM permeates through the membrane to the fermentation broth or biofilm across the membrane wall. In shell-side feed (outside-in) configuration the fermentation broth circulates inside the fibres lumen. Given the small inner diameter of the fibres, typically used for gas-liquid contacting, the outside-in configuration is not advised because biofilm formation in the lumen might block broth flow. Therefore, in the field of syngas fermentation this configuration has been mainly tested for abiotic gas-liquid mass transfer measurements (32).

In terms of gas supply and depending on their design and fabrication, HFM modules can be operated in dead-end or open-end configuration. In an open-end configuration, both ends of the fibre bundle tubesheets are open. For lumen-side feeding this implies that the gas feed is supplied from one end of the bundle and the retentate exits from the opposite end. If gas is not recycled, inherently this configuration leads to lower extent of gas conversion since there is loss of syngas substrate with the gaseous retentate. On the other hand, the gas velocity throughout the membrane is usually high. Therefore, the advective mass transport in the lumen is much faster than the diffusive transfer across the membrane, which results in

relatively uniform syngas concentrations in the lumen, leading to high average fluxes (71).

In a closed-end configuration, the fibre bundles are sealed at one end (24, 59) or are looped back to form a "U" shape in the bundle (72). All the gas supplied to the membranes is delivered through the membrane fibre, allowing 100% extent of syngas transfer (24). However closed-end HFM are usually susceptible to gas back-diffusion where produced CO_2 diffuses into the membrane lumen, which lowers the transfer rate of CO and H_2 (71). Furthermore, in HFMs for gas transfer there is also the risk of water condensation in the HFM lumen. This problem can be caused by the supply of dry feed gas at the temperature of the aqueous fermentation medium (73, 74). Since the gas permeable membranes are also highly permeable to water, the gas inside the hollow fibres becomes saturated by water within a few centimeters from the gas feed entrance. Therefore a closed-end HFM should be designed such that condensate and lumen gases are vented (73). Perez-Calleja *et al.* (71) has stated that periodic venting of the lumen of the HFM has great potential to improve the gas transfer rate and extent, increasing the performance of the HFM module and decrease the capital and operational costs. Steady state operation of an open-end system with minimized gas outflow could be an equivalent option.

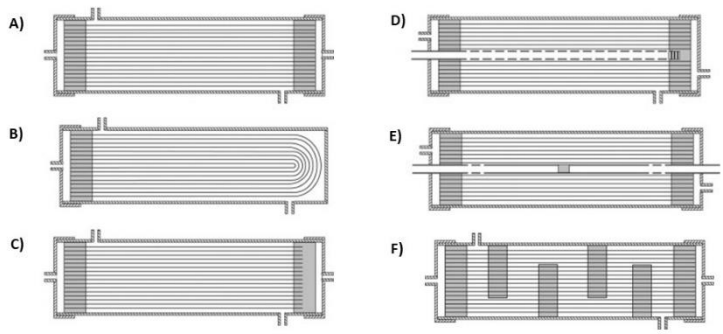

Figure 2.3 HFM modules with (A) tubesheets at both ends; (B) a single tubesheet in a U shaped bundle; (C) one tubesheet and one sealed end; (D, E) gas feed entering the bundle from the perforations on the central tube and exiting from (D) the port on the housing or (E) the perforations towards the other end; (F) Baffles with alternating clearances at top and bottom to force the flow up and down. Based on Wan *et al.* (56).

Depending on the relative flow directions of the two fluid phases, HFM modules can be classified as longitudinal/axial-flow (operated either counter-current or co-current) or as cross-flow. An axial flow pattern is often achieved in parallel hollow fibre bundles. Perez-Calleja *et al.* (71) reported higher dissolved gas concentration towards the end of the membrane fibre when operating in co-current mode. Cross-flow is designed to provide a perpendicular flow to the membrane surface, which

results in a higher mass transfer coefficient than that achieved with parallel flow. The radial flow pattern can be imposed by using, for example, a HFM module with perforated central tube to deliver the liquid feed to the shell-side, a helically wound bundle, or by introducing flow diverters and baffles in the HFM module design - Figure 2.3.

2.5.2 Side-stream and submerged HFMs

In stand-alone HFM modules, the liquid has a plug flow behaviour, whereas liquid mixing is required to achieve pH control such as necessary for most industrial fermentations. Thus, in case high performance fermentation is desired, the liquid is circulated through a mixed compartment. The HFM module can be submerged in a mixed bioreactor (internal module) or can be coupled with an external mixed tank. In the internal configuration, the HFM bundle is fabricated as an integral part of the fermentation vessel or submerged in the fermentation broth. In these systems, liquid mixing can be achieved by using a microporous membrane as a gas micro-diffuser, designated as a hollow fibre membrane bubble column reactor (HFM-BCR) (58, 59). This is also done by implementation of impellers in the reactor (70), or addition of a liquid recirculation circuit (29, 75).

In the external configuration, fermentation broth is circulated between the HFM module and a reservoir tank. This configuration is inherently very flexible, allowing the connection of available commercial modules to the external tank, therefore being investigated in several laboratory studies - Table 2.5. The fermentation broth is commonly supplied to the shell side of the membrane module and the liquid velocity entering the module is controlled by a cross-flow pump. If the external vessel is a stirred tank, the rotor can be used for additional mixing of the fermentation broth. The pump settings and tube sizing should be selected to minimize the shear stress induced on the microorganisms. The liquid feed, containing nitrogen source and mineral medium, is supplied to the external tank. Depending on the configuration and simplicity of the external tank, sensors can be installed, and pH, temperature and level of the broth can be controlled. Non-volatile products are collected from the tank effluent. For simplicity, laboratory setups can use an overflow bottle as the external reservoir (75). Both configurations have been tested in liquid batch, sequential batch or continuous configuration mode - Table 2.5. Gas delivery to the reactor is always continuous.

2.5.3 Mass transfer under abiotic conditions

The typical approach to evaluate syngas to liquid mass transfer performance in HFM bioreactors is the design of experiments to measure, directly or indirectly, the dissolved gas concentrations in the liquid, in the absence of cells and biochemical

conversion, and determine the mass transfer coefficients of the system from this concentration. The volumetric mass transfer coefficient, K_La, is not only useful to compare mass transfer capacity of different setups and at different operational conditions, but also to provide valuable information for the reactor design or process modelling. Different HFM bioreactor configurations for permeation of syngas substrates under abiotic conditions have been tested at lab scale and the respective K_La values have been reviewed, although not all literature values can be directly compared (24, 57). Therefore, a detailed explanation is given here. The approach to calculate K_La is highly dependent on the configuration and characteristics of the reactor (mixed external reservoir vessel, submerged in a reactor or stand-alone) and on the method and experimental design used.

In mass transfer studies with HFM modules with an external liquid recirculation configuration, the following equation applies in case of a liquid concentration gradient over the fibre length and no concentration gradients at the gas side.

$$\ln\left(\frac{C^* - C_0}{C^* - C_L}\right) = \frac{Q_L}{V_R}\left[1 - \exp\left(-K_L a \frac{L}{v_L}\right)\right] t \qquad 2.13$$

C^*, C_0 and C_L are, respectively, the saturated concentration, the initial concentration and actual concentration of dissolved gas in the aqueous phase in the reservoir tank (assuming well mixed conditions), Q_L is the liquid recirculation rate through the membrane module, V_R is working volume of the reservoir tank vessel, K_L the overall mass transfer coefficient, and according to the derivation of Ahmed and Semmens (52), a is the volume specific interfacial area of the membrane module (per liquid volume in the membrane module), L is the hollow fibre length, v_L is the liquid velocity in the HFM module and t is the sampling time. Then, K_La for a gas is determined by a dynamic method. During batch operation, the transient dissolved gas concentration in the well-mixed liquid reservoir is periodically measured and plotted against the sampling time according to equation 2.13. K_La is obtained from the slope of this linear relation. equation 2.13 can be rearranged to the exponential form to reduce errors resulting from linear regression.
Since K_La according to equation 2.13 is calculated per liquid volume in the membrane module solely, it must be recalculated when accounting for the total working volume of the bioreactor, V_L, that is, the external reservoir working volume, V_R, in addition to the membrane module liquid volume, V_M.

If the characteristic time for liquid recirculation (V_R/Q_L) is much shorter than the characteristic time for mass transfer ($1/K_La$), equation 2.13 simplifies to equation 2.14.

$$\ln\left(\frac{C^* - C_0}{C^* - C_L}\right) = K_L a.\frac{V_M}{V_R}.t \qquad 2.14$$

Then, there is no concentration gradient along the fibres. This condition has been achieved at submerged HFM reactor configurations, for which K_La can similarly be determined by a dynamic method according to equation 2.15 (29, 58, 59).

$$\ln\left(\frac{C^* - C_0}{C^* - C_L}\right) = K_L a.t \qquad 2.15$$

For stand-alone HFM reactors, K_La has been calculated by a steady state mass transfer analysis (static method) according to equation 2.16 (30, 57).

$$K_L a = \frac{C_{L,out}.Q}{V_M.\Delta C_{lm}} \qquad 2.16$$

This applies to HFM reactors in steady state in which there are gradients along gas side as well as liquid side of the fibre axis, but no gradients perpendicular to the axis.

K_La is based on membrane module liquid volume, V_M, $C_{L,out}$ is the quasi-steady state concentration of dissolved gas in the liquid outlet, and ΔC_{lm} is the logarithmic mean dissolved concentration difference between saturated liquid (at the partial pressure of the gas) and liquid phase (calculated differently depending on co-current or counter-current flow operation).

The K_La values in Table 2.4 differ by three orders of magnitude and should be compared with caution given the different methodologies used for their calculation, the different volumes considered (total reactor working volume or solely liquid volume of the membrane module), and the different operational parameters used in distinct experimental setups (23, 30). It is crucial to report these factors in detail, particularly the HFM module volume, total system volume, and volume used to calculate K_La (57).

2.5.4 Syngas fermentation performance in HFM reactors

Pure cultures

A minority of studies mentioned in Table 2.5 investigated HFMs submerged in bubble column reactors (58, 59). Yasin *et al.* (58) investigated fermentation of a mixture of CO/CO_2 by *Eubacterium limosum* KIST612, which yielded acetate, and as bijproduct butyric and isobutyric acids with trace amounts of ethanol and 1-butanol. The liquid phase was operated in batch mode, whereas the syngas was continuously supplied through the hydrophobic microporous hollow fibres (closed-end), resulting in formation of bubbles on the liquid side. In these type of systems, the HFM is used as a micro-sparger of the syngas substrates, and micro-bubbles

delivered by the membrane not only contribute to K_La but also to liquid mixing and to reduced gas retention in the liquid. Jang *et al.* (59) used an analogous experimental setup to study the effect of electrolyte addition to the medium on CO mass transfer to the liquid and on biomass, ethanol and acetate production. This study utilized *Clostridium autoethanogenum* DSM10061 for the fermentation of CO/CO_2 (80:20) supplied via submerged microporous HFMs, with recirculation of the headspace gas. Addition of 1% $MgSO_4$ increased ethanol productivity, ethanol concentration, cell concentration and ethanol/acetate ratio. This was explained by mass transfer increase due to bubble coalescence suppression in the presence of electrolyte.

Other studies with pure cultures investigated HFM biofilm reactors coupled with an external reservoir. Shen *et al.* (40) tested an HFM module made of microporous hydrophobic polypropylene coupled with an agitated reservoir vessel for continuous fermentation of syngas (20% CO, 5% H_2, 15%, CO_2, and 60% N_2) to ethanol and acetate and characterized fermentation performance at different syngas flow, liquid recirculation and dilution rates. A modest ethanol concentration of 23.93 $g.L^{-1}$ and ethanol to acetic acid molar ratio of 4.79 was achieved for a liquid recirculation of 25 $mL.min^{-1}L^{-1}$, a dilution rate of 0.12 d^{-1} and for a syngas flow of 37.5 and 25 $mL.min^{-1}L^{-1}$, respectively. Yet, this is the highest titer achieved for this type of reactor configuration and comparable to published data for reactors employing gas bubbling (40). The maximum ethanol productivity of 0.14 $g.L^{-1}h^{-1}$ was reported at a different dilution rate (0.96 d^{-1}). The authors reported the formation of biofilm on the membrane surface, but did not quantify mass or thickness. The formation of biofilm proved to be beneficial as a cell retention method, as it was possible to grow the microorganism at dilution rate higher than reported in suspended growth syngas fermentation reactors using the same strain (40).

Anggraini *et al.* (63) compared the performance of liquid batch syngas fermentation in a STR with and without an HFM integration, concluding that higher ethanol yield, ethanol titer, and ethanol-acetate ratio can be achieved in the former due to an increase in syngas mass transfer rates.

Abubackar *et al.* (11) reviewed a number of HFM reactor configurations patented for syngas fermentation. Tsai *et al.* (69) for example, showed the usefulness of an asymmetric HFM module that retained the cells as a biofilm layer in the membrane pores (shell side), of approximately 400 μm. The syngas stream was fed to the shell side while ethanol and other products formed in the membrane pore biofilm were transferred through the membrane (hydration layer) to the liquid medium, which recirculated between the fibre's lumen and an external stirred reservoir. With this

configuration, *C. ragsdalei* produced 15 $g.L^{-1}$ ethanol after 20 days of continuous operation.

Mixed cultures

Table 2.5 also includes studies that coupled HFMs with external reservoirs for mixed culture fermentation of syngas to carboxylic acids or methane. Operational conditions tested include membrane interfacial area, syngas composition, continuous or batch liquid operation mode, temperature, and pH. Shen *et al.* (67) investigated the conversion of CO/H_2 (40:60) by a mixed culture in a closed-end HFM biofilm reactor by varying the membrane surface area, liquid operation mode, and temperature. The main products obtained for a sequential batch experiment at 35 °C were acetate, butyrate, hexanoate and octanoate. The main product at 55 °C was acetate (minimal butyrate detected), at a maximal concentration and productivity of 24.6 $g.L^{-1}$ and 16.4 $g.L^{-1}.day^{-1}$, respectively, for continuous liquid operation of the reactor. More membrane area per working volume, hence higher available mass transfer area, led to increased production (67). *Clostridium* and *Thermoanaerobacterium* strains played major roles in this at 35 and 55 °C. In mixed culture fermentation of carbon dioxide and hydrogen, again acetate was the major product (64, 65, 68). Wang *et al* (68). achieved the highest acetate titers (42.0 $g.L^{-1}$) in a mixed culture HFM biofilm reactor, converting CO_2 and H_2 (40:60) in a liquid batch operation at 55 °C. Continuous liquid flow operation was also tested, reaching lower titers but acetate productivity up to 10.5 $g.L^{-1}.day^{-1}$ at hydraulic retention time (HRT) of 1 day.

Luo *et al.* (70) tested biogas production in a HFM reactor for simultaneous continuous sewage sludge treatment and CO biomethanation at 55 °C. Complete consumption of CO was reported, with a maximal productivity of methane of 1992 $mL.L^{-1}.d^{-1}$. The microorganisms mainly responsible for CO biomethanation were distributed differently in the liquid and in the biofilm formed on the HFM. The efficiency of microporous membrane used for the CO supply to the liquid was reported to be limited due to its relatively low bubble point pressure (70).

2.6. Biofilm formation in HFM bioreactors

As HFM bioreactors can support biofilm formation, this phenomenon needs attention. Biofilms are microbial consortia composed of one or more types of cells adhering to each other or to a surface, enclosed in a matrix of extracellular polymeric substances (EPS). Biofilm formation is linked to quorum sensing, a cell-to-cell communication mechanism via self-produced extracellular chemical signals, which allows microorganisms to monitor population density and regulate gene expression accordingly (76).

Depending on the hydrodynamic conditions achieved in the HFM, and propensity of the microbial culture to form biofilms or to attach to the membrane material, a biofilm can form in the outer layer of the membrane and cell retention in the module can be achieved. For a liquid continuous operation, the biofilm attached to the membrane surface continues to grow until the biofilm reaches a thickness equilibrated with the operating conditions (77). This membrane biofilm reactor is typically known as a counter-diffusional biofilm operation, that is, when substrate (electron donor or acceptor) diffuses through the membrane toward a biofilm naturally forming on the membrane outer surface, while complementary substrates or nutrients typically diffuse from the bulk liquid into the biofilm (78). Product usually diffuses to the bulk liquid, but depending on membrane characteristics, volatile product can also diffuse to the lumen of hollow fibres. In that case, it would be stripped with the gas feed (in open fibre configuration) or achieve equilibrium in closed-end fibre.

Biofilm reactors can offer several advantages in comparison with planktonic cells configurations as they can enable higher cell density and stability. This can lead to higher volume specific productivity, long-term continuous operation at high dilution rates without cell wash-out and easier downstream processing (79). Moreover, the biofilm offers a confined microenvironment which might protects cells from inhibitory compounds, substrates or products (79, 80).

Understanding of biofilm formation and composition is essential for the design and optimization of biofilm-based processes (79), although limited knowledge is available for anaerobic syngas-fermenting microorganisms. Philips *et al.* (81) observed that addition of NaCl (200 $mmol.L^{-1}$) to their growth medium strongly induced biofilm formation as stress response of *Clostridium ljungdahlii*, a well-known syngas fermenting bacterium. The biofilm matrix was composed of extracellular proteins, polysaccharides and DNA. Several other *Clostridium* species, including syngas fermenting bacteria, are also known to be capable of biofilm formation (82). As shown in Table 2.5, biofilms have been formed in HFMs for syngas fermentation by *Clostridium carboxidivorans* P7, *Clostridium ljungdahlii* and *Carboxydothermus hydrogenoformans*, although biofilm density (usually defined as the biomass concentration in the biofilm), biofilm thickness, molecular composition or mechanical properties were not fully characterized. Shen *et al.* (40) concluded that liquid recirculation rate through the membrane module is crucial for the fermentation performance, as it is responsible for maintaining an appropriate thickness of the biofilm in the module. A high recirculation rate corresponds to high shear stress and results in biofilm abrasion, while a low recirculation rate tends to cause membrane biofouling in HFM reactor. Zhao *et al.* (62) observed a heterogeneous colonization of the membrane and mushroom-shaped micro-

colonies in the most populated regions of the fibres, typical of biofilms grown under low laminar flow conditions. The irregular radial biofilm distribution was related with the possibly uneven fibre packing in the module causing irregular flow of liquid and substrate and nutrient maldistribution. Moreover, EPS accounted for 14% of total attached biomass.

Syngas transfer to biofilm requires the use of large membrane areas while the membrane modules need to accommodate a desired volume of biofilm. Therefore, the challenge with HFM biofilm reactors is to achieve and control biomass accumulation on properly dimensioned membrane units that contain well performing membrane materials (73).

2.7. Comparison with commercial syngas bioreactors

Membrane bioreactors and the current industrial-scale gas-lift bioreactors should be compared on syngas fermentation potential. However, no full-scale process data or conceptual studies at comparable operational conditions (syngas composition, pH, temperature), scale of reactor, and microbial strain are available, as the only current commercial process is owned and protected by LanzaTech. From industrial data, a maximum mass transfer coefficient (K_La) of 374 h^{-1} has been estimated for CO in bubble columns for a superficial gas velocity of 0.14 $m.s^{-1}$ (9). Higher gas flow rates, lower pressure and non-coalescing media could increase this value. On the other hand, values up to 1096 h^{-1} are found for lab-scale HFM reactors - Table 2.4, and such K_La values will not be scale-dependent in case of modular scale-up of HFM reactors. Thus, HFM reactors need a smaller volume for transferring the same amount of syngas.

Exploiting high K_La values requires operation at high biomass concentration. At steady-state operation, HFM reactors with biofilms need little cell growth, whereas gas-lift reactors and bubble columns need either substantial cell growth, or cell retention systems, for similar performance. Estimates of costs involved in this are not available.

Per m^3, bubble column costs should decrease with increasing size because of decreasing area/volume ratio. HFM reactor costs per m^3 are determined by membrane costs and membrane area per volume. Since this will not show much dependency on scale, HFM reactors become less likely to be competitive if very large production volumes are needed such as in case of bulk products like ethanol. Fine-chemicals may be a better target for HFM reactors.

2.8. Conclusions and future perspectives

Technical feasibility of membrane modules for syngas permeation and fermentation has been demonstrated at lab scale. They can offer cell retention and high syngas mass transfer, potentially leading to high productivities. To achieve this, HFM modules with dense or asymmetric membranes such as PDMS or PMP, respectively, seem suitable. Gas feed configurations (open-/closed-end) and liquid patterns configurations (co-/counter-/cross-current) in these modules have not been systematically studied. Liquid flow operation, though, should prevent biofouling of the module while maximizing mass transfer rates. In case of external liquid recirculation, external volume should be minimized to avoid volumetric mass transfer losses. Comparison of published mass transfer performances of HFM reactors for syngas permeation is not straightforward given the variability between setups, operational conditions and calculation methodologies.

Economic feasibility of membrane modules for syngas supply in fermentations is not clear yet, because it requires prior process optimization. However, the number of design parameters is large; they are related to:

i. Mass transfer kinetics (membrane permeabilities, K_La determination and standardization)
ii. Reaction kinetics and stoichiometry
iii. Biofilm kinetics (cell growth and detachment)

Using mathematical models would allow a more systematic design and optimization of HFM reactors and understanding of each variable's contribution to the overall performance.

Chapter 3

Modelling syngas fermentation in a hollow fibre membrane bioreactor

(Manuscript in preparation)

Marina P. Elisiário, Lars Puiman, Wouter Van Hecke, Heleen De Wever, Henk Noorman, Cristian Picioreanu, Adrie J. J. Straathof, Syngas fermentation in a hollow fibre membrane bioreactor: a predictive model.

Abstract

To allow optimization of the performance of syngas fermentation in hollow fibre membrane (HFM) bioreactors, a computational model was developed, incorporating hydrodynamics, mass transfer and kinetics microbial kinetics. The model allows for systematic study and optimization of the process, considering various operational settings. A specific case of CO fermentation to ethanol was used for illustration due to available kinetic data. The model results were compared with experimental data from literature, showing promising agreement. Parametric analyses were performed to investigate the influence of process variables on key performance indicators such as ethanol productivity, concentration, and CO conversion. The hydraulic retention time was identified as a critical parameter affecting the ethanol concentration and productivity trade-off. While the model provides valuable insights and predictions, future improvements should focus on experimental validation of key assumptions and parameters, including stoichiometry and reaction kinetics. By refining the model, it can serve as a valuable tool to guide the design of efficient HFM bioreactors for syngas fermentation and predict optimal operational conditions.

Keywords: *Syngas, Fermentation, Membrane bioreactor, Modelling, Ethanol, Kinetics*

3. Modelling syngas fermentation in a hollow fibre membrane bioreactor

3.1. Introduction

Syngas fermentation uses chemolithoautotrophic microorganisms that have the unique ability to convert a mixture of gas substrates (CO, CO_2 and H_2) to carbon-containing commodity products such as ethanol, acetate, and 1-hexanol. This microbial process has demonstrated potential in the reduction of greenhouse gas emissions since it enables the utilisation of captured carbon. Therefore, it can make a pertinent contribution regarding climate change action (83).

One of the main bottlenecks in gas fermentation is the low solubility of CO and H_2 in water, and the consequential low productivity of acetogens (1, 13, 84). This poor solubility hampers the transfer of these gases to the microorganisms resulting in low dissolved gas concentrations. The low growth rate motivates the use of biomass retention systems to obtain sufficient biomass concentrations and to increase the rate of production of the desired carbon compound. To achieve high gas transfer and cell retention, several reactor configurations and operational conditions have been studied and investigated for syngas fermentation (23).

In this respect, hollow fibre membrane (HFM) bioreactors are important options (Chapter 2). The HFM works as a gas-liquid contactor, allowing syngas permeation. The HFM's high specific mass transfer area may enable high mass transfer. The driving force for gas permeation can be increased by increased transmembrane pressure. Moreover, the aqueous side of the membrane may function as a physical support for attachment of growing microbes, leading to biofilm formation and cell retention (40). Additionally, membrane bioreactors have been claimed to offer several advantages such as low energy consumption, enabling continuous operations, easy operation and scale-up (34, 35). Coupling to an external reservoir, based on a stirred-tank reactor, yields control of the liquid residence time and thus product titre and productivity.

A variety of process settings influence process performance in HFM bioreactors: gas pressure, gas flow velocity and composition, the shell liquid flow pattern and inflow rate, reservoir inflow rate, membrane parameters such as thickness, material and type (porous, dense or composite), and reactor dimension factors like fibre length, fibre diameter, spacing and total fibre number (Chapter 2). These can be adjusted to improve the reactor performance. Given the numerous variables that can be simultaneously tuned, it is impractical and time consuming to use experimental studies for performance optimization. Instead, the influence of these process

variables on the process key performance indicators can be determined with a computational model of an HFM reactor.

Previous research has developed computational models to assess mass transfer in membrane reactors. However, some models do not incorporate biomass formation (13, 85) or do not specify membrane characteristics (86). Other models have been developed by fitting experimental data to determine mass transfer coefficients (30, 32). More comprehensive models have been developed incorporating mass transfer and biofilms, for wastewater treatment (87-90) and for hydrogen-based denitrification (91, 92). Edel *et al.* (93) developed a simple 1D model for syngas fermentation to acetate in membrane reactors with attached biofilm. They concluded from their model that the biofilm thickness and the biomass concentration in the biofilm are the most important values that influence the productivity of the reactor. However, they did not systematically determine the underlying dominant transport phenomena and the impacts of concentration gradients on the biological conversion. Overall, literature models on syngas fermentation in HFM bioreactors address only a modest part of the design space.

The current study aims to develop a descriptive model of syngas fermentation in a lab-scale HFM reactor with biofilm that allows systematic study and optimization of the performance. The model will incorporate hydrodynamics, mass transfer and microbial kinetics. Although the model structure will allow numerous process settings to be evaluated, we limit the evaluations that will be presented by fixing the HFM reactor dimension and membrane type and by varying only a selection of the operational settings. The model structure will be generic, hence widely applicable for several use-cases concerning relating to gas fermentation and permeation. As example conversion, we will take the fermentation of CO to ethanol, because of the availability of kinetic data of the reaction. An attractive window of operation will be derived by assessing possible trade-offs between key performance indicators: productivity, product titre, and extent of CO conversion. The model will also enable comparison with other reactor types and guide scale-up.

3.2. Methods

3.2.1 Description of bioreactor configuration

A schematic overview of the lab scale HFM bioreactor and process configuration is shown in Figure 3.1. A mathematical model for gas permeation and fermentation in a bioreactor was developed for steady-state conditions. In the modelled process, the gaseous substrates are fed in the lumen (inside) of the membrane fibres in an open-end fibre configuration. The substrates permeate the dense poly-dimethylsiloxane (PDMS) membrane material, to reach the biofilm at the shell side and, if not

converted, the liquid compartment of the HFM bioreactor. PDMS was chosen since it offers long term high syngas permeability and mechanical stability (Chapter 2). This will be described in more detail in the next section. The aqueous phase is recirculated via a continuous stirred tank reactor (CSTR) which is ideally mixed and controls outflow of the aqueous product. Some nitrogen gas may be sparged into this reservoir via a separate gas inflow to decrease concentrations of dissolved gases. This prevents that gases can reach supersaturation and also simulates the lab scale provision for online dissolved gas analysis. A gas condenser in the gas outlet of the reservoir limits evaporation of water and ethanol. Isothermal conditions are assumed for the whole system.

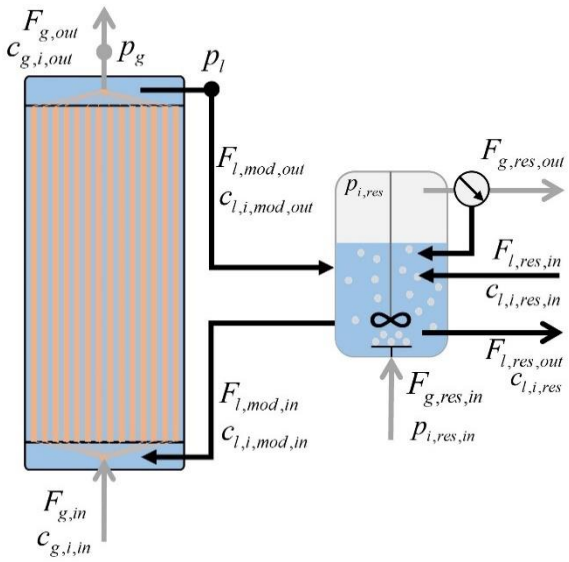

Figure 3.1. Schematic representation of the lab scale HFM bioreactor module (*mod*, left) with a liquid recirculation reservoir (*res*, right). The process streams are represented by arrows. *F* is flow, c_i is concentration of species *i*, and *p* is pressure; these are defined for gas *g* and liquid *l*.

3.2.2 Model description

The numerical model assumes that the fibres are identical parallel cylinders that are equally spaced in a hexagonal or honeycomb structure over the membrane module length. Maldistribution in gas and liquid flow velocities and module wall effects are neglected. Hence, one single fibre is modelled as representative of all the fibres in the membrane module (

Figure 3.2a-b). The geometry of the HFM bioreactor is approximated by one fibre in a two-dimensional (2D) axisymmetric configuration, where a symmetry axis is imposed in the centre of the fibre (Figure 3.2c). This accounts for the 3D patterns around the fibre, as it assumes that there is an equal distribution of all properties in

the azimuthal direction. In Figure 3.2c, the geometry of each compartment (lumen gas *g*, membrane *m*, biofilm *b*, and shell liquid *l*) is depicted together with the respective most relevant transport phenomena and species fluxes. The domain of fluid surrounding each fibre is approximated by a cylinder with cross-section radius r_l, given by equation 3.1, which depends on the packing density ϕ according to equation 3.2 via the volumes *V* (94). From this, the fibre spacing of the membrane module d_{spacing} was derived as equation 3.3.

$$r_l = r_{mb}^{\text{int}} \sqrt{\frac{1}{\phi}} \tag{3.1}$$

$$\phi = \frac{V_g + V_m}{V_{\text{shell}}} \tag{3.2}$$

$$d_{\text{spacing}} = 2\left(r_l - r_{mb}^{\text{int}}\right) \tag{3.3}$$

The numerical model describes fluid flow and also mass transport and reaction of the fermentation substrate (CO) and the products (biomass, ethanol and CO_2) in the gas, membrane, biofilm and liquid compartments, if applicable (sections 3.2.3 and 3.2.4). In the gas and liquid phases, radial diffusion and axial convection are considered, while in the membrane and biofilm only radial diffusion was taken into account for solutes transport. Partitioning (constant *K*) is assumed at the interfaces between the gas phase and the membrane and between the membrane and the biofilm layer.

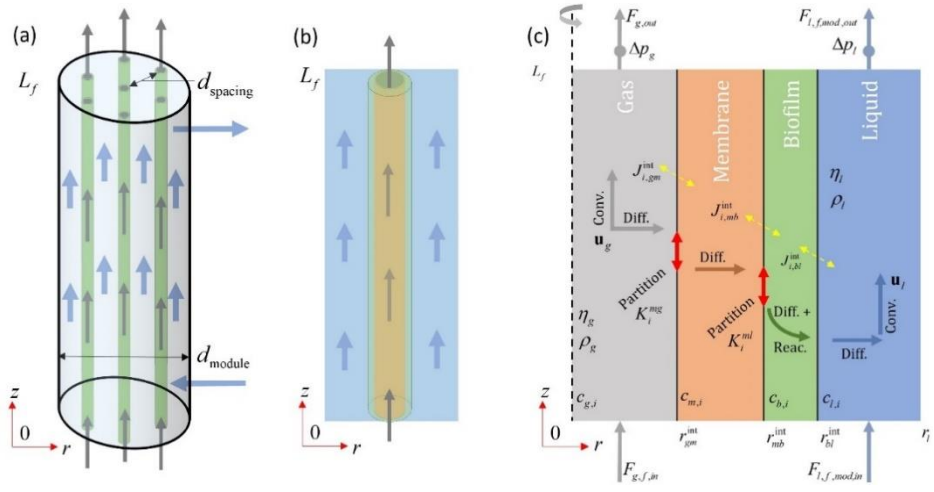

Figure 3.2. Schematic configurations used for designing the model of the HFM module. (a): 3D module of a HFM system with three fibres, although the module used has 550 fibres. (b): the used approximation, with only one fibre in 3D. (c): The 2D axisymmetric system which was eventually used for modelling this system.

3.2.3 Flow balances

Gaseous flow through the fibre was assumed to be a compressible and laminar flow. Gravity was excluded due to the low gas density ρ_g and the short length of the fibre. The viscosity η_g of the syngas was calculated at the inlet composition and assumed not to change along the fibre length L_f. Momentum continuity was modelled, at steady-state, by the constitutive Navier-Stokes equation, equation 3.4, which accounts for momentum changes due to advection, pressure differences and gas viscosity and compressibility effects. This was coupled (95) with mass continuity according to equation 3.5, while taking into account that a gas pressure gradient over the length of the lumen of the fibre will cause density variations to according to equation 3.19, which will be given later.

$$\rho_g\left(\mathbf{u}_g\cdot\nabla\right)\mathbf{u}_g=\nabla\cdot\left(-p_g\,\mathbf{I}+\eta_g\left(\nabla\,\mathbf{u}_g+\left(\nabla\mathbf{u}_g\right)^T\right)-\frac{2}{3}\eta_g\left(\nabla\cdot\,\mathbf{u}_g\right)\mathbf{I}\right) \tag{3.4}$$

$$\nabla\cdot\left(\rho_g\mathbf{u}_g\right)=0 \tag{3.5}$$

As boundary conditions, symmetry was imposed at r = 0 according to equation 3.6. At the gas-membrane interface a no-slip condition was imposed according to equation 3.7. The fibre gas flow at the inlet was assumed to be fully developed as the length of the fibre is much larger than the diameter of the fibre (72) and equals the total gas flow into the lumen divided by the number of fibres N_f according to equation 3.8. At the fibre outlet, the boundary condition imposed a normal flow pressure regulated with a pressure controller, which suppresses the backflow according to equation 3.9.

$$u_{g,r}\Big|_{r=0}=0 \quad \text{and} \quad \frac{\partial u_{g,z}}{\partial r}\Big|_{r=0}=0 \tag{3.6}$$

$$\mathbf{u}_g(r=r_{gm}^{\text{int}})=0 \tag{3.7}$$

$$F_{g,f,in}(z=0)=\frac{F_{g,in}}{N_f} \tag{3.8}$$

$$p_g(z=L_f)=p_{ref}+\Delta p_g \tag{3.9}$$

The shell liquid flow was modelled assuming laminar flow (Re ≤ 15). Effects of the solutes (nutrients, ethanol, dissolved gases and biomass) on the viscosity and the density of the liquid phase were always neglected. At steady state, momentum continuity was described by the constitutive Navier-Stokes equation for incompressible flow according to equation 3.10 – taking into account advective,

pressure, viscosity and gravity effects on momentum. Mass continuity was modelled by equation 3.11.

$$\rho_l \left(\mathbf{u_l} \cdot \nabla\right)\mathbf{u_l} = \nabla \cdot \left(-p_l\ \mathbf{I} + \eta_l \left(\nabla\ \mathbf{u_l} + \left(\nabla\ \mathbf{u_l}\right)^{\mathrm{T}}\right)\right) + \rho_l \mathbf{g} \qquad 3.10$$

$$\rho_l \nabla \cdot \mathbf{u_l} = 0 \qquad 3.11$$

As boundary conditions, a no-slip condition was applied at the liquid-biofilm interface according to equation 3.12, and flow symmetry was applied at $r = r_l$ by using equation 3.13. At the liquid outlet, the pressure was controlled, and backflow was suppressed according to equation 3.14. At the inlet, the liquid flow to the shell was divided by the amount of fibres according to equation. 3.15.

$$\mathbf{u_l}(r = r_{bl}^{\mathrm{int}}) = 0 \qquad 3.12$$

$$u_{l,r}\Big|_{r=r_l} = 0 \quad \text{and} \quad \left.\frac{\partial u_{l,z}}{\partial r}\right|_{r=r_l} = 0 \qquad 3.13$$

$$p_l(z = L_f) = p_{ref} + \Delta p_l \qquad 3.14$$

$$F_{l,f,in}(z = 0) = \frac{F_{l,mod,in}}{N_f} \qquad 3.15$$

The shell-side Reynolds number is given by equation 3.16.

$$\mathrm{Re} = \frac{\rho_L v_L d_{spacing}}{\eta_l} \qquad 3.16$$

3.2.4 Species material balances

Gas phase

Steady state mass balances for all chemical species *i* in the gas phase were solved for the mass fractions $\omega_{g,i}$ and involved convection and diffusion transport mechanisms:

$$\rho_g \left(\mathbf{u}_g \cdot \nabla\right)\omega_{g,i} + \nabla \cdot \mathbf{J}_{g,i}^{d} = 0 \qquad 3.17$$

The species relative diffusion flux $\boldsymbol{J}_{g,i}^{d}$ was defined according to the Maxwell-Stefan model (96) as the gaseous species fractions are all in the same order of magnitude:

$$\mathbf{J_{g,i}^{d}} = -\rho_g \omega_{g,i} \sum_{j=1}^{n} D_{i,j} \left(\nabla x_{g,j} + (x_{g,j} - \omega_{g,j})\frac{\nabla p_g}{p_g}\right) \qquad 3.18$$

This includes the Maxwell-Stefan diffusion coefficients ($D_{i,j}$ for species i in j), and as driving forces gradients of mole fractions ($\nabla x_{g,j}$) and total gas pressure (∇p_g).The gas density ρ_g was computed assuming ideal gas behaviour with mass averaged molar masses M_i:

$$\rho_g = \frac{p_g}{RT}\left(\sum_{i=1}^{n}\frac{\omega_{g,i}}{M_i}\right)^{-1} \quad 3.19$$

The gas pressure p_g and velocity $\boldsymbol{u_g}$ follow from the gas flow equations, which in turn make use of the variable gas density ρ_g.

A Danckwerts-type boundary condition was assumed at the fibre inlet (z = 0):

$$u_{g,z}c_{g,i,in} = \left(u_{g,z}c_{g,i} + J^{d}_{g,i,z}\right)_{z=0} \quad 3.20$$

with the inlet mass concentrations of the gas species $c_{g,i,in}$ defined as:

$$c_{g,i} = x_{g,i}\frac{p_g}{RT}M_i \quad 3.21$$

Symmetry was imposed at the fibre axis, $\left(J^{d}_{g,i,r}\right)_{r=0} = 0$. An outflow condition (zero diffusion flux) was set at the end of the fibre, $\left(J^{d}_{g,i,z}\right)_{z=L_f} = 0$.

A flux continuity condition was set for each species at the gas-membrane interface ($r = R_{gm}$), assuming that the diffusion flux on the membrane side equals the diffusion flux plus Stefan effective convection flux at the gas side of the interface (97).

Membrane

In a dense PDMS membrane, steady state species transport is modelled according to the solution-diffusion model and is therefore described by Fick's law for all compounds dissolved in the membrane (38), as function of molar concentration $c_{m,i}$ while assuming an isotropic diffusion coefficient $D_{m,i}$:

$$\nabla\cdot\left(D_{m,i}\nabla c_{m,i}\right) = 0 \quad 3.22$$

No-flux conditions were imposed at z = 0 and z = L_f. At the gas-membrane interface, the species concentration in the membrane was coupled with the gas phase concentration via a partition coefficient $K_i^{m,g}$:

$$\left(c_{m,i}\right)_{r=R_{gm}} = K_i^{m,g}\left(c_{g,i}\right)_{r=R_{gm}} \quad 3.23$$

The flux through the membrane was coupled to the flux in the biofilm, assuming flux continuity according to equation 3.24.

$$J_{i,mb}^{int} = -D_{b,i}\frac{\partial c_{b,i}}{\partial r} \quad 3.24$$

The membrane diffusion and partition coefficients of the dissolved species were calculated (98). The biofilm species diffusion coefficient was calculated from the liquid diffusion coefficient (98), while assuming a biofilm diffusivity factor f_B (38) according to equation 3.25.

$$D_{b,i} = f_B D_{l,i} \quad 3.25$$

Biofilm and liquid

The mass balances in the biofilm, equation 3.26, included transport in the biofilm by Fick's law and a reaction kinetics term, as convection was assumed to be absent in the biofilm. The reaction kinetics term includes the biomass-specific rate q_i and the biomass concentration c_x. No flux (J_i = 0) was imposed at z = 0 and $z = L_f$. Flux continuity was imposed at the biofilm-liquid interface according to equation 3.27. The liquid flow and biomass distribution in the membrane module were assumed to be uniform, for simplification, therefore the biofilm thickness d_b and its biomass concentration were assumed to be constant along the fibre's length. The biofilm thickness (Table 3.1) was assumed based on a study on HFM biofilm reactor with mixed culture syngas (H_2/CO_2) fermentation by Wang *et al.*(68) , which reported scanning electron microscopy (SEM) photos of the cross-section of a single fibre. At the membrane-biofilm interface, the solute concentrations were coupled to the concentrations in the biofilm, while taking partition equilibria at the interfaces into account according to equation 3.28. However, for larger pressures, supersaturation and subsequent bubble formation could occur in the biofilm. It was assumed that in these cases the concentration of solutes in the biofilm equals the maximum solubility.

$$D_{b,i}\nabla^2 c_{b,i} = q_i c_{b,x} \quad 3.26$$

$$J_i^{\mathrm{bl,int}} = -D_{l.i}\frac{\partial c_{l,i}}{\partial r} \quad 3.27$$

$$c_{b,i}^{\mathrm{mb,int}} = \begin{cases} c_{m,i}^{\mathrm{ml,int}} / K_i^{ml} & \text{when } c_{m,i}^{\mathrm{ml,int}} / K_i^{ml} < c_{l,i}^{sol} \\ c_{l,i}^{sol} & \text{when } c_{m,i}^{\mathrm{ml,int}} / K_i^{ml} \geq c_{l,i}^{sol} \end{cases} \quad 3.28$$

The liquid mass balances are given by equation 3.29. Transport in the shell liquid phase was governed by axial convection and radial diffusion. Microbial conversion of CO in the liquid was considered when suspended biomass was present in the

liquid. At the liquid inlet, a Danckwerts boundary condition was imposed, equation 3.30, as this takes axial dispersion into account (99). At the liquid outflow, equation 3.31 was applied as no-flux condition. Equal partitioning was imposed at the biofilm-liquid boundary, according to equation 3.32, as both compartments are aqueous. Lastly, symmetry was applied in the middle of the liquid phase by using equation 3.33.

$$u_l \cdot \nabla c_{l,i} + D_{l,i} \nabla^2 c_{l,i} = q_i c_{l,x} \quad 3.29$$

$$u_l c_{l,i}(z=0) = u_l c_{l,i,in} + D_{l,i} \frac{\partial c_{l,i}}{\partial z} \quad 3.30$$

$$\frac{\partial c_{l,i}}{\partial z}(z=L_f) = u_l \nabla c_{l,i} \quad 3.31$$

$$c_{l,i}^{\mathrm{bl,int}} = c_{b,i}^{\mathrm{bl,int}} \quad 3.32$$

$$\frac{\partial c_{l,i}}{\partial r}(r=r_l) = 0 \quad 3.33$$

Evaporation of water and ethanol from liquid to gas phase was included in the model by analogy with CO mass transfer. The partial pressure gradient over the membrane, which was based on the saturation pressure in the gas phase and the concentration in the liquid phase, was taken as the driving force for evaporation.

Microbial conversion of CO was modelled according to equation 3.34. This equation is based on the CO uptake kinetics which were derived by Mohammadi *et al.* (100) and a linear fit of ethanol inhibition data from Fernández-Naveira *et al.* (101). For ethanol concentrations $c_{k,EtOH}$ exceeding the tolerance $K_{I,EtOH}$ (45 g.L^{-1}), we used q_{CO}=0 instead of equation 3.34. By derivation of a black-box stoichiometric model for *Clostridium spp.* (102) for the metabolic and catabolic reactions, the reaction stoichiometry was determined. Incorporating the maintenance requirement m_{ms}, the microbial-specific growth rate was calculated using equation 3.35. With the Herbert-Pirt relationship, the compound-specific reaction rates were calculated using equation 3.36. Details on the derivation of the kinetic model for CO uptake, CO inhibition, ethanol inhibition and the reaction stoichiometry have been reported by Puiman (98).

$$-q_{CO} = -q_{CO}^{max} I_{CO} I_{EtOH} = -q_{CO}^{max} \times \frac{c_{k,CO}}{K_{p,CO} + c_{k,CO} + \frac{c_{k,CO}}{K_{I,CO}}} \left(1 - \frac{c_{k,EtOH}}{K_{I,EtOH}}\right) \quad \text{with} \quad k = [b,l] \quad 3.34$$

$$\mu = \frac{q_{CO} - m_{ms}}{Y_{CO}^{met}} \quad 3.35$$

$$q_i = Y_i^{met}\mu + \frac{m_{ms}Y_{CO}^{cat}}{Y_i^{cat}} \quad 3.36$$

External Reservoir

As mentioned, the reservoir was also at steady-state and was ideally mixed. It was assumed that reaction in the reservoir can be neglected. The liquid inflow to the system and outflow from the system via the reservoir were assumed to have equal rates. Assuming ideal mixing and steady-state behaviour in the reservoir, the compound-specific concentration in the liquid phase in the reservoir is described by equation 3.37, which is derived from solute-specific mass balances (which depends on inlet and outlet liquid flow rates and compound mass transfer to the gas phase in the reservoir). The liquid hydraulic retention time HRT in the HFM bioreactor including reservoir, is inversely proportional to the dilution rate *D* and defined by equation 3.38.

$$c_{l,i,res} = \frac{F_{l,res,in}c_{l,i,res,in} + F_{l,mod,out}c_{l,i,mod,out} + \left(k_{L,i}^{ov}a\right)_{res}V_{res}\frac{p_{i,res}}{RT}K_i^{lg}}{F_{l,mod,in} + F_{l,res,out} + k_{L,i}^{ov}aV_{res}} \quad 3.37$$

$$HRT = \frac{1}{D} = \frac{V_{l,tot}}{F_{l,res,out}} = \frac{V_{res} + V_{shell} - V_{biof}}{F_{l,res,out}} \quad 3.38$$

3.2.5 Model parameters

Table 3.1 Non-compound-specific parameters used for modelling the HFM membrane module. Some parameters were provided by the membrane producing company (OxyMem).

Parameter	Symbol	Value	Unit	Source
General parameters				
Temperature	T	37	°C	a
Reference pressure	p_{ref}	1	atm	a
HFM module parameters				
Inner fibre diameter	d_i	340	µm	Oxymem
Membrane thickness	d_m	110	µm	Oxymem
Fibre and module length	L_f	40	cm	Oxymem
Number of fibres	N_f	550	-	Oxymem
Shell volume	V_{shell}	500	mL	Oxymem
Fibre spacing	$d_{spacing}$	0.123	cm	(98)
Packing density	ϕ	9.7	%	a
Volume-specific surface area	a	774	m^{-1}	(98)
Gas phase parameters				
Lumen gas flow rate	$F_{g,in}$	4 - 400	$mL.min^{-1}$	b
Fibre gas flow rate	$F_{g,f,in}$	0.0073 - 0.727	$mL.min^{-1}$	a
Lumen gas overpressure	Δp_g	0.5	bar	c
CO gas viscosity at inlet	η_g	$1.8{\cdot}10^{-5}$	Pa.s	(98)
CO gas density at inlet	ρ_g	1.63	$kg.m^{-3}$	(98)
Biofilm and reaction parameters				
Diffusivity factor	f_B	0.8	-	d
Biofilm thickness	d_b	100 or 190	µm	b, d
Biomass concentration	$c_{b,x}$	15	$kg.m^{-3}$	d
Maintenance requirement	$-m_{ms}$	0.066	$mol_{CO}.mol_x^{-1}.h^{-1}$	(98)
Max. CO uptake rate	$-q_{CO}^{max}$	0.0344	$mol_{CO}.g_x^{-1}.h^{-1}$	(100)
CO saturation constant	$K_{p,CO}$	0.0178	$mol_{CO}.m^{-3}$	(100)
CO inhibition constant	$K_{I,CO}$	0.510	$mol_{CO}.m^{-3}$	(100)
Ethanol inhibition constant	$K_{I,EtOH}$	978	$mol_{EtOH}.m^{-3}$	(98)
Liquid phase parameters				
Shell liquid flow rate[a]	$F_{l,mod,in}$	10 - 500	$mL.min^{-1}$	a
Shell liquid flow rate per fibre	$F_{l,f,mod,in}$	0.00036 - 0.909	$mL.min^{-1}$	a
Liquid overpressure	Δp_l	0	atm	b
Liquid viscosity	η_l	$7.0{\cdot}10^{-4}$	Pa.s	(98)
Liquid density	ρ_l	993.6	$kg.m^{-3}$	-
Reservoir parameters				
Gas inflow rate (co-current)	$F_{g,res,in}$	1 - 100	$mL.min^{-1}$	b
Inlet pressure	$p_{res,in}$	1	atm	a
Liquid inflow rate	$F_{l,res,in}$	0.025 - 2	$mL.min^{-1}$	b
Reservoir volume	V_{res}	0.5	L	a
Volumetric mass transfer coefficient	$\left(k_{L,i}^{ov}a\right)_{res}$	30	h^{-1}	(98)

[a] Process parameter. [b] Process parameter value used is mentioned when discussing models. [c] Process parameter having a different value in cases where mentioned. [d] No source available, hence assumed.

Table 3.2 Compound-specific parameters used for modelling the HFM membrane module (98). Partition and membrane diffusion values for ethanol and water are calculated for 37 ◦C, while the values of the gasses were calculated temperature of 35 ◦C. All the other parameters were calculated for a temperature of 37 ◦C.

Parameter	Symbol	Unit	CO	CO_2	H_2	N_2	EtOH	H_2O	Biomass
General parameters									
Molecular mass	M_i	$\mathrm{g.mol^{-1}}$	28	44	2	28	46	18	24.6[a]
Gas phase parameters									
CO gas inlet composition	$x_{g,i,in}$	$\mathrm{mol_i.mol_{gas}^{-1}}$	0.5 or 1	10^{-8}	10^{-8}	10^{-8}	-	-	-
Maxwell-Stefan diffusion coefficient	$D_{g,i,av}$	$10^{-5}\mathrm{m^2.s^{-1}}$	1.5	1.2	6.0	1.6	∼1	∼1	-
Membrane parameters and partition coefficients									
Membrane permeability	P_i	$10^{-9}\mathrm{m^2.s^{-1}}$	0.382	2.93	0.723	0.316	34.1	5410	-
Diffusion coefficient	$D_{m,i}$	$10^{-9}\mathrm{m^2.s^{-1}}$	3.40	2.20	14.0	3.40	1.46	4.87	-
Membrane-gas partition coefficient	K_i^{mg}	-	0.112	1.333	0.052	0.093	23.36	1111	-
Membrane-liquid partition coefficient	K_i^{ml}	-	5.201	2.048	2.731	6.752	0.0024	$1.59{\cdot}10^{-4}$	-
Liquid-gas partition coefficient	K_i^{lg}	-	0.0216	0.651	0.0189	0.014	9721	22647	-
Biofilm and reaction parameters									
Diffusion coefficient	$D_{b,i}$	$10^{-9}\mathrm{m^2.s^{-1}}$	2.17	2.05	4.81	2.01	0.97	-	-
Catabolic reaction yield	Y_i^{cat}	$\mathrm{mol_i.mol_{EtOH}^{-1}}$	-6	4	0	0	1	-3	0
Metabolic reaction yield	Y_i^{met}	$\mathrm{mol_i.mol_x^{-1}}$	-46.06	30.41	0	0	7.33	-22.58	1
Liquid parameters									
Diffusion coefficient	$D_{l,i}$	$10^{-9}\mathrm{m^2.s^{-1}}$	2.71	2.56	6.01	2.51	1.21	-	$1.98{\cdot}10^{-4}$
Solubility	$c_{l,i}^{sol}$	$\mathrm{mol_i.m^{-3}}$	0.85	25.6	0.74	0.54	-	-	-
Reservoir parameters									
Inlet partial pressure	$p_{i,res,in}$	atm	0	0	0	1	0	0	0
Liquid inlet concentration	$c_{l,i,res,in}$	$\mathrm{mol_i.m^{-3}}$	0	0	0	0	0	55555	0

[a] Considering a biomass composition of $CH_{1.8}O_{0.5}N_{0.2}$.

3.2.6 Model solution

The model was solved with the finite-element simulation platform COMSOL Multiphysics (COMSOL 5.4, Comsol Inc., Burlington, MA, www.comsol.com) using a steady Newton nonlinear solver. A mesh was developed with varying element size, 100 cells in the axial direction, in gas, membrane, biofilm, liquid phases, and radially varying cell numbers of 30, 50, 20, 100, respectively.

3.2.7 Key process performance indicators

The volume-averaged volumetric mass transfer coefficient for CO, for the HFM module, was calculated for an abiotic system (without the presence of cells or biofilm) and without recirculation through the reservoir by using equation 3.39. The total mass transfer rate $T_{CO}^{ml,int}$ was calculated as the amount transferred from the membrane to the shell, in the whole HFM module, whereas Δc_{CO} is the substrate concentration gradient between gas and liquid side, with $\langle c \rangle_{A_s}$ denoting the surface average of concentration.

$$k_{L,CO}^{ov} a = \frac{T_{CO}^{ml,\mathrm{int}}}{\Delta c_{CO}} = \frac{\dfrac{N_f}{V_{shell}} \int_0^{A_{s,ml}^{\mathrm{int}}} J_{CO}^{ml,\mathrm{int}} \mathrm{d}A_{\mathrm{s,ml}}^{\mathrm{int}}}{\left\langle c_{g,CO}^{gm,\mathrm{int}} \right\rangle_{A_{s,gm}} K_{CO}^{\mathrm{lg}} - \left\langle c_{l,CO}^{ml,\mathrm{int}} \right\rangle_{A_{s,ml}}} \qquad 3.39$$

The performance of syngas permeation and fermentation in HFM bioreactor was evaluated in terms of ethanol concentration (in the reservoir) using equation 3.37, volumetric ethanol productivity using equation 3.40, biomass-specific ethanol productivity using equation 3.41 and extent of CO conversion using equation 3.42. The extent of CO transfer was calculated using the amount entering (denominator of equation 3.42) and the similarly the amount leaving with the off gas at $z = L_f$.

$$P_{V,i} = M_i \frac{N_f}{V_{\mathrm{shell}}} \int_0^{V_k} q_i c_{k,x} \, \mathrm{d}V_k \quad \text{with} \quad k = [b, l] \qquad 3.40$$

$$P_{X,i} = M_i \frac{N_f}{V_{\mathrm{shell}}} \int_0^{V_k} q_i \, \mathrm{d}V_k \quad \text{with} \quad k = [b, l] \qquad 3.41$$

$$\text{CO conversion} = \frac{\displaystyle\int_0^{V_b} q_{CO} \mathrm{c}_{b,x} \mathrm{d}V_b}{\displaystyle\int_0^{A_{c,g}} \boldsymbol{u_g} c_{g,CO} \mathrm{d}A_{c,g} \Big|_{z=0}} \qquad 3.42$$

3.3. Results and Discussion

3.3.1 Abiotic mass transfer coefficient

By changing the liquid flow rate on the shell side, and consequently the Reynolds number (Re), the resulting volume-averaged volumetric mass transfer coefficient $k_{L,CO}{}^{ov}a$ gives a measure of the bioreactor efficiency for mass transfer.

Figure 3.3 shows the $k_{L,CO}{}^{ov}a$ value for the HFM module given different CO concentrations in the feed gas; and, for a fixed CO concentration, the $k_{L,CO}{}^{ov}a$ dependence on Re (hence varying liquid flow rates).

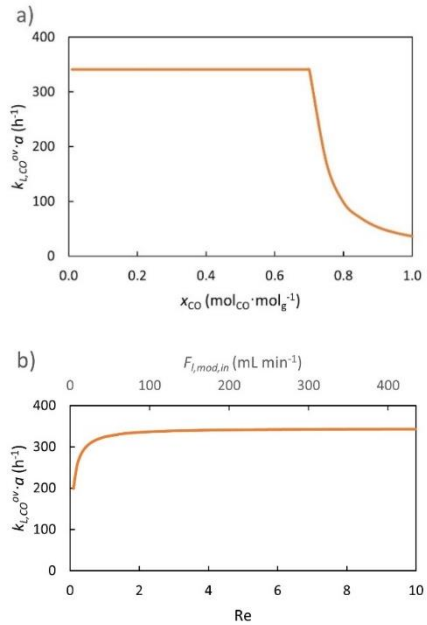

Figure 3.3 Overall mass transfer coefficient in an abiotic HFM module at $F_{g,in}$=20 mL.min^{-1}. (a) At Re = 4.6 (hence $F_{l,mod,in}$=200 mL.min^{-1}) and varying CO inlet molar fraction, $x_{CO,in}$. (b) At varying Re (hence varying liquid flow rates), at a CO inlet molar fraction of 0.5.

For an abiotic system, a maximum volume-averaged volumetric $k_{L,CO}{}^{ov}a$ for the HFM module of 343 h^{-1} is achieved for CO inlet molar fractions, $x_{CO,in}$, below 0.70, as shown in Figure 3.3a. For higher $x_{CO,in}$ values, the $k_{L,CO}{}^{ov}a$ value decreases, reaching a minimum of 40 h^{-1} (for 100% CO). The low mass transfer rates obtained in this regime are explained by saturation of the water by CO at a certain length of the fibres. By decreasing the fraction of CO in the gas phase below 0.7, the maximum solubility is not reached in any region of fibre, increasing the mass transfer rate and thereby the volume-average $k_{L,CO}{}^{ov}a$. For a biotic system, the consumption of CO by the microorganism is expected keep the dissolved concentration below its solubility.

Thereby, for increased mass transfer performance, a biotic system could operate at higher CO inlet molar fractions than 0.7. The abiotic $k_{L,CO}^{ov}a$ calculations are, therefore, a useful conservative estimation of the biotic $k_{L,CO}^{ov}a$.

When the Reynolds number is increased (by increasing the shell liquid flow rate), the mass transfer coefficient increases as well Figure 3.3b. This increase is due to the larger convection rates obtained, which cause a thinner mass transfer boundary layer at the membrane-liquid side. A thinner liquid boundary layer leads to less diffusion in the liquid phase and thus increases the mass transfer rate and its coefficient. At higher liquid flow rates, the concentration in the liquid at the membrane-liquid interface is lower, therefore, the mass transfer driving force is also higher.

For Re higher than 3, the mass transfer coefficient reaches a maximum of 343 h^{-1}. At increased liquid flow velocities, the thickness of the liquid boundary layer becomes constant and, thereby, the liquid side mass transfer resistance reaches its minimum. At this regime, the membrane is expected to be the main resistance for mass transfer. Orgill *et al.* (57) experimentally obtained the $k_{L,CO}^{ov}a$ of a PDMS HFM module, for different Reynolds, measuring a maximum of 420 h^{-1} for a Reynolds of 3.4. This result is comparable (same order of magnitude) and expected to be higher than $k_{L,CO}^{ov}a$ obtained by our model (Figure 3.3b), since the former used a HFM of the same membrane material but at a different geometry (higher fibre packing density and lower membrane thickness). A lower membrane thickness corresponds to lower membrane mass transfer resistance (Chapter 2) and thereby to an increased $k_{L,CO}^{ov}a$ (when the membrane phase is the main mass transfer resistance).

3.3.2 Comparison between biofilm and suspended biomass configuration

When using an HFM for syngas permeation and fermentation, it is still unclear if the formation of biofilm is beneficial for the process performance. Biofilm formation leads to cell retention, which can increase the volumetric productivity, by increasing cell concentration. An example of solutes' concentration profiles in the multiple HFM module compartments is shown by Puiman (98). On the other hand, the biofilm might hinder mass transfer and consequently ethanol productivity. To elucidate which is the preferred operational scenario, both configurations were simulated and are compared in Figure 3.4. The biofilm configuration can achieve higher biomass concentration (per volume of biofilm) than the suspended configuration due to inherent higher biomass densities which are typically contained in the biofilm (89). Figure 3.4a shows that the volume-specific productivity P_V of ethanol can reach higher values in case of a biofilm. Figure 3.4b shows that the maximum biomass-specific ethanol productivity P_x is the same for both configurations (0.15 $g_{EtOH}.g_X^{-1}.h^{-}$

^{1}) and, while it is reached at a concentration of 2 g_X L^{-1} for suspended biomass configuration, it is reached at a biofilm density of 48 g_X L_{biof}^{-1} .

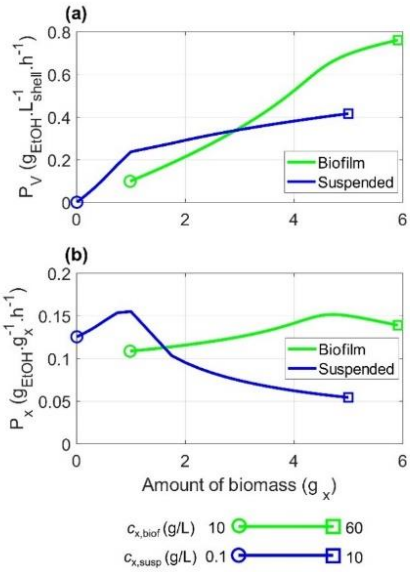

Figure 3.4 The shell-volume-specific ethanol productivity for different amount of suspended and biofilm biomass in the HFM module. The circles depict the lowest and the squares the highest possible value used for the concentrations of biomass in the suspended and biofilm configurations (see Table 3.1).The biofilm thickness was fixed at 100 μm, pure CO was used as feed gas and the module liquid flow rate $F_{l,mod,in}$ was fixed at 200 $mLmin^{-1}$ in all cases.

The optimal biomass-specific productivity and the decline of the slope of the volume-specific productivity can be explained by comparing the characteristic times of reaction and of radial diffusion (98). For suspended biomass, at a concentration of 2 g_X L^{-1} (0.9 g_X in the module), the characteristic time of reaction matches the characteristic time of radial diffusion in the liquid (Figure 3.5a). At this biomass concentration, CO diffuses through the entire liquid phase, allowing all biomass to be used for reaction. At higher biomass concentrations, CO is consumed by biomass located closer to the membrane and it is completely depleted further way (in the radial direction). Increasing biomass concentration increases mass transfer rate to the liquid phase since the reaction is not limited by mass transfer, thereby ethanol volumetric productivity increases accordingly.

For the biofilm configuration, the characteristic time of reaction equals the time of diffusion in the biofilm when biomass density in biofilm is 48 g_X L_{biof}^{-1}, equivalent to 4.7 g_X in the module (Figure 3.5b), thereby the maximum biomass-specific ethanol productivity is achieved at this concentration. The reaction is constrained by the kinetics of the organism at lower biomass concentrations, where the reaction rate is insufficiently slow. Increasing the biomass concentration results in an increased

conversion capacity. Above 48 g_X L_{biof}^{-1}, CO mass transfer is limited by the rate of diffusion in the biofilm. Not all CO reaches the biofilm-liquid boundary, yielding some biomass ineffective, and a decreased slope in P_v.

Figure 3.4a suggests that the achievable volume-specific productivity of ethanol is higher for a biofilm thickness of 100 µm than for a suspended biomass configuration, when the biofilm can retain more than 3 g_X in the membrane module (which corresponds to 31 g_X L_{biof}^{-1}). If that biomass concentration could not be reached in the biofilm, then these results suggest that suspended biomass in this HFM module would lead to the highest productivities, and that the HFM would act as an efficient gas permeating device. Obviously, this trade-off point will change if other liquid flow rates will be taken, for example.

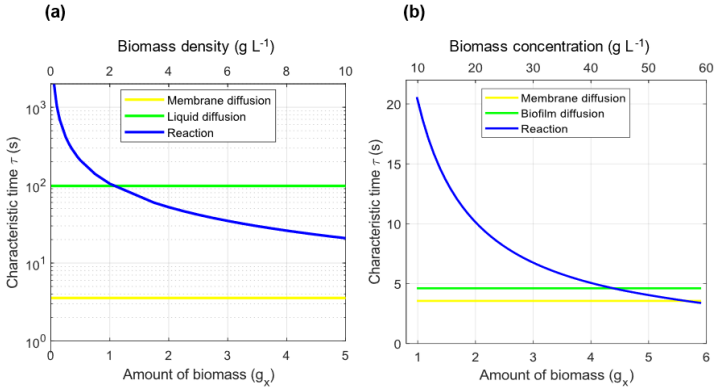

Figure 3.5 For (a) the suspended biomass and (b) the biofilm configuration, characteristic times for CO membrane diffusion, biofilm diffusion and reaction were calculated for different amounts of biomass in the module and respective biomass concentration. The biofilm thickness was fixed at 100 µm, pure CO was added in the gas phase and the module liquid flow rate $F_{l,mod,in}$ was fixed at 200 mL·min^{-1} in all cases.

3.3.3 Parametric analyses (process performance indicators vs operational parameters)

The influence of important process variables on process performance was assessed by parametric analyses (Figure 3.6). The impact of the lumen gas flow rate, lumen gas overpressure, liquid overpressure and hydraulic retention time (HRT) was investigated. The ethanol volumetric productivity, ethanol concentration and the extent of CO conversion were considered as key performance indicators (KPIs). No analysis is shown of the impact of external reservoir volume and shell liquid recirculation flow as they were found to have a marginal influence on the considered KPIs (98). For the parametric analysis, the base value of each studied process variable was kept constant while changing another variable. The base values and operational window are reported in Table 3.3.

Table 3.3 Operational window of the key process variables studied by parametric analysis.[a]

Parameter	Symbol	Unit	Base Value	Lower value	Upper value
Lumen gas flow rate	$F_{g,in}$	mL min^{-1}	20	4	200
Lumen gas overpressure	Δp_g	atm	1.5	1	1.5
Liquid overpressure	Δp_l	atm	1	1	2
HRT [b]	-	day	5.7	0.31	25

[a] Fixed values were $F_{l,mod,in}$ = 150 mL/min, $F_{g,res,in}$ = 1 mL/min, and d_b = 190 µm.
[b] Modified by changing $F_{l,res,in}$ according to Table 3.1.

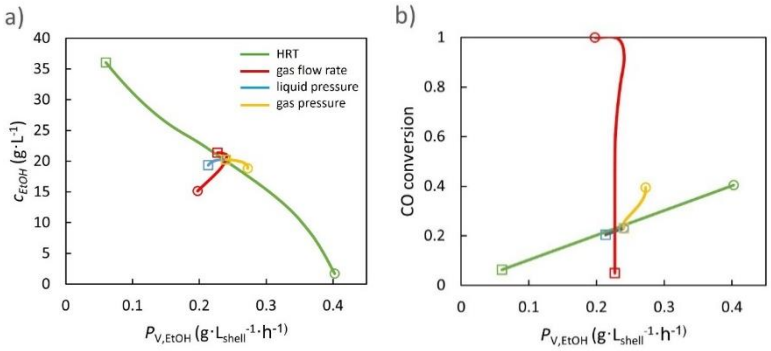

Figure 3.6 Trade-off trends within the operating ranges of the different process parameters While changing one parameter, the others were kept constant according to their base values in Table 3.3. The circles depict the lower boundary, while the squares depict the upper boundary. a) The trade-off between the volumetric ethanol productivity and the ethanol concentration. b) The trade-off between productivity and the extent of CO conversion.

Regarding HRT, there is a clear trade-off between the concentration of ethanol and the productivity. Higher productivities lead to lower concentrations and vice versa. Also, variation of HRT leads to changes of the productivity and the concentration in a very wide range, compared to the other variables. Varying the lumen gas flow rate could create a change in concentration of around 5 g L^{-1}, while the influence of the gas pressure and the liquid pressure is negligible in these cases (Figure 3.6a). Furthermore, the influence of the gas flow rate on the volumetric productivity is marginal compared to the influence of HRT on the volumetric productivity. However, the gas flow rate could be used to manipulate the extent of CO conversion in the HFM reactor. By varying the lumen gas flowrate, one can steer the extent of conversion from almost 0% to 100% (Figure 3.6b). The gas flowrate leading to the highest volumetric productivity leads to a CO conversion of about 90% (Figure 3.6b) without harming the ethanol concentration (Figure 3.6a).

Since HRT has the most prominent impact on the considered KPIs, its contribution to process performance was further evaluated (Figure 3.7).

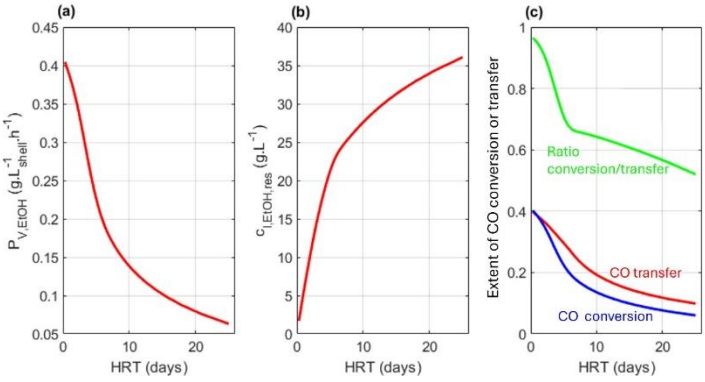

Figure 3.7 Simulated values (a) the shell volume-specific ethanol productivity, (b) the ethanol concentration in the reservoir and (c) the extents of CO conversion and transfer. The HRT was varied between 0 and 25 days and other process parameters were kept at their base values as given in Table 3.3.

The dilution rate and hence HRT influence accumulation of solutes. From Figure 3.7 it can be observed that lower HRT results in higher productivities, but low ethanol titres. At low HRT, the concentration of ethanol approaches zero, while at higher HRT (25 days) the concentrations increase to around 35 g L^{-1}. This large change in the achievable ethanol concentration range also implies that this parameter can be used to steer the effect of the ethanol inhibition on the volume-specific ethanol productivity. Experimentally, the HRT could be easily controlled to achieve the desired ethanol concentration and change the biomass productivity (if steady states can be reached). A larger extent of the feed gas is transferred through the membrane at high HRTs, and also a larger extent is converted in the biofilm, although the proportion of the transferred gas that is converted in the biofilm decreases with lower HRTs; the rest of the transferred gas leaves the system unconverted via the reservoir exits The diminishing amount of ethanol inhibition at high liquid outflow rates (high HRTs) cause that relatively much CO is consumed. The higher reaction rate leads to a higher driving force for CO transfer across the membrane.

The results predicted by our simulations were compared with experimental results reported in literature (Figure 3.8). Shen *et al.* (40) conducted syngas fermentations in a HFM bioreactors to investigate the impact of HRT on ethanol concentration and productivity. They cultivated *Clostridium carboxidivorans P7*, growing on syngas (containing 25% CO), using a gas flow rate of 300 mL min^{-1}, in a commercial microporous HFM module coupled to a reservoir (also sparged with the same gas flow). To get the same metrics as in the literature, we calculated productivity per total liquid volume rather than per shell volume, but the comparison performed still cannot serve as an experimental validation of the model results given the wide

difference between fermentation operational settings (microbial strain, HFM material, gas composition and flow, etc.). Nonetheless, the results obtained by our simulations and experimentally by Shen *et al.* (40) regarding ethanol concentration and productivity dependence on HRT are in the same order of magnitude and show the same trade-off (Figure 3.8). These similarities support the value of the model to predict trends regarding performance of syngas fermentation in HFM bioreactors. Given that the model predicted performance and maximum ethanol productivity (0.4 g $L^{-1}h^{-1}$), the bioreactor configuration is far from optimal industrial production targets (10 g $L^{-1}h^{-1}$) (103). Current industrial fermentation settings are expected to be highly optimized both regarding reactor configuration and operation and strain/medium engineering.

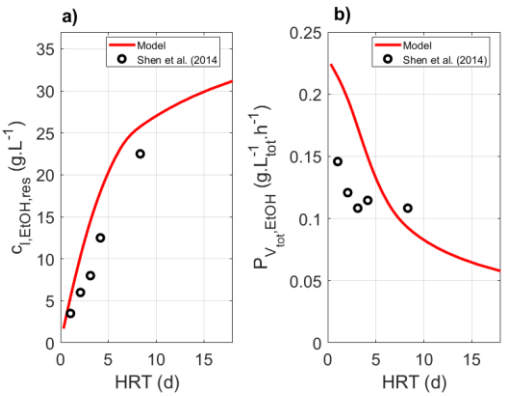

Figure 3.8 The influence of the hydraulic retention time (a) on the ethanol concentration in the reservoir and (b) on the total-volume-specific ethanol productivity. Lines are simulations using parameters from Table 3.3 and markers are experimental data from Shen *et al.* (40).

3.4. Model Evaluation

For a proper model evaluation, all the model assumptions and results should be critically analysed and, if possible and applicable, they should be validated. A systematic list of experiments that would validate model assumptions (regarding process conditions, process parameters) and results has described in detail (98). Regarding process conditions, it would be essential to verify that the liquid and gas flows distribution is homogenous, such that one fibre approximation would indeed be representative of the whole HFM module, and that the biofilm is flat and homogeneous. The most sensitive model assumptions to analyse are the reaction stoichiometry and kinetics (microbial CO uptake, CO inhibition, and ethanol inhibition), given the lack of relevant and accurate literature to describe these properties (104). For biofilm systems, additional knowledge gaps have also been identified (Chapter 2). The most sensitive process parameters to examine are the biofilm thickness, biomass density in the biofilm, and the diffusion coefficients in the

biofilm, which may be process-specific. The model allows to perform sensitivity analyses to study their impact on the results (namely on KPI) (98), and when more experimental data are available the model can be adjusted.

The diffusion of ethanol through the dense PDMS membrane and the resulting permeation to the gas phase was negligible at low gas flow rates, allowing model simplification. On the other hand, increase of gas flows might be used as strategy for *in-situ* removal of volatile products with the unused feed gas stream. This could reduce product inhibition effects and consequently increase volumetric production rates, and potentially facilitate downstream separation processes.

3.5. Conclusions

A model was successfully developed for the description and evaluation of gas fermentation and permeation processes in HFM bioreactors. The model results allow for a systematic analysis of the influence on process performance of crucial process variables including variables that are usually not measured (such as CO dissolved concentration). The results regarding abiotic and biotic simulations are comparable with literature experimental results. The predicted HFM mass transfer coefficient is promising and aligns with literature data. For the modelled process conditions, the gas mass transfer resistance in the membrane does not hinder process performance given that the reaction rate proved to be rate limiting. The model predicts an operational window where a biofilm configuration could lead to increased productivities compared with suspended biomass. The HRT governs a trade-off between ethanol concentration and production rate. An important step for advancing the model would be a better description and validation of the microbial stoichiometry and kinetics for CO consumption and ethanol formation. New insights in the metabolism could lead to enhanced predictions of ethanol concentrations, ethanol productivity and extent of CO conversion. The same holds for biofilm characteristics (thickness, biomass concentration and diffusion coefficients). Overall, the model can be used as a tool to evaluate dense HFM modules for permeation and fermentation of gaseous substrates to ethanol. It may guide experimentation and subsequent optimization. The model structure is suitable for adaptation to other products and substrate gases.

Chapter 4

The impact of broth components on mass transfer

This chapter has been published as:

Puiman, L.*, Elisiário, M. P.*, Crasborn, L. M., Wagenaar, L. E., Straathof, A. J. J., & Haringa, C. (2022). Gas mass transfer in syngas fermentation broths is enhanced by ethanol. *Biochemical Engineering Journal*, *185*, 108505

*These authors contributed equally to this work.

Abstract

In gas fermentations (using O_2, CO, H_2, CH_4 or CO_2), gas-to-liquid mass transfer is often regarded as one of the limiting processes. However, it is widely known that components in fermentation broths (e.g. salts, biomass, proteins, antifoam, and organic products such as alcohols and acids) have tremendous impact on the volumetric mass transfer coefficient K_La We studied the influence of ethanol on mass transfer in three fermentation broths derived from syngas fermentation. In demineralized water, we observed that the addition of ethanol, the expected product, increased K_La two-fold in the 0-5 $g.L^{-1}$ range, after which near-constant K_La values were obtained. In the fermentation broths, K_La was increased significantly (2-4 fold compared to water) by ethanol supplementation, and to be highly influenced by broth salinity. Our results indicate that k_La is a dynamic parameter in gas fermentation experiments and can be significantly increased due to broth components.

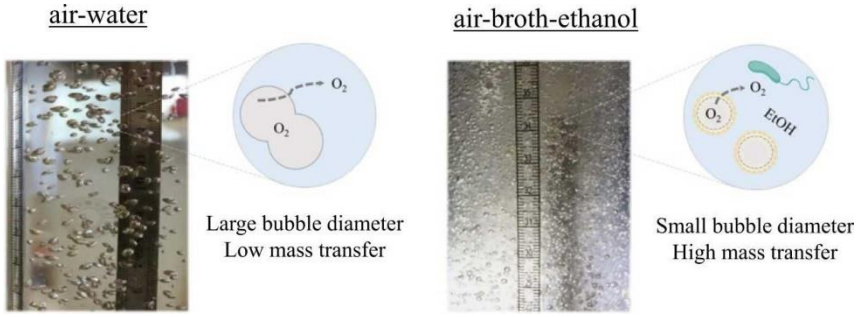

Keywords: *syngas fermentation, mass transfer, fermentation broths, ethanol, bubble column*

4. The impact of broth components on mass transfer

4.1. Introduction

Many fermentations with gaseous substrates (e.g. O_2, CO, H_2, CO_2, CH_4) are considered as promising conversion processes for a multitude of useful products (e.g. succinic acid, ethanol, butanol, hexanoic acid, lactic acid) (105 - 107). For many of these processes, poor gas-to-liquid mass transfer and low dissolved gas concentrations, have been identified as a limiting factor (108 - 111). Based upon that, a lot of research, for example in syngas fermentation, is focused on increasing the volumetric mass transfer coefficient (k_La) by developing innovative reactor configurations (23, 30, 108). Understanding of the k_La values obtained is essential in the gas fermentation field.

For a long time, it has been known that medium components and products (such as salts, acids, alcohols, surfactants, biomass and antifoam) can significantly affect k_La (18 - 21, 112). For a broad range of alcohols in water, a 5-fold increase in k_La was observed in a narrow concentration range (112), which was explained by a decrease in Sauter mean bubble diameter (d_{32}) (from 4 to 1 mm) and a two-fold increase in the gas hold-up (ε_G) (113). The presence of alcohol decreases the surface tension and stabilizes low-diameter gas bubbles, preventing repulsions and thereby inhibiting coalescence (113, 114). Similar effects on mass transfer were not only observed for alcohols, but also for organic acids, ketones and compounds like lactic acid (18, 113, 115). Changes in the gas solubility at alcohol concentrations relevant for gas fermentations were, however, expected to be negligible (116).

Similar effects were noticed for electrolytes, Lessard and Zieminski (19) observed significant coalescence inhibition (more than 90%) for different salt solutions with ionic strength above 0.3 mol.L^{-1}, resulting in increases in k_La (112). The presence of biomass, however, may decrease k_La by absorption to the bubble surface (the so-called “blocking effect”), as well as by increasing the viscosity, which stimulates coalescence (20) and reduces the diffusion coefficient (117). Dissolved proteins, however, are known to improve mass transfer as they stabilize bubbles and prevent coalescence (21). Furthermore, in air-water systems, the mass transfer coefficient (k_L) is known to be, amongst others, a function of the bubble diameter: Small bubbles (d_b around 1 mm) have a rigid surface with a k_L around 1.10^{-4} m.s^{-1}, while larger bubbles (d_b > 2 mm) have a mobile surface and k_L between 3 and 5.10^{-4} m.s^{-1} (17).

Typically, biomass, salts, proteins, products, and substrates are jointly present in fermentation broth, and might change the medium physical properties (i.e. surface tension, viscosity, density) with respect to pure water. Some empirical relations

(Table S1) predict the influence of these properties on k_La (111, 118 - 122). As these relations have been developed using air-water mixtures without taking into account biomass and salts concentrations, their validity for fermentation broths remains unclear.

The aforementioned studies on mass transfer mostly focus on mixtures with water and one compound of interest, while the joint influence of different compounds has hardly been studied. Studies with fermentation broths have only been performed to characterize the effect of the biomass concentration on k_La (20) and on d_{32} (123). In wastewater technology, however, it is common to measure aeration performance in process water (with contaminants and biomass sludge), which is often characterized with the alpha-factor, which relates the k_La in process water with clean water (124). Analyses on the joint influence of broth components in gas fermentations on mass transfer are lacking in the scientific literature, making it challenging to estimate. Knowledge on the most influential parameters and their respective ranges would be essential for accurate prediction in real fermentation broths, both during experiments and modelling. With the growing interest in fermentation and bioprocess design, understanding on the most influential parameters and their respective ranges would be essential for accurate k_La prediction.

In this study, we aim to determine mass transfer characteristics (k_La, d_{32}, ε_G, k_L) in different fermentation broths to show that there are complex interactions between the compounds present and that this has significant consequences in gas fermentation processes. Syngas fermentation is used as an example of a gas fermentation process, as it is a frequently studied process wherein mass transfer is often mentioned as a factor for poor performance (23, 108). For safety and analytical reasons, oxygen mass transfer is studied, but the same trends are expected for other gases that also have a very low solubility in water, such as CO, H_2, and CH_4. The very low concentration of dissolved O_2 is expected not to change k_La, d_{32}, ε_G, or k_L. The investigated product is ethanol, since it is a major product in the commercialized syngas fermentation process (125). First, we will determine the range wherein ethanol addition affects k_La. After that, we will study the influence of ethanol on the mass transfer characteristics in five mixtures (water, fermentation medium, and three syngas fermentation broths). The experimentally obtained k_La values will be compared with k_La values from published empirical relations, after determining the physical properties of the mixtures.

4.2. Materials and methods

4.2.1 Influence of ethanol concentration on kLa

k_La was determined in water-ethanol solutions using the dynamic absorption method (111) in a 1.5 L temperature-controlled stirred tank reactor (STR) with 1 L working volume (Applikon Biotechnology, the Netherlands). After desaturation with pure nitrogen, dissolved oxygen (DO) was measured every second with an AppliSens Dissolved Oxygen probe (Applikon Biotechnology, the Netherlands) while suppling 1 vvm of air at 800 rpm stirring rate. Experiments were performed at 20°C and 37°C and at least in trifold for all demineralized water-ethanol mixtures (0, 2.5, 5, 10, 15, 25 and 50 $g.L^{-1}$).

4.2.2 Determination of mass transfer characteristics of different mixtures

For this study several mixtures were tested in a bubble column reactor (BCR): demineralized water, mineral fermentation medium ("medium"), and three fermentation broths derived from syngas fermentation experiments (e.g. "broth-1"). A BCR was used since it enables more detailed analyses on d_b and ε_G than a STR does. The influence of ethanol on the mass transfer characteristics was determined by supplementing with the industrially obtained ethanol concentration (50 $g.L^{-1}$) (126), after experiments without supplemented ethanol. The Supplementary material provides the composition of the mineral fermentation medium as well as the media and methods for cultivation of the fermentation broths (Table S2).

Mass transfer characteristics of the different mixtures were determined in a lab-scale glass bubble column (7 cm internal diameter, 70 cm liquid height) with a multi-orifice sparger (0.6 mm orifice diameter). Experiments were performed with air at a low superficial gas flow velocity of 1.8 $mm.s^{-1}$ to ensure that flow was homogenous and that the individual bubbles could be pictured for bubble size determination. The liquid temperature was kept at 37°C. Gas hold-up was determined by measuring the ratio between aerated and unaerated volumes (127) using a ruler at the column wall. k_La was determined using the same method as described above, with the oxygen probe located 42 cm above the sparger, at least in triplicate for each mixture.

The bubble size was analysed using two methods, one for the small bubbles in mixtures with supplemented ethanol and another for larger bubbles in the mixtures without ethanol. During aeration, pictures of the small bubbles were made with a photo-optical endoscopic probe (SOPAT-VF GX 2750) (SOPAT, Germany) with the focal plane at 0.5 mm, located 47 cm above the sparger. From 600 images, between 100 and 1400 bubbles (depending on the mixture) were captured with the Hough circle detection method in the Python OpenCV package, and their diameters were calculated using a camera-specific pixel-to-mm conversion factor. As these bubbles

were spherical, the Sauter mean bubble diameter d_{32} was calculated using equation 4.1, in which $V_{b,i}$ is the volume of bubble i, $A_{b,i}$ its surface area and $d_{b,i}$ its diameter.

$$d_{32} = 6\frac{\sum_i V_{b,i}}{\sum_i A_{b,i}} = 6\frac{\frac{4}{3}\pi\sum_i\left(\frac{1}{2}d_{b,i}\right)^3}{4\pi\sum_i\left(\frac{1}{2}d_{b,i}\right)^2} \quad 4.1$$

To obtain the (equivalent) diameter of the larger bubbles, pictures were made with a CANON EOS 200D camera. A metal ruler was placed inside the column to decrease the influence of light refraction and to obtain a pixel-to-mm ratio. With image analysis software (ImageJ) d_b was measured for spherical bubbles, and for spheroidal bubbles the radii of the semi-major r_a and semi-minor axes r_c was measured to determine their eccentricity e and equivalent diameter d_{eq} (equation 4.2). Subsequently, d_{32} was calculated with the obtained (equivalent) diameters of the spherical and spheroidal bubbles using equation 4.1. The two bubble size determination methods were cross-validated using broth-4, see Figure S1 and Table S3.

$$d_{eq} = 6\frac{V_{b,i}}{A_{b,i}} = 6\frac{\frac{4}{3}\pi r_a^2 r_c}{2\pi r_a^2 + \pi\frac{r_c^2}{e}\ln\left(\frac{1+e}{1-e}\right)} \text{ with } e = \sqrt{1-\frac{r_c^2}{r_a^2}} \quad 4.2$$

After determining d_{32}, k_La and ε_G, equation 3 was used to calculate k_L.

$$k_L = \frac{k_La}{a} \text{ with } a = \frac{6\varepsilon_G}{d_{32}} \quad 4.3$$

The standard deviation σ of k_L was evaluated using classical error propagation (equation 4). The unpaired t-test with Welch's correction was used to determine statistical significance for all mass transfer characteristics.

$$\sigma_{k_L} = k_L\sqrt{\frac{\sigma_{k_La}^2}{k_La} + \frac{\sigma_a^2}{a}} \text{ with } \sigma_a = a\sqrt{\frac{\sigma_{\varepsilon_G}^2}{\varepsilon_G} + \frac{\sigma_{d_b}^2}{d_{32}}} \quad 4.4$$

4.2.3 Determination of mixture properties

After aeration in the BCR, the mixtures' physical properties were determined at 37°C. Density was measured with a benchtop density meter (DMA 5000, Anton Paar, Austria). The dynamic viscosity was determined with a Haake Viscotester 500 (Thermo Fisher Scientific, US) with NV sensor system. Dynamic surface tension was measured using a BPT Mobile tensiometer (KRÜSS Scientific, Germany), at least in duplicate.

The biomass concentration for fermentation broth-2, broth-3 and broth-4 was measured by determination of volatile suspended solids (VSS) concentration in the broth, from 150 mL broth samples (128). For broth-1, the biomass concentration was obtained by measuring its optical density at 660 nm (OD_{660}). This was converted to VSS concentration using calibration curves previously obtained during cultivation. Acetate and ethanol concentrations in filtered broth samples (0.22 µm pore size, Millipore, Millex-GV, Ireland) were determined using ultra high performance liquid chromatography (UPLC) with an Aminex HPX-87H column (BioRad, United States) at 50°C coupled to a refractive index (RI) detector RefractoMax 520 (Thermo Fisher Scientific, US), using 1.5 $mmol.L^{-1}$ aqueous phosphoric acid was used as eluent. Lastly, protein concentrations were determined with the Pierce™ BCA Protein Assay Kit (Thermo Fisher Scientific, US) according to the manufacturer recommendations. From the cultivation media composition (Table S2), ionic strength I was calculated (equation 5), from the ion concentrations c and charge z.

$$I = \frac{1}{2}\sum_i c_i z_i^2 \qquad 4.5$$

4.3. Results and Discussion

In this section, we will first present the influence of the concentration of ethanol in water on the k_La, which was determined in a stirred tank reactor (section 4.3.1). After that, detailed results for the different mixtures in a bubble column reactor are presented (section 4.3.2), which will be followed by a discussion on k_L for fermentation broths (section 4.3.3). Lastly, a comparison with empirical correlations (sections 4.3.4) is performed with the determined physical properties.

4.3.1 Influence of ethanol on k_La

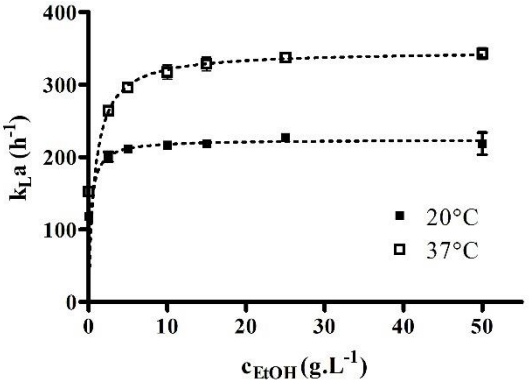

Figure 4.1 Influence of the ethanol concentration on kLa, data obtained at 20°C (filled squares) and 37°C (open squares) in the stirred tank. Error bars: standard deviations from triplicates.

The influence of the concentration of ethanol in water on k_La has been determined in a stirred tank (Figure 4.1). Sharp increases in k_La were observed in the lower concentration range, until a plateau is reached (between 5-10 $g.L^{-1}$, independent from the temperature). For both temperatures, the maximum k_La was measured around twice as large as it would be without ethanol. Visually, we observed a significant reduction in bubble size upon the addition of ethanol, explaining the increased k_La (Figure S2).

The k_La increases roughly 40% between 20 and 37°C, which corresponds with predictions for this temperature-increase (17, 129). This indicates that the temperature-increase and the ethanol addition show an independent influence on k_La. This temperature increase predominantly causes an increase in k_L (by increasing the diffusion coefficient, and reducing the kinematic viscosity (117, 130)).

In STRs with added ethanol, similar increases in k_La were observed before (131), but not with such a clear plateau formation. The plateau formation in k_La has been observed for other organic compounds in STRs (112), and was explained since a constant bubble diameter is obtained after a certain concentration range (113). Similar results on plateau formation were seen in a plunging jet contactor with propanol (132) and in an external-loop airlift reactor with methanol, ethanol and propanol (133).

The ethanol concentration range wherein the steep change in k_La values was observed (0-5 $g.L^{-1}$) corresponds to the range of achieved ethanol titres met in e.g. lab-scale syngas fermentation experiments (108, 134, 135). The rapid change in this

range indicates that k_La is a dynamic parameter and cannot be assumed constant during gas fermentation processes. This means that, for example during batch operation, different values of k_La may apply. Moreover, we recommend to obtain k_La values using representative fermentation conditions rather than using water, to compare reactor configurations (29, 30) or to determine dissolved gas concentrations (136).

Based on this, we expect that k_La differs between fermentation broths derived from syngas fermentation experiments and synthetic aqueous solutions containing some broth solutes. As more detailed analyses on d_b and ε_G can be performed in BCRs, we will use them in the upcoming sections. Due to the plateau formation by ethanol addition, we will perform experiments with the expected industrial ethanol concentration of 50 g.L^{-1} (126).

4.3.2 k_La determination in different mixtures with ethanol

Physical properties of the mixtures are shown in Table 4.1. As the fermentation broths contain only little amounts of ethanol, we supplemented the mixtures with 50 g.L^{-1} to reach the industrially relevant concentrations. From the determination of the physical properties, we saw a clear decrease in surface tension upon supplementation of ethanol. Broth-4 was not included in the dataset in the table as there was possible interference with the reducing agent during the k_La-determination (see section 4.3.5), so that the k_La and k_L could not reliably be predicted.

Table 4.1 Physical properties of the different mixtures that were analysed in this study. All properties were measured at 37°C. Provided are the liquid-phase density (ρ_L), liquid-phase viscosity, surface tension (η_L), ionic strength (I), and the concentrations of biomass (c_x), proteins (c_{prot}), total acetic acid(c_{Ac}), and ethanol (c_{EtOH}) of each mixture.

	ρ_L kg m^{-3}	η_L mPa s	σ mN m^{-1}	I mol L^{-1}	c_x g L^{-1}	c_{prot} g L^{-1}	c_{Ac} g L^{-1}	c_{EtOH} g L^{-1}
Water	992.91	0.768	69.02	N/A	N/A	N/A	0	0
Mineral medium	996.28	0.768	68.62	0.296	N/A	N/A	0	0
Broth-1	997.97	0.821	70.43	0.296	0.061	0.369	1.14	0
Broth-2	997.62	0.732	68.82	0.171	0.246	1.278	2.22	0.18
Broth-3	996.6	0.763	69.08	0.136	0.087	0.062	1.37	0.12
Water + 5% ethanol	984.36	0.827	52.2	N/A	N/A	N/A	0	49.2
Mineral medium + 5% ethanol	986.63	0.825	51.49	0.277	N/A	N/A	0	49.2
Broth-1 + 5% ethanol	989.28	0.815	51.66	0.277	0.057	0.345	1.07	49.2
Broth-2 + 5% ethanol	988.06	0.84	51.83	0.16	0.23	1.196	2.07	49.37
Broth-3 + 5% ethanol	987.93	0.759	51.76	0.127	0.082	0.058	1.28	49.32

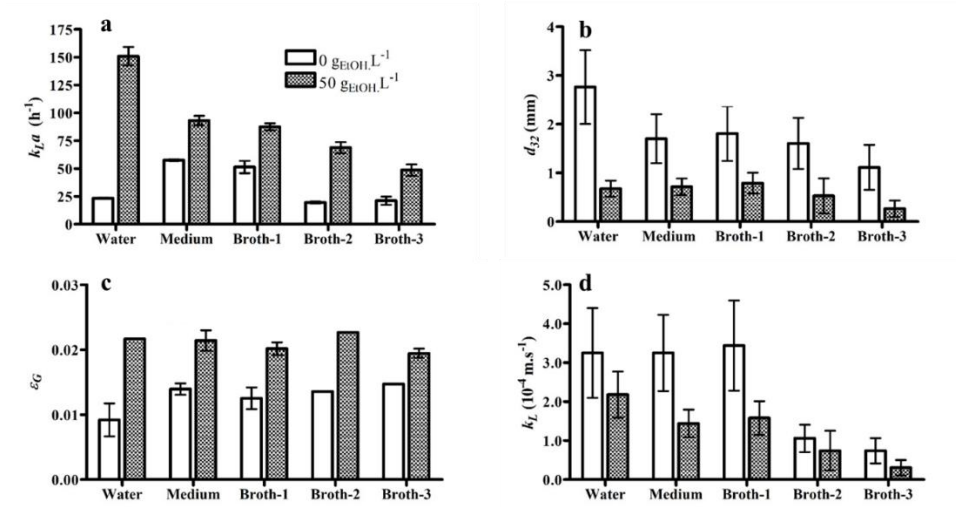

Figure 4.2 Mass transfer characteristics obtained in a bubble column ($u_{G,s}$ = 1.8 mm.s^{-1}) for different mixtures (see Table 4.1) without (white bars) and with supplemented ethanol (patterned bars). a) Volumetric mass transfer coefficient k_La, b) Sauter mean bubble diameter d_{32}, c) gas hold-up ε_G, and d) mass transfer coefficient k_L . Error bars: standard deviations between at least three measurements.

For all other mixtures, a significant increase in k_La was observed (Figure 4.2a) upon the addition of ethanol (p = 0.038). In water, a six-fold higher k_La was encountered after adding ethanol. Such increases have been obtained before with ethanol (112, 137). This is explained by the decrease in d_{32} (from 2.7 mm to 0.7 mm) and the doubling of the gas hold-up due to the addition of ethanol.

The mineral medium and broth-1 show an increased k_La compared to the demineralized water. This might be due to the broth's ionic strength (0.3 mol.L^{-1}, Table 4.1) since little coalescence was observed when ionic strength is above 0.2 mol.L^{-1} (19). This suggests that k_La might easily be increased in fermentation broths by increasing ionic strength by slightly changing the mineral medium composition.

Although ethanol decreases the bubble size and makes the bubbles more spherical and rigid (Figure S3), the beneficial effect of ethanol on k_La is less pronounced in the mineral medium than in pure water. This lower increase in k_La can be attributed to a decrease in k_L, which might be due to unresolved complex interactions between salts and ethanol in the boundary layers.

In all fermentation broths, k_La is observed to be lower than in the mineral medium. As d_{32} and ε_G remain similar in broth-1 and broth-2, the decrease in k_La is attributed to a decrease in k_L (see section 4.3.3), resulting in broth-2 and broth-3 having a similar k_La as water (without ethanol). Hence, the presence of biomass in these

broths seems to diminish the beneficial effects of salts on k_La. Supplemented ethanol causes a shrink in d_{32}, but the net increase in k_La is less pronounced than for the mineral medium. Still, the k_La values in the ethanol-rich broths are two to four times larger than the value in water without ethanol, indicating that the mass transfer properties of these broths can neither be represented with those of pure water, nor with those of water with added ethanol only.

In all cases with ethanol, a significant decrease in bubble diameter was observed (p = 0.023), as well as a narrower bubble size distribution by analysing the standard deviations (Figure 4.2b) and the bubble size distribution plots (Figure S4). This confirms that ethanol stabilizes the homogeneous flow regime (127, 138), while the coalescence inhibition causes a hold-up increase (Figure 4.2c) (114).

In the mineral medium and broths, d_{32} does not change much, except for some decrease with broth-3. This implies that the biomass, acetate and proteins have little effect on the bubble size at the observed concentrations. Broth-3 also shows a remarkably low d_{32} without ethanol, compared to the other mixtures. This effect cannot be explained, because more data are required to achieve correlation to the physical properties or the concentration of components.

The addition of ethanol significantly (p = 0.0003) increased the gas hold-up for all media (Figure 4.2c). Increases in gas hold-up were explained by coalescence inhibition: smaller bubbles rise slower, thereby increasing the gas residence time in the reactor and thus the hold-up (114). The same applies for the mineral medium and broths: salts and surface-active compounds decrease d_{32} by inhibiting coalescence and thus increase the hold-up. For more details about the underlying mechanisms, one is referred to Keitel and Onken (113) and Jamialahmadi and Müller-Steinhagen (114).

The obtained data hints at a decrease in k_L due to supplemented ethanol (Figure 4.2d), but this was not statistically significant (p = 0.10). A decrease would be explained by ethanol causing extra mass transfer resistance around the gas bubble, or by increasing surface rigidity due to the small and spherical bubbles.

4.3.3 k_L as function of biomass concentration

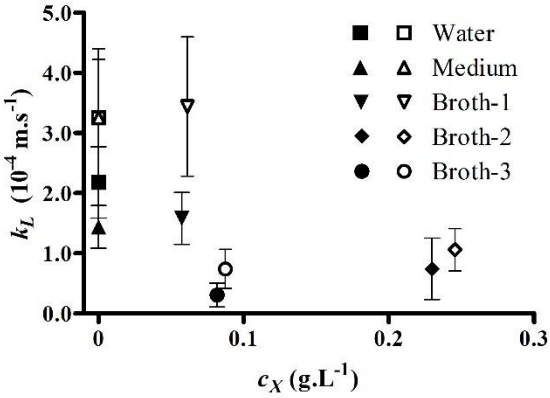

Figure 4.3 Mass transfer coefficient k_L for different values of the biomass concentration in the studied mixtures. Open symbols: mixtures without ethanol, filled: mixtures with 50 g.L^{-1} ethanol. Error bars: standard deviations.

From the different mixtures, it was observed that the fermentation broths have a lower k_L than water. This weakly correlates (Pearson's r = -0.57) with the biomass concentration in the broth (Figure 4.3). It has been argued (111) that biomass increases broth viscosity and thus decreases k_L. However, the viscosities of the measured samples are in such a narrow range that a viscosity-based k_L model cannot adequately describe these changes (139) (Figure S5). Any such reduction might be explained by a bubble surface blocking effect of the biomass, creating additional mass transfer resistance, even though direct oxygen consumption was not expected for syngas fermenting bacteria (111). We expect that there are complex interactions between the (type of) microbe, salts and nutrients in the medium, and the products, that influence the value of k_L. Unfortunately, at this moment, we are not able to provide general guidelines for prediction of k_L in fermentation broths without further experiments.

4.3.4 Comparison with empirical correlations

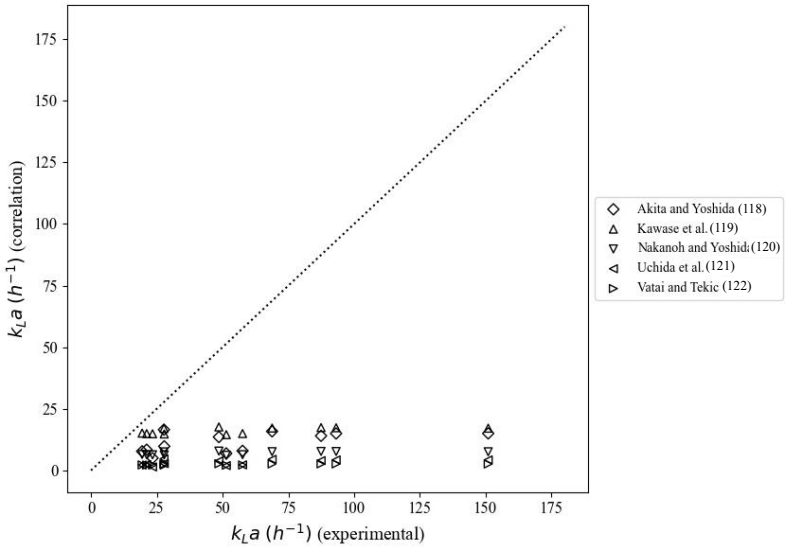

Figure 4.4 Parity plot of experimental k_La data in the different mixtures vs. the values calculated using empirical relations (118 - 122).

Empirical relations (Table S1) are often used for the prediction of k_La in bubble column fermentations (111). After determining surface tension, density, viscosity and k_L for all the different media (with and without ethanol) (Table 4.1), the k_La values were calculated using these equations (Figure 4.4). However, a large discrepancy is visible between the experimental and predicted values. These relations systematically underestimate k_La since they do not consider the influence of biomass, the salts and ethanol on the bubble properties. For example, the decrease in surface tension by ethanol has a smaller influence on k_La in the empirical relations than observed in our experiments. As we saw that variables as ionic strength, ethanol and biomass concentration are important regarding mass transfer in fermentation broths, these variables should also be part of such relationships.

4.3.5 Implications and future studies

This study shows several observations on mass transfer characteristics obtained in different liquid mixtures relevant for gas fermentations. The obtained results show that the influence of medium components is significant and should be considered in further practical and modelling work in gas fermentations. Although it is widely known that antifoam promotes coalescence (21, 111) and decreases mass transfer by creating a monolayer around the bubbles (140), and that dissolved solids (e.g.

silica) can both improve and worsen mass transfer (depending on the concentration) (141), we did not consider their presence.

To reduce the redox potential, which is required for anaerobic (syngas) fermentation, a reducing agent was added to the fermentation broths (Table S2). Reaction of oxygen and the reducing agent (sodium sulphide) might have disturbed the dynamic absorption method for k_La determination (for broth-4), such that this broth had to be left out from the aforementioned evaluation. In such a case the method might be adapted to, for example, the method proposed by Bandyopadhyay *et al.* (142). Future studies should also note that the dynamic absorption method for k_La determination has low validity at high power inputs (P/V > 1000 W.m^{-3}) (143).

Industrial syngas fermentation requires higher biomass concentrations (around 10 g.L^{-1}) (9) than the concentrations achieved in our experiments. Such high biomass concentrations are expected to influence the broth viscosity and thus the k_L. Furthermore, the used bubble column (7 cm diameter) is not representative for an industrial fermentation. To represent a large-scale bubble column, the column diameter should be more than 15 cm to exclude wall effects for mild viscous liquids (144). For an industrial-scale syngas fermentation, a significantly higher gas flow velocity can be expected. We noted that at such gas velocities, determination of d_{32} in media without ethanol would be challenging due to the regime change to slug flow. To prevent slugs, we decided to compare d_{32} and k_La at low gas flow velocities. In literature, at higher gas flow rates and in wider and higher columns, the beneficial effect of ethanol on gas hold-up (127, 138) and k_La were observed (133). Because of that, we think that in large-scale reactors the observed phenomena in this paper would still be present.

Further research is needed in order to quantitatively predict the relevant parameters (e.g. k_L, d_{32}) in order to develop more realistic mass transfer models for fermentations. Although the exact mechanism might remain unknown, structural experiments and technologies like machine learning might be used to develop algorithms for reliable prediction of mass transfer properties in fermentation broths of various compositions. Additional and more fundamental research might provide explanations on the mechanisms behind our observations (e.g. why k_La is lower in the mixture with mineral medium and ethanol compared to the water-ethanol mixture).

Although our results were only obtained with supplemented ethanol, we stress that similar phenomena were obtained with other compounds (longer alcohols, acids, ketones) (18, 112, 113). This indicates that similar deviations in mass transfer characteristics can be expected in a wide range of gas fermentations (105), e.g.

syngas fermentation (to alcohols/acids), microbial electrosynthesis (to acids) (109) as well as sugar-based fermentations (e.g. 1,4-butanediol production (145)). As there are methods available to measure mass transfer characteristics (k_La, d_{32}, ε_G, k_L, a) easily, we highly recommend to perform these experiments with realistic broths to prevent underestimation of mass transfer rates.

4.4. Conclusions

By supplementing ethanol to water, k_La sharply and significantly increases, primarily by decreasing d_{32}. This effect is also present, but weaker, in the studied syngas fermentation broths. Broth salinity (ionic strength) and biomass concentration seem to affect k_La in fermentation broth as well. Future mass transfer studies should consider the influence of broth components because literature models fail to predict their effects.

Supplementary material

Relations used for k_La determination by physical properties

Table S1. Relations used for the prediction of k_La in bubble column reactors. Constants: D_r=0.07 m, $u_{G,s}$ = 1.8 mm.s^{-1}, $D_{L,O2}$=2.1e^{-9} m^2.s^{-1}, g = 9.81 m.s^{-2}.

Dimensionless relations	**Equation**
Akita and Yoshida (118)	$(Sh)a \cdot D_r = 0.6Eo^{0.62}Ga^{0.3}Sc^{0.5}\varepsilon_G^{1.1}$
Kawase *et al.* (119)	$(Sh)a \cdot D_r = 0.452Eo^{0.6}Sc^{0.5}Fr^{0.12}Re^{1}$
Nakanoh and Yoshida (120)	$(Sh)a \cdot D_r = 0.09Eo^{0.75}Ga^{0.4}Sc^{0.5}Fr^{1}$
Uchida *et al.* (121)	$(Sh)a \cdot D_r = 0.17Eo^{0.62}Ga^{0.3}Sc^{0.5}\varepsilon_G^{1.1}$
Vatai and Tekic (122)	$(Sh)a \cdot D_r = 0.031Eo^{0.75}Ga^{0.4}Sc^{0.5}Fr^{1}$

Dimensionless numbers	**Equation**
Schmidt	$Sc = \frac{\eta_L}{\rho_L D_{L,O_2}}$
Eötvös	$Eo = \frac{\rho_L g D_r^2}{\sigma}$
Galileo	$Ga = \frac{\rho_L{}^2 g D_r^3}{\eta_L^2}$
Froude	$Fr = \frac{u_{G,s,in}}{\sqrt{gD_r}}$
Reynolds	$Re = \frac{\rho_L u_{G,s,in} D_r}{\eta_L}$
Sherwood	$Sh = \frac{k_L D_r}{D_{L,O_2}}$

Cultivation strategies and media composition

Fermentation broth 1 was effluent resulting from a CO fermentation by *Clostridium autoethanogenum* (DSM 10061) in a continuous stirred-tank reactor (CSTR). The cultivation was carried out in a 1.5 L glass jacketed chemostat (Applikon, The Netherlands) with a working volume of 1 L. The temperature was controlled at 37°C, the agitation rate was set to 500 rpm and the pH was maintained at 5.9. The bioreactor was continuously supplied with a gas phase consisting of CO (6 mL.min^{-1}) and N_2 (4 mL.min^{-1}). The sterile growth media (composition reported in Table S2) was supplied continuously at the dilution rate of 0.024 h^{-1}. The fermentation effluent was continuously sparged with 100% N_2 to maintain anaerobic conditions, kept at room temperature (~20°C) and collected anaerobically in a glass bottle during 4 days, and then used for the mass transfer experiments.

Fermentation broth 2 was the effluent resulting from CO fermentations by *C. autoethanogenum* (DSM 10061) in a custom-built rotor stator spinning disc reactor (RS-SDR) coupled to a buffer tank. The fermentation broth was cultivated in a 600 mL glass mixed buffer vessel (300 mL working volume) and recirculated though the RS-SDR (60 mL working volume), made of polymethyl methacrylate. The reactor was operated in a sequential batch mode, with a cycle time of 24 hours. Each cycle, 10 mL of fermentation broth in the buffer tank was exchanged by the same volume of fresh sterile feed medium (composition reported in Table S2). The headspace of the buffer tank (300 mL) was completely refreshed with 100% CO once a day and kept at 1.5 bar of absolute pressure. The buffer tank was placed on a heating stirring plate. The temperature was controlled between 35 and 37°C, the broth was agitated at 200 rpm with a magnetic stirrer and the pH was maintained between 5.3 and 5.8. The fermentation broth was recirculated through the RS-SDR at a recirculation liquid flow rate of 120 mL.min^{-1}. The RS-SDR operated at varying rotation speeds (100, 500, 1000 or 1500 rpm). After 72 hours of cultivation, the fermentation effluent was collected in 1 L plastic bottles and stored in the fridge (~2°C). The effluent of 8 consecutive independent fermentations was stored (during a maximum 4 weeks), mixed and then used for the mass transfer experiments.

Fermentation broth 3 was the effluent of a mixed culture converting CO into H_2 and acetate in a continuous stirred tank reactor (CSTR). The cultivation was carried out in a 500 mL chemostat with a working volume of 400 mL. The temperature was controlled at 30°C, the agitation rate was set to 800 rpm and the pH was maintained at 7.0. The bioreactor was continuously supplied with a gas phase consisting of CO (2 mL/min), N_2 (1.06 mL/min) and CO_2 (0.27 mL.min^{-1}). The sterile growth media (composition reported in Table S2) was supplied continuously to maintain the dilution rate of 0.014 h^{-1}. The fermentation effluent was collected anaerobically into

1 L serum glass bottles sealed with butyl rubber stoppers and aluminium caps, under N_2/CO_2 (80:20) headspace, at 1.4 bar of absolute pressure. The effluent was stored at room temperature (~20 °C) during 5 days, and then used in the mass transfer experiments.

Fermentation broth 4 was produced by the fermentation of CO by *C. autoethanogenum* (DSM 10061) in batch bottles. The cultivation medium (which composition is reported in Table S2) was dispersed into 1 L glass bottles (300 mL working volume) sealed with butyl rubber stoppers and aluminium caps. The headspace of each bottle (700 mL) was filled with 100% CO to a final absolute pressure of 1.5 bar, using an anaerobic gas-exchange system. The bottles were sterilized in a autoclave immediately after preparation, for 20 minutes at 121°C. Each bottle was inoculated with 1% (v/v) of exponential growing inoculum, at initial pH of 5.9 and incubated without shaking at 37°C until reaching optical density at wavelength of 660 nm (OD_{660}) of 0.2. The fermentation broth from each bottle was then collected and mixed, and used for bubble size characterization (Figure S1, Table S3).

Table S2. Media composition used for the cultivation of the fermentation broths. Media compounds concentrations are reported in g L^{-1} or mg L^{-1} (in the case of metal trace elements and vitamins).

	Mineral media	**Broth-1**	**Broth-2**	**Broth-3**	**Broth-4**
	$g.L^{-1}$	$g.L^{-1}$	$g.L^{-1}$	$g.L^{-1}$	$g.L^{-1}$
Ammonium chloride	0.9	0.9	0.3	0.3	0.3
Sodium chloride	0.9	0.9	0.3	0.3	0.3
Magnesium sulfate heptahydrate	0.2	0.2	0.1	0.03	0.03
Monopotassium phosphate	0.7	0.7	0.408	0.408	0.408
Dipotassium phosphate	1.5	1.5	-	-	-
Sodium phosphate dibasic dihydrate	-	-	0.534	-	-
Calcium chloride dihydrate	0.02	0.02	0.11	0.11	0.11
Sodium bicarbonate	-	-	4.0	4.0	4.0
Resazurin sodium salt	0.0005	0.0005	0.0005	0.0005	0.0005
Yeast extract	0.5	0.5	1.0	0.1	0.1
Triptone	-	-	1.0	-	-
L-cysteine hydrochloride monohydrate	-	0.75	0.5	0.1	0.1
Sodium sulfide nonahydrate	-	-	0.24	-	0.24
Metal trace elements	$mg.L^{-1}$	$mg.L^{-1}$	$mg.L^{-1}$	$mg.L^{-1}$	$mg.L^{-1}$
Iron(II) chloride tetrahydrate	1.50	1.50	1.50	1.50	1.50
Iron(III) chloride hexahydrate	2.50	2.50	-	-	-
Zinc chloride	0.07	0.07	0.07	0.07	0.07
Manganese(II) chloride tetrahydrate	0.10	0.10	0.10	0.10	0.10
Boric acid	0.006	0.006	0.062	0.062	0.062
Cobalt(II) chloride hexahydrate	0.190	0.19	0.119	0.119	0.119
Copper(II) chloride dihydrate	0.002	0.002	0.017	0.017	0.017
Nickel(II) chloride hexahydrate	0.024	0.024	0.024	0.024	0.024
Sodium molybdate dihydrate	0.040	0.040	0.024	0.024	0.024
Sodium selenite	0.004	0.004	0.017	0.017	0.017
Sodium tungstate dihydrate	0.200	0.200	0.033	0.033	0.033
Vitamins	$mg.L^{-1}$	$mg.L^{-1}$	$mg.L^{-1}$	$mg.L^{-1}$	$mg.L^{-1}$
Biotin	0.02	0.02	0.02	0.02	0.02
Nicotinamide	0.20	0.20	0.20	0.20	0.20
P-aminobenzoic acid	0.10	0.10	0.10	0.10	0.10
Thiamine	0.20	0.20	0.20	0.20	0.20
Pantothenic acid	0.10	0.10	0.10	0.10	0.10
Pyridoxamine	0.50	0.50	0.50	0.50	0.50
Cyanocobalamin	0.10	0.10	0.10	0.10	0.10
Riboflavin	0.10	0.10	0.10	0.10	0.10

Bubble size method cross-validation

With broth-4, and in the same conditions as used with the other mixtures, bubbles were obtained that could be analysed using both methods (the one designed for the small bubbles with the photo-optical probe and the one for the larger bubbles with the CANON EOS 200D camera). The resulting bubble size distributions are given in Figure S1. As can be seen, the resulting BSDs are very similar, with the exception that the method used for the small bubbles is not able to capture bubbles bigger than 1.3 mm and that it has a slightly higher probability peak between 0.5 - 0.75 mm. As the obtained average bubble diameters, Sauter mean bubble diameters and standard deviations (Table S3) were similar, it was concluded that both methods could be used for bubble size comparison purposes.

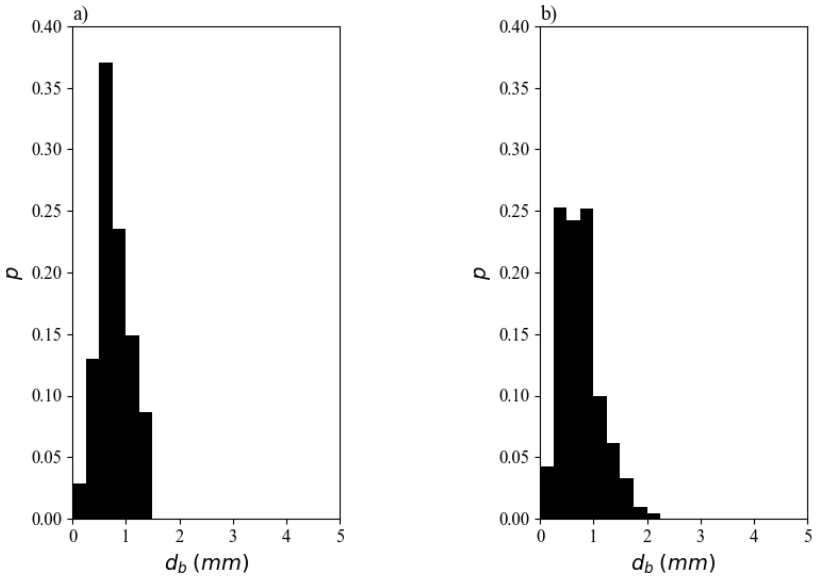

Figure S1. Bubble size distributions obtained using the method designed for a) the smaller bubbles, and b) the larger bubbles.

Table S3. Bubble diameter method cross-validation. For broth-4, the average bubble diameters, Sauter mean bubble diameter, and the standard deviation of the bubble diameter were determined via both methods.

	SOPAT method	**CANON method**
$\overline{d_b}$ (mm)	0.78	0.77
d_{32} (mm)	0.98	1.11
σ_{d_b} (mm)	0.29	0.36

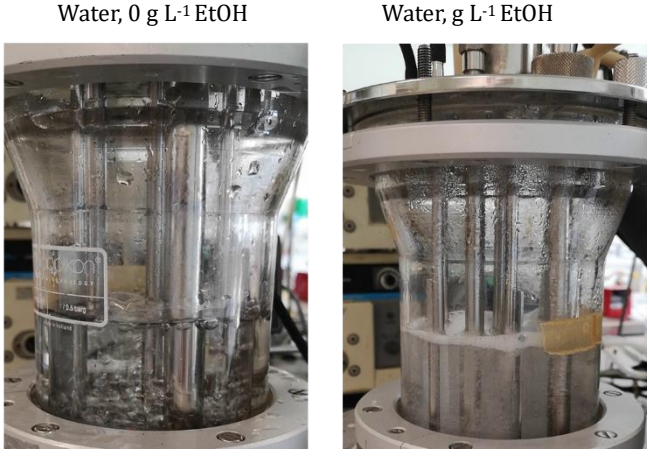

Figure S2. Photographs of bubbles in the STR with and without supplemented ethanol.

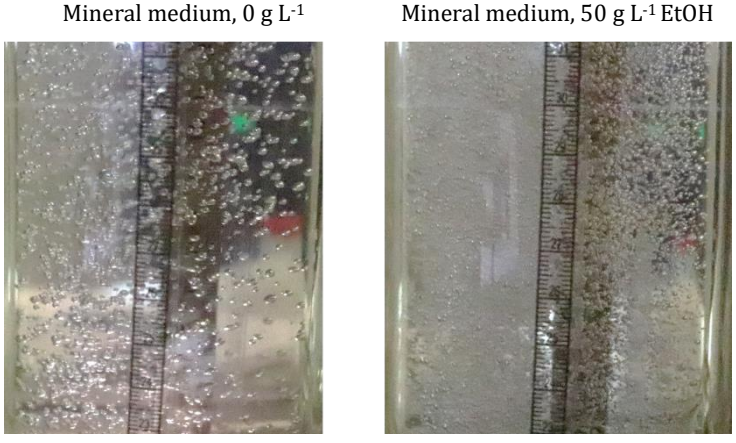

Figure S3. Photographs of bubbles in the BCR with mineral medium with and without supplemented ethanol. In the solution without ethanol, small but less stable, wobbling, bubbles were observed, while the ethanol leads to rigid, spherical, bubbles.

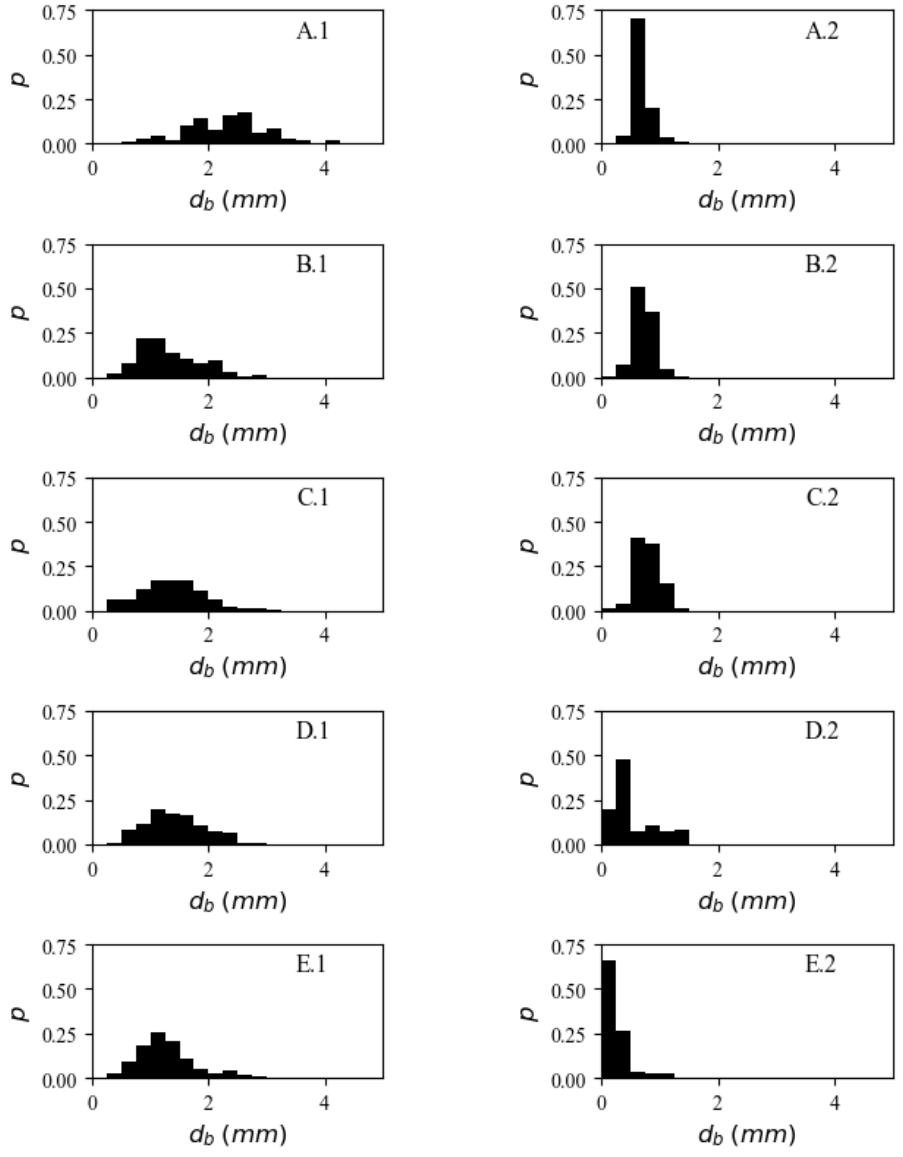

Figure S4. Bubble size distributions obtained for the different mixtures. A: water, B: mineral medium, C: broth-1, D: broth-2, E: broth-3, 1: without ethanol, 2: with ethanol.

k_L as a function of the biomass concentration

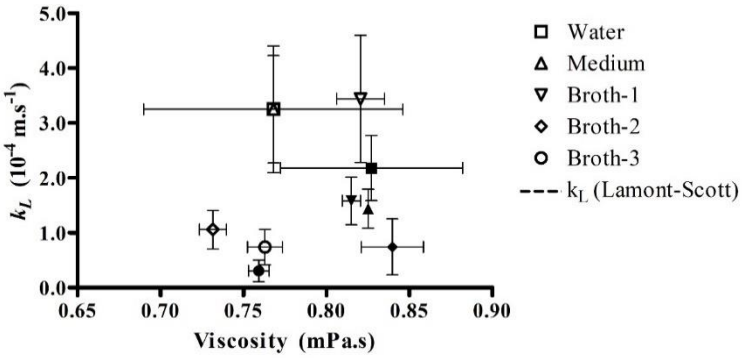

Figure S5. k_L as a function of the mixture viscosity. Error bars: standard deviations. Filled symbols: mixtures with ethanol, empty symbols: mixtures without ethanol.

Chapter 5

The impact of mass transfer and fermentation variables on the metabolism of acetogenic bacteria

This chapter has been published as:

Elisiário, M. P., Van Hecke, W., De Wever, H., Noorman, H., & Straathof, A. J. J.(2023). Acetic acid, growth rate, and mass transfer govern shifts in CO metabolism of *Clostridium autoethanogenum*. *Applied Microbiology and Biotechnology*, *107*(17), 5329-5340.

Abstract

Syngas fermentation is a leading microbial process for the conversion of carbon monoxide, carbon dioxide and hydrogen to valuable biochemicals. *Clostridium autoethanogenum* stands as a model organism for this process, showcasing its ability to convert syngas into ethanol industrially with simultaneous fixation of carbon and reduction of greenhouse gas emissions. A deep understanding the metabolism of this microorganism and the influence of operational conditions on fermentation performance is key to advance the technology and enhancement of production yields. In this work, we studied the individual impact of acetic acid concentration, growth rate and mass transfer rate on metabolic shifts, product titres and rates in CO fermentation by *C. autoethanogenum*. Through continuous fermentations performed at a low mass transfer rate, we measured the production of formate in addition to acetate and ethanol. We hypothesise that low mass transfer results in low CO concentrations, leading to reduced activity of the Wood–Ljungdahl pathway and a bottleneck in formate conversion, thereby resulting in the accumulation of formate. The supplementation of the medium with exogenous acetate revealed that undissociated acetic acid concentration increases and governs ethanol yield and production rates, assumedly to counteract the inhibition by undissociated acetic acid. Since acetic acid concentration is determined by growth rate (via dilution rate), mass transfer rate and working pH, these variables jointly determine ethanol production rates. These findings have significant implications for process optimization as targeting an optimal undissociated acetic acid concentration can shift metabolism towards ethanol production.

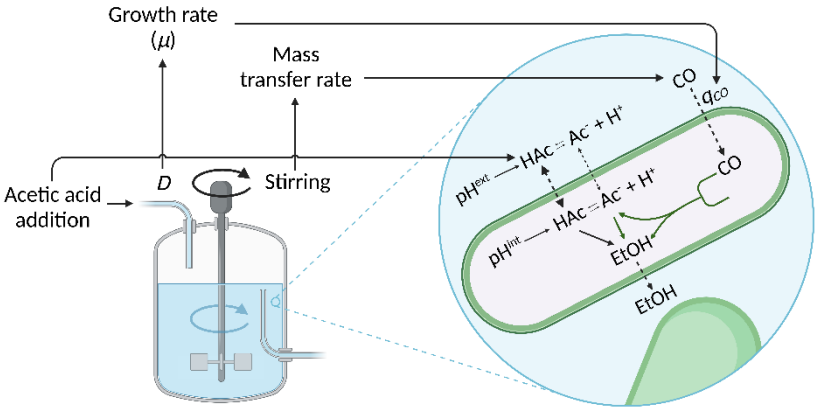

Keywords: *CO metabolism; Clostridium autoethanogenum; acetic acid concentration; growth rate, mass transfer*

5. The impact of mass transfer and fermentation variables on the metabolism of acetogenic bacteria

5.1. Introduction

Syngas fermentation is a microbial process through which acetogenic microorganisms convert carbon monoxide (CO), carbon dioxide (CO_2) and hydrogen (H_2) into added-value biochemical compounds (3, 11). This technology offers a ground-breaking option for green-house gas emission reduction and sustainable biochemical production (1). The acetogen *Clostridium autoethanogenum* is a syngas fermenting model organism, which can natively produce ethanol (EtOH), acetate (Ac), 2,3-butanediol (BDO) and lactate (126); therefore it has been vastly studied and is employed for industrial production of ethanol (4, 7, 146). This microorganism uses the Wood–Ljungdahl pathway (WLP) for reductive synthesis of acetyl-CoA from CO_2, CO, and H_2 (Figure 5.1).

Understanding the metabolism of this microorganism and the impact of fermentation conditions on fermentation performance is key to advance the technology. Among other factors, the gas-to-liquid mass transfer rate has a very pertinent role, as it directly affects the substrate availability to the microorganism (147). For example, the substrate uptake rate depends on the dissolved gas concentration. Different substrate gas-to-liquid mass transfer rates can be imposed, for example by changing the agitation rate in stirred tank reactors or the superficial gas velocity in stirred tank and bubble column reactors (23, 147).

In addition to the gas-to-liquid mass transfer rate, the biomass-specific microbial growth rate, μ, also has a crucial role in the fermentation performance (148). In chemostat fermentations, the biomass-specific growth rate μ is equivalent to and imposed by the operational dilution rate D, up to the critical dilution rate. The growth rate influences the product concentration and substrate to product yields. Increasing the growth rate might also change product distribution because the microbe may shift its metabolism (135, 148) to cope with higher energy requirements for biomass formation. Process rates are affected, which has an impact on process economics.

The combined influence of growth rate and mass transfer rate also determines the production rate and concentration of total acetate (anion plus undissociated species). Simultaneously, the extracellular pH determines the extracellular ratio of acetate anion to undissociated acetic acid, which can differ from the intracellular ratio (103) since the intracellular pH is metabolically controlled at about 6.0 (149) and the external pH can be imposed.

Since many factors determine the syngas fermentation performance (microorganism, pH, medium composition, gas flow, gas composition, dilution rate, etc.) and literature covers only part of the operational window, understanding of the impact of operational settings on the fermentation performance is still incomplete.

In this work, we will obtain and characterise chemostat fermentations of *C. autoethanogenum* grown on CO as sole carbon and energy source, to simplify the system. We will investigate the individual effects of CO mass transfer rate (100 or 500 rpm agitation in a stirred bioreactor), growth rate (~0.008 h^{-1} to ~0.04 h^{-1} dilution rate), and acetate concentration on products distribution, titres, rates and yields. An assessment will be made of how the individual effects jointly affect the observed fermentation performance and shifts in the metabolic network Figure 5.1. Previous studies have hypothesized on the role of acetic acid as a critical factor in increasing ethanol production in syngas fermentation (103, 150). We will further provide experimental evidence to support this hypothesis for *C. autoethanogenum*, by analysing experiments supplementing exogenous acetic acid to fermentation while keeping other fermentation conditions constant. Furthermore, we will conduct a comprehensive analysis and comparison of literature experimental results to clarify the role of acetic acid concentration on ethanol yield.

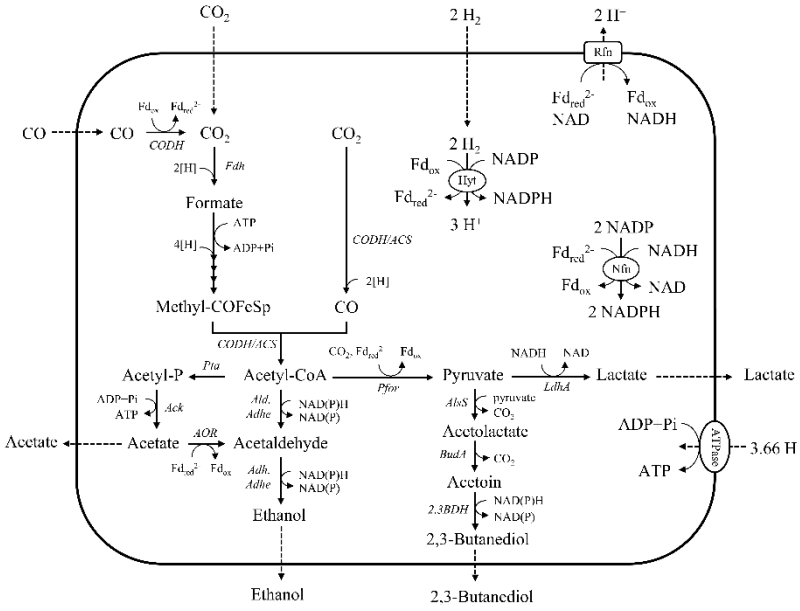

Figure 5.1 Simplified overview of carbon fixation through WLP and autotrophic product formation in *C. autoethanogenum*, including key enzymes and product excretion. Figure adapted from Liew et. al (1) and Liew et. al (151), wherein abbreviations are depicted.

5.2. Materials and methods

5.2.1 Microorganism, growth medium and inoculum cultivation

C. autoethanogenum (DSM 10061) from the DSMZ strain collection (Braunschweig, Germany) was used in all fermentations and stored as glycerol stock at -80 °C. Pre-cultures were cultivated in batch operation in anaerobic bottles capped with rubber stoppers and aluminium caps (50 mL working volume), at 37 °C without agitation, after inoculation in a 1:50 ratio (v/v). The glycerol stock cells were first revived in modified YTF (Yeast extract-Tryptone-Fructose) medium (containing per litre: 10 g Bacto™ Yeast Extract, 16 g tryptone, 4 g NaCl, 4 mg $Cl_2Fe \cdot 4\ H_2O$, 0.5 mg resazurin sodium salt and 0.75 g L-cysteine · HCl · H_2O dissolved in demineralized water) adjusted to pH 6.2 with 2 mol L^{-1} HCl and under 100% N_2 headspace (1.5 atm). Once this culture reached exponential growth, the cells were propagated and further cultivated under 100% CO headspace (1.5 atm) in anaerobic bottles with the feed medium. Once exponentially growing, this culture was used as inoculum for bioreactor experiments, in a 1:20 v/v ratio. The feed medium contained per litre: 0.9 g NH_4Cl, 0.9 g NaCl, 0.2 g $MgSO_4 \cdot 7\ H_2O$, 0.7 g KH_2PO_4, 1.5 g K_2HPO_4, 0.02 g $CaCl_2$, 0.5 mg resazurin sodium salt, 0.5 g Bacto™ Yeast Extract , and 0.75 g L-cysteine · HCl · H_2O dissolved in demineralized water; and it was supplemented with the following metal trace-elements per litre of medium: 1.5 mg $FeCl_2 \cdot 4\ H_2O$, 2.5 mg $FeCl_3 \cdot 6\ H_2O$, 0.07 mg $ZnCl_2$, 0.1 mg $MnCl_2 \cdot 4\ H_2O$, 0.006 mg H_3BO_3, 0.19 mg $CoCl_2 \cdot 6\ H_2O$, 0.002 mg $CuCl_2 \cdot 2\ H_2O$, 0.024 mg $NiCl_2 \cdot 6\ H_2O$ and 0.04 mg $Na_2MoO_4 \cdot 2\ H_2O$, 0.004 mg Na_2SeO_3 and 0.2 mg $Na_2WO_4 \cdot 2\ H_2O$; and the following vitamins per litre of medium: 0.02 mg biotin, 0.2 mg nicotinamide, 0.1 mg p-aminobenzoic acid, 0.2 mg thiamine · HCl, 0.1 mg pantothenic acid, 0.5 mg pyridoxamine, 0.1 mg cyanocobalamin and 0.1 mg riboflavin. The pH of the feed medium was adjusted to 6.2 with 2 mol L^{-1} HCl. Both media were sterilized by autoclaving at 121 °C during 20 min. The yeast extract, vitamins and cysteine were added to the media as sterile concentrated stock solutions after autoclavation. The feed medium for the steady-state fermentation VI was additionally supplemented with a concentrated sterile acetic acid solution to reach the concentration mentioned in Table 5.1.

5.2.2 Bioreactor operation

Continuous fermentations for cultivation of *C. autoethanogenum* were performed in a 1.5 L glass jacketed stirred tank bioreactor (Applikon, Delft, The Netherlands). Three baffles and two Rushton impellers (46 mm diameter) were installed; the impellers were placed at 33% and 66% of the liquid height. The fermentation pH, temperature, agitation and mass flow) were controlled (In-Control, Applikon, The Netherlands). Conditions were strictly anaerobic at 37 °C. Off-gas was condensed at 4 °C, such that water and ethanol loss was insignificant. The pH of the fermentation

was maintained at 5.90 ± 0.05 by addition of 2 mol L^{-1} NaOH via a peristaltic pump. The start-up, inoculation and batch operation of the bioreactor were performed as reported by Diender *et al.* (152). Peristaltic pumps (Masterflex, Gelsenkirchen, Germany) were used for continuous supply of feed medium and removal of effluent, applying different dilution rates Table 5.1. The bioreactor was continuously supplied with a gas phase of 10 mL min^{-1} (on basis of standard temperature and pressure) consisting of CO and N_2 (composition in Table 5.1). Variable stirring rates were applied. Effluent samples of 2 mL were analysed daily for biomass concentration using optical density. Each sample supernatant was analysed for product concentration using ultra performance liquid chromatography (UPLC). Off-gas composition was continuously monitored. The steady-state (SSt) results were obtained from three independent chemostat runs and were reported once concentrations were constant for at least 3 working volume changes.

Table 5.1 Operational conditions of fermentations at steady-steady.

Steady-State	I	II	III	IV	V	VI
Working volume (L)	0.9	0.9	1.0	1.0	1.0	1.0
Stirring rate (rpm)	100	100	500	500	500	500
Inlet CO concentration (%)	40	40	50	50	50	50
Dilution rate (h^{-1})	0.0081 ±0.0004	0.025 ±0.001	0.0088 ±0.0004	0.024 ±0.001	0.039 ±0.002	0.040 ±0.002
Total acetate concentration in the feed media (g L^{-1})	0	0	0	0	0	10.15 ±0.11

5.2.3 Analytical techniques

Optical density of broth was measured daily at 660 nm (OD_{660}). When constant, the biomass concentration was measured (at least in triplicate) by determination of the volatile suspended solids (VSS) concentration in the broth (153), from 150 mL broth samples collected continuously and anaerobically from the effluent of the bioreactor. Acetate, ethanol, 2,3-butanediol and formate concentrations in filtered broth samples (0.22 µm pore size, Millipore, Millex-GV, MA, USA) were determined using ultra high performance liquid chromatography (UPLC) with an Aminex HPX-87 H column (BioRad, CA, USA) and 1.5 mmol L^{-1} phosphoric acid as eluent at 50 °C with RI detection (RefractoMax 520, Thermo Fisher Scientific, MA, USA).

The bioreactor exhaust gas was continuously diluted 1:10 (v/v) with pure nitrogen gas to obtain the minimum flow required for gas analysis (Rosemount™ X-STREAM XEGP, Emerson, MO, USA). This custom-built analyser was equipped with a nondispersive infrared (NDIR) sensors for CO and CO_2 measurement and a thermal conductivity detector (TCD) for H_2 measurement.

5.2.4 Quantification of fermentation data

Production rates

Production rates, R_i (mmol h^{-1}) were quantified for analysis of fermentation performance. The off-gas flow rate, $F_n^{G,out}$, was calculated using an N_2 (inert) gas mass balance with its concentrations measured in the gas inlet and outlet. The production rates were calculated from compound mass balances, taking into account gas phase inlet and outlet molar fractions, x_i^G, and molar flow rates, F_n^G, for gaseous products (CO_2, CO and H_2) - equation 5.1 - and considering liquid outlet product concentration, $C_i^{L,out}$, and volumetric flow rate, F_L^{out}, for aqueous products (Ac, EtOH, formate and biomass) - equation 5.2.

$$R_i = x_i^{G,out} F_n^{G,out} - x_i^{G,n} F_n^{G,in} \quad 5.1$$

$$R_i = C_i^{L,out} F_L^{out} \quad 5.2$$

The biomass specific production rates q_i (mmol g_X^{-1} h^{-1}) were calculated from $R_{i,}$ liquid working volume, $V_{L,}$ and biomass concentration c_X using equation 5.3.

$$q_i = \frac{R_i}{c_X . V_L} \quad 5.3$$

5.2.5 Carbon and electron balances

Fermentation data analysis and reconciliation was performed using carbon and electron balances.

Carbon recoveries were calculated from production rate R_i (mol h^{-1}) per compound i (positive or negative), with its number of carbon atoms $n_{C,i}$ (mol_C mol_i^{-1}), see equation 5.4. Electron recoveries were calculated from R_i and the degree of reduction γ_i (mol_e mol_i^{-1}), see equation 5.5. The reference degrees of reduction were: C = 4, H = 1, N = -3, O = -2, ($^+$) = -1 and ($^-$) = 1. For these calculations, CO was considered to be the sole carbon source and electron donor. The biomass (X) composition was assumed to be $CH_{1.8}O_{0.5}N_{0.2}$ (154), resulting in 24.6 mol_x g_x^{-1}.

$$C_{rec} = \frac{\sum_i^n R_i . n_{C,i}}{-R_{CO} . n_{C,CO}};\ i = \{CO_2, \text{Ac, EtOH, BDO, formate, X}\} \quad 5.4$$

$$e_{rec} = \frac{\sum_i^n R_i . \gamma_i}{-R_{CO} . \gamma_{CO}};\ i = \{H_2, \text{Ac, EtOH, BDO, formate, X}\} \quad 5.5$$

5.3. Results

5.3.1 Comparison of different mass transfer rates

We compared the impact of agitation rate (100 or 500 rpm) at two fixed growth rates (~0.009 h^{-1} and ~0.024 h^{-1}; Steady States I to IV – in Table 5.1). This 5× rise in agitation speed corresponds to a 125× increase in the power input per volume (P/V), considering properly operating impellers in the turbulent flow regime and for coalescing broth. Subsequently, the corresponding volumetric mass transfer coefficient is expected to increase 6 to 7 times, according to van't Riet (1979), and hence the CO transfer capacity as well. The observed mass transfer rate of CO, and the associated CO consumption rate were expected to increase by such a factor only in case of mass transfer limitation occurring at either stirring rate. Higher agitation indeed led to an increase of CO consumption from about 2 mmol L^{-1} h^{-1} (estimated from production rates and catabolic stoichiometries) to 10 mmol L^{-1} h^{-1} (measured experimentally), which indicates mass transfer limitation at these conditions.

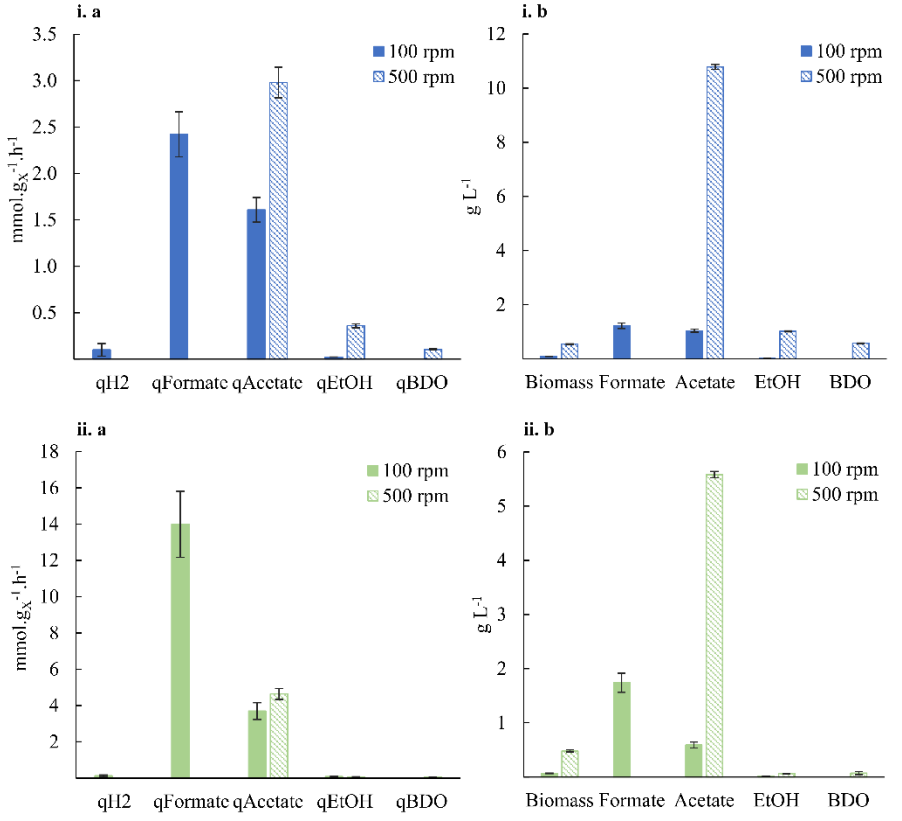

Figure 5.2 Biomass specific production rates (a) and product concentrations (b) for steady-state fermentations grown at ~0.009 h^{-1} (i) and ~0.024 h^{-1} (ii).

For growth rates of ~0.009 and ~0.024 h^{-1} the biomass concentration increased 6 and 7 times, respectively.

Figure 5.2 shows that the fermentations at 500 rpm led to the expected products (acetate, ethanol and 2,3-butanediol), with relatively high titres and biomass-specific production rates for acetate and ethanol. However, for the fermentations at 100 rpm, production of formate was substantial (14.6% and 41.4% of the converted carbon, for SSt I and II, respectively).

In Figure 5.3, we propose a combination of reactions that allows the microorganism to gain some adenosine triphosphate (ATP) from CO conversion into formate (0.14 mol_{ATP}/mol_{CO}), in case no ATP is required for formate export. The yield of ATP is significantly higher (0.375 mol_{ATP}/mol_{CO}) if acetate would be produced (155). A reason for the organism to excrete formate instead of converting it into acetate could be severe limitation of CO, of which a second molecule is required per acetyl-CoA and hence acetate (see Figure 5.1). As explained before, at 100 rpm agitation rate, mass transfer limitation is severe, so dissolved CO concentrations can be assumed to be very low, but quantification would require specific equipment (156) or methods for reliable k_La determination in the presence of broth components (Chapter 4).

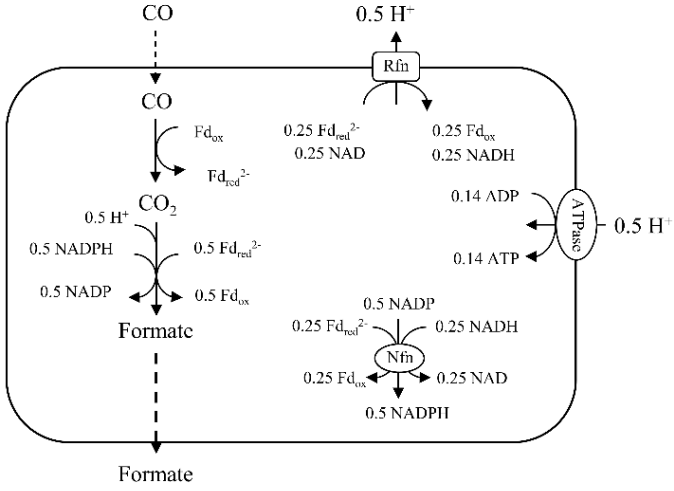

Figure 5.3 Schematic overview of the proposed pathway for CO conversion to formate with ATP production in *C. autoethanogenum*.

5.3.2 Comparison of different growth rates

At fixed agitation rate and volumetric CO supply rate, we tested different growth rates by changing the dilution rate accordingly (Steady states III, IV and V – Table 5.1). For these experiments, correct gas measurements were available, and the carbon and electron recoveries indicate highly consistent data. Namely, for μ = 0.009, 0.024 and 0.04 h^{-1}, carbon recoveries (equation 5.4) were 95 ± 2%, 94 ± 1% and 98 ± 1%, respectively, and electron recoveries (equation 5.5) were 95 ± 2%, 99 ± 2% and 99 ± 5%, respectively. Figure 5.4 shows the carbon distribution, indicating acetate and CO_2 as main products.

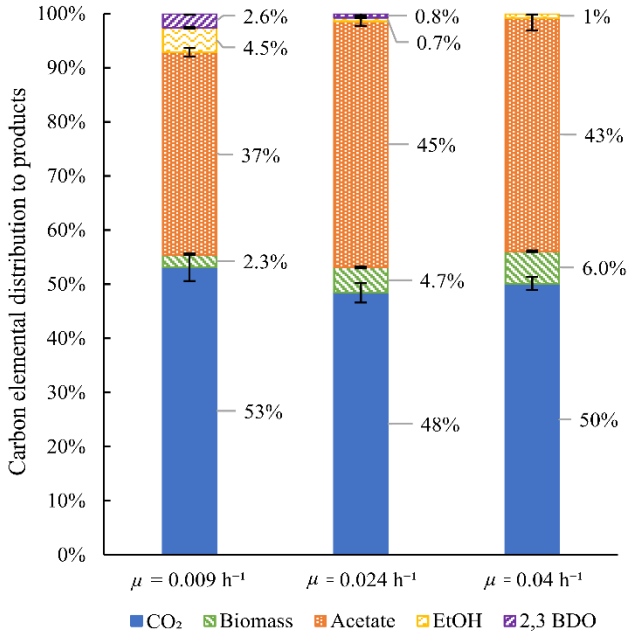

Figure 5.4 Carbon distribution from CO to products in steady state fermentations at 500 rpm stirring rate. Carbon recoveries were normalized to 100% to facilitate comparison of carbon distributions between different conditions.

As expected in a substrate limited regime, an increase of μ resulted in an linear increase of $-q_{CO}$ as shown in Figure 5.5. The higher $-q_{CO}$ value correlates with an increase in q_{Ac} and q_{CO2} as the catabolic reaction to acetate and CO_2 generates most ATP for biomass production. On the other hand, q_{EtOH} and q_{BDO} generally decreased with increasing μ. Our results also show that, at the studied fermentation settings, faster growth rates do not result in increased production rates of the more reduced products (ethanol and BDO). This is supported Figure 5.5c, where an increase of μ leads to lower ethanol and BDO concentrations. Also, the acetate concentration in broth decreases.

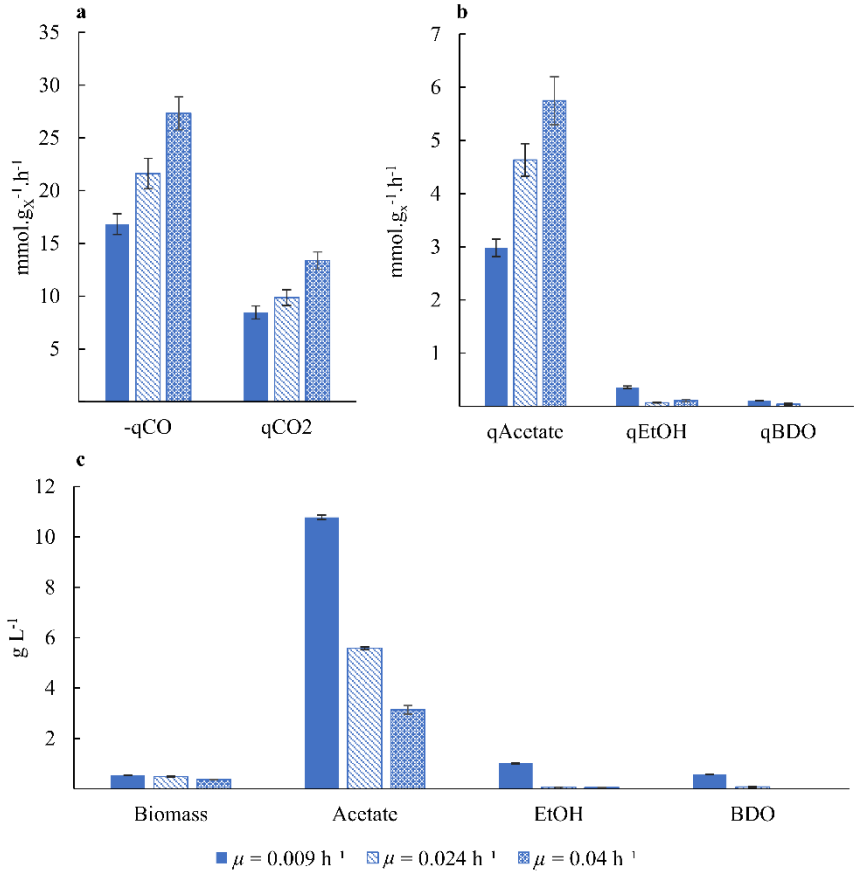

Figure 5.5 Continuous fermentation of *C. autoethanogenum* grown at 500 rpm stirring rate (Steady states III-IV-V corresponding to μ = 0.009 - 0.024 - 0.04 h^{-1}, respectively). a) and b) Biomass-specific production rates. c) Product concentrations.

5.3.3 Influence of acetate addition

For μ = 0.04 h^{-1} at 500 rpm agitation rate, the impact of extracellular acetate (and consequently undissociated acetic acid) on ethanol yield and productivity was studied by supplementing acetate to feed medium at fixed pH. The operating conditions for the obtained Steady States V and VI are given in Table 5.1 and the results are compared in Table 5.2.

For SSt VI, q_{Ac} was significantly lower than for SSt V, where total acetate concentration (resulting only from microbial production) was much lower . On the other hand, q_{EtOH} and yield of ethanol on CO, $Y_{EtOH/CO}$, increased both almost 10 fold at the increased acetate concentration. This coincided with an increase of 13.5% in $-q_{CO}$ and 22.4% in q_{CO2}, and a decrease of 27.8% in biomass concentration. BDO production was not measured upon the addition of acetate to the feed medium.

Table 5.2 Comparison of steady-state conditions and conversion between experiments with (SSt VI) and without (SSt V) acetate in the feed medium.

Steady-state fermentation	V	VI
Volume-specific acetate feed rate (g L^{-1} h^{-1})	0	0.408 ± 0.004
Growth rate (h^{-1})	0.039 ±0.002	0.040 ±0.002
Biomass concentration (g L^{-1})	0.36 ± 0.01	0.26 ± 0.01
Acetate concentration (g L^{-1})	3.13 ± 0.17	11.38 ± 0.11[a]
EtOH concentration (g L^{-1})	0.045 ± 0.009	0.318 ± 0.006
BDO concentration (g L^{-1})	0	0
q_{CO} (mmol g_x L^{-1})	-27.3 ± 1.6	-31 ± 2
q_{CO2} (mmol g_x L^{-1})	13.4 ± 0.8	16.4 ± 1.6
q_{Ac} (mmol g_x L^{-1})	5.8 ± 0.5	3.2 ± 0.3
q_{EtOH} (mmol g_x L^{-1})	0.11 ± 0.02	1.05 ± 0.07
$Y_{EtOH/CO}$ (mol_{EtOH} mol_{CO}^{-1})	0.0039 ± 0.0008	0.0340 ± 0.0009

[a] Substracting the added acetate leads to 1.23 ± 0.11 g L^{-1} produced acetate.

5.4. Discussion

5.4.1 Acetic acid increases ethanol yield on CO

The maximum amount of ATP produced for the catabolic conversion of CO to acetate and to ethanol is given by (155, 157):

$$4\,CO + 2\,H_2O \rightarrow Ac + 2\,CO_2 + 1.5\,ATP \qquad 5.6$$

$$6\,CO + 3\,H_2O \rightarrow EtOH + 4\,CO_2 + 2.1\,ATP \qquad 5.7$$

Per converted CO, more ATP is produced in case of acetate than in case of ethanol production. Therefore, acetate is the main product if CO is limiting, but still sufficiently available to prevent formate production. However, like Diender (158), we found that addition to acetate to the feed resulted in decreased acetate production, increased volumetric ethanol production rates, and decreased biomass concentrations. Toxicity of undissociated acetic acid to the microorganism was proposed (158). Similar results on ethanol productivity have been obtained by others with other microbial strains or other gas compositions (159 - 161).

The undissociated acetic acid concentration depends on pH and measured total acetate concentration (dissociated plus undissociated).

Figure 5.6 compares our results with literature data from CO fermentations by *C. autoethanogenum*. Despite different fermentation conditions among studies, the general trend is that ethanol yield on CO increases with increasing extracellular acetic acid concentration until a plateau is reached. While the maximum catabolic yield is 0.17 mol_{EtOH} mol_{CO}^{-1} according to equation 5.7, the maximum experimental yields reported are close to 0.090 mol_{EtOH} mol_{CO}^{-1} for acetic acid concentrations higher than 25 mmol L^{-1}.

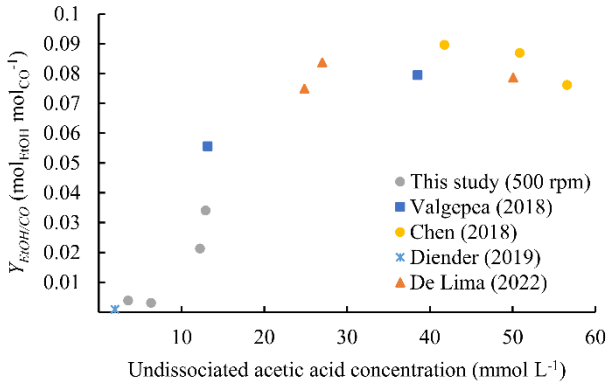

Figure 5.6 Ethanol yield on CO for different continuous fermentations of *C. autoethanogenum* grown on CO (148, 152, 170, 171) as function of the extracellular acetic acid concentration, which was calculated from the concentration of total acetate and pH at steady state.

At extracellular pH around 6.0, a small part of total acetate is protonated. The higher the extracellular total acetate concentration or the lower the pH, the higher is the resulting undissociated acetic acid concentration. Acetic acid has a significantly higher permeability coefficient than acetate (150) and therefore it diffuses faster into the cell. When acetic acid diffuses back into the cell it carries a proton that is not being imported through ATPase, therefore not producing ATP. This explains the inhibitory effect of acetic acid on the microrganism, as higher concentrations of acetic acid lead to the uncoupling of proton motive force and respective higher ATP maintenance requirements (150). As a strategy to restrict such ATP loss, the microorganism drives the metabolism towards acetate conversion to ethanol, even though $Y_{ATP/CO}$ is lower when CO is overall converted into ethanol than in acetate - equations 5.6 and 5.7. Similarly, for *Clostridium ljungdahlii*, Richter *et al.* (103) has stated that at a thermodynamic threshold concentration of undissociated acetic acid with a surplus of reducing equivalents, ethanol production occurs as an overflow mechanism.

Comparably to our experimental results, Xu *et al.* (162) demonstrated that ethanol production is increased (through acetate reduction via an aldehyde:ferredoxin oxidoreductase (AOR)), upon supplementation of additional extracellular (^{13}C-labeled) acetate to the cultivation medium of *C. autoethanogenum,* growing on 100% CO in batch experiments, and posterior detection of ^{13}C-labeled ethanol. The indirect ethanol pathway, through acetate reduction via AOR, has been postulated and discussed before (27, 149, 163) and its role in autotrophic ethanol production in *C. autoethanogenum* has been confirmed by Liew *et al.* (151).

Product inhibition in chemostats leads to lower biomass concentration (164), in line with our observation in Table 5.2. These results emphasize that acetic acid concentration is a key fermentation variable that determines metabolic shifts in CO fermenting acetogenic bacteria *C. autoethanogenum*, and consequently, also impacts product distribution, ethanol yield and volumetric productivities. Since mass transfer rate and growth rate affect the resulting total extracellular acetate concentration, and pH the undissociated acetic acid concentration, these factors are equally fundamental to determine product distribution to ethanol (see subsequent sections). This finding has pertinent implications for industrial process operation and for tuning metabolic shifts towards solventogenesis. For example, by lowering operational pH or recovering and recycling acetate to the bioreactor, one could drive production towards higher ethanol yields and productivity.

5.4.2 Influence of mass transfer

Decreasing the fermentation agitation rates corresponds to decreased gas-to-liquid mass transfer rates, dissolved CO concentration in the broth, and CO uptake rate. For *C. autoethanogenum* fermentations we observed excretion the intermediate metabolite formate. Formate production in syngas fermentation has been previously observed during batch cultivation of *Clostridium ljungdahlii* (165, 166) and in *Acetobacterium woodii* (167, 168) and has been linked to high partial pressure of dissolved CO_2 or H_2. Our continuous fermentations have no CO_2 or H_2 feeding, and we expect very low CO concentrations when formate is excreted. Formate excretion might be caused by its accumulation due to a bottleneck in a consecutive conversion step in the WLP. Formate formation is the first step in the methyl branch and reducing equivalents are required to convert it to methyl-COFeSp which is a substrate for CODH/ACS. In the case of low CO concentration conditions, there could be a deficiency of reducing equivalents, which are typically supplied by CO oxidation to CO_2. The lack of reducing equivalents (due to severe limitation in CO availability) could potentially hinder the further conversion of formate to methyl-COFeSp, resulting in the accumulation of formate.

C. autoethanogenum harbours more than one CO dehydrogenase (CODH) enzyme, which can catalyse the reversible CO oxidation to CO_2 (1) - Figure 5.1. One of the CODHs combines with acetyl-CoA synthase (ACS) to form the bifunctional CODH/ACS complex for CO_2 reduction to CO and acetyl-CoA fixation (Figure 5.1). In the case that the activity for CO conversion would be much higher for the CODH which catalyses CO to CO_2, than for ACS which catalyses CO to acetyl-CoA, formate accumulation could be explained. A reason for the relatively low activity of ACS complex in case of low CO concentration might be that the Michaelis constant of the CODH for CO is well below the CO concentration, in combination with a Michaelis

constant of ACS for CO well above the CO concentration, such that only ACS loses activity. Enzyme affinities for CO will need to be measured to test this hypothesis, using, for example approaches and methods similar to Techtmann *et al.* (169).

Increasing mass transfer triggers other effects. Assuming a carbon-limited continuous cultivation, for a fixed growth rate, Valgepea *et al.* (150) expected to obtain the same q_{CO} for different stirring rates (and corresponding substrate transfer and uptake rate, and biomass concentrations). Instead, Valgepea *et al.* (170) observed an increase in $-q_{CO}$ from ~22 to ~31 mmol g_X^{-1} h^{-1} when increasing stirring rate from 510 to 650 rpm, in case of growing *C. autoethanogenum* solely on CO at μ = ~0.04 h^{-1}. Besides, increased agitation rate resulted in higher production of acetate and ethanol and a higher acetate to ethanol ratio.

We explain this as follows: For a fixed growth rate, an increase in agitation rates also translates into higher biomass concentration and q_{Ac} and, consequently in higher acetic concentration. This is aligned with our experimental results (Figure 5.2) and by Valgepea *et al.* (170). Given the inhibitory effect of undissociated acetic concentration on the microorganism, this consequence elucidates the metabolic shifts and carbon distribution in *C. autoethanogenum*, when varying substrate mass transfer rate. It also explains the increase of $-q_{CO}$ for higher mass transfer rates obtained by Valgepea *et al.* (170) and the resulting increased acetic acid concentrations, since cells dissipate more CO as CO_2 for maintenance and consequently a lower carbon fraction is allocated to biomass growth.

5.4.3 Influence of growth rate

Figure 5.7 shows the dependence of q_{CO} and q_{EtOH} on μ for our experimental data at 500 rpm and diverse literature studies, for continuous CO fermentations by *C. autoethanogenum* under diverse cultivation conditions that avoided formate production. No q_{CO} data were obtained at 100 rpm due to equipment malfunctioning. While our experiments and those reported by Diender *et al.* (152) used media containing yeast extract and at pH 5.9 and 6.2, respectively, other studies used chemically defined medium at pH 5 (148, 170, 171). All studies used a stirred tank reactor, except Chen *et al.* (171) who used a bubble column reactor. Furthermore, gas flow, CO composition in inlet gas, and agitation rate (if applicable) vary widely between the different studies analysed here.

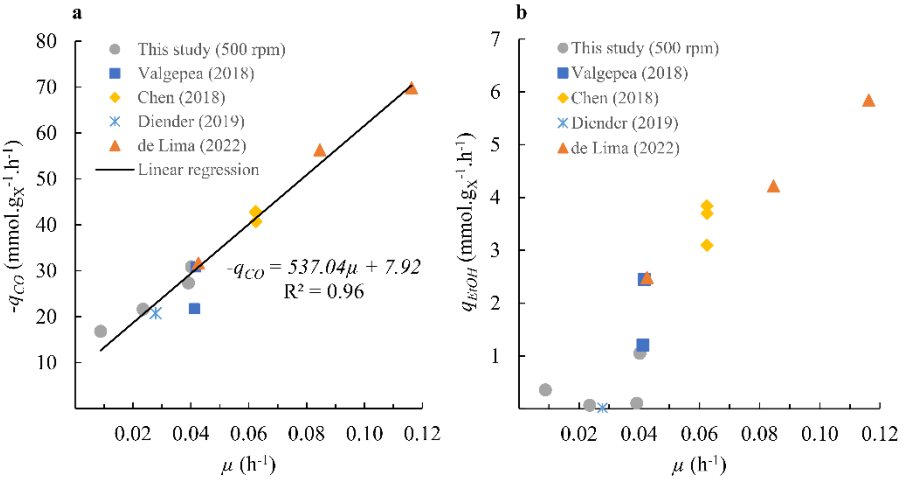

Figure 5.7 Biomass-specific rates of (a) CO and (b) EtOH as function of specific growth rate in continuous fermentations of *C. autoethanogenum* grown on CO (148, 152, 170, 171).

Still, q_{CO} clearly correlates with μ, largely according to the Pirt equation (154):

$$-q_{CO} = \frac{1}{Y_{x/CO}^{max}}\mu + m_{CO} \qquad 5.8$$

However, the obtained maximum yield of biomass on substrate, $Y_{x/CO}^{max}$ = 0.076±0.005 $mol_X\ mol_{CO}^{-1}$ and maintenance coefficient, m_{CO} = 0.20±0.05 $mol_{CO}\ mol_X^{-1}\ h^{-1}$ from this figure are merely apparent values because the undissociated acetic acid concentration results influences the amount of ATP required for maintenance (150), and different amounts of CO are consumed depending on the catabolic product. de Lima *et al.* (148) claimed that increasing the growth rate increases q_{EtOH} and or the volume-specific productivity of EtOH (r_{EtOH}) but our experiments did not confirm this for q_{EtOH} (Figure 5.7b) or r_{EtOH} (not shown). de Lima *et al.* (148) increased the agitation rate for faster growing rates experiments to obtain equivalent biomass concentrations between the different steady states, which also resulted in higher total acetate concentrations and, consequently higher undissociated acetic acid concentrations than in our experiments (Figure 5.6). As discussed previously, higher acetic acid concentrations drive metabolic shifts towards ethanol production. In our study, the fermentations were cultivated at pH 5.9, which, using acetic acid pK_a of 4.77, results in a fraction of 6.7% undissociated acetic acid over total acetate; whereas this fraction increases to 36% at pH 5, which was used by de Lima *et al.* (148). For a fixed growth rate, there are other experimental conditions that can affect ethanol production. Namely, pH and CO mass transfer rate (which are directly

linked to acetic acid concentration) and media composition (including yeast extract concentration) have a major relevance.

Yeast extract has been reported to provide the required trace nutrients for the structural integrity of CO fermenting *Clostridium* bacteria (172), besides being an importance nitrogen source for the microorganisms and having a positive effect in lag phase duration (173). Nonetheless, lowering yeast extract concentration in the feed medium has been shown to result in enhanced production of more reduced products (such as ethanol) (11, 84, 174). This could explain some differences regarding ethanol productivity with faster growth rates between our experimental results and the discussed literature.

5.4.4 Implications for Ethanol Yield, Titer and Production Rate

By imposing different agitation rates in steady-state fermentations, we showed that insufficient mass transfer rate results in the excretion of the intermediate metabolite formate, while increasing mass transfer rates results in higher acetate and ethanol titres, yields and productivities. Our study did not focus on maximizing ethanol concentration. Nevertheless, based on our results we conclude that to obtain commercially interesting ethanol concentrations, much higher CO mass transfer rates will be needed (to provide sufficient carbon and reducing equivalents), while the dilution rate should still be modest to prevent dilution. We hypothesize that the extracellular undissociated acetic acid concentration is the crucial variable determining ethanol yield and production rate. In fact, our results strongly suggest that, by increasing the extracellular undissociated acetic acid concentration, *C. autoethanogenum* shifts CO metabolism towards ethanol production as a strategy to cope with acetic acid inhibition. A high yield of ethanol on CO requires > 20 mmol/L undissociated acetic acid, which can be obtained by (a combination of) high CO transfer rate, low pH, low dilution rate, and external acetate addition. Our research extends beyond previous studies on *C. ljungdahlii* (103, 159) by investigating the strain *C. autoethanogenum*, showcasing the impact of acetic acid inhibition across CO fermenting acetogen species. These outcomes could shed light on strategies for industrial process operations and to drive metabolic shifts towards solventogenesis in CO fermentations. Additionally, acetic acid inhibition should be included in stoichiometric and kinetic models for accurate prediction of CO uptake rate, product distribution, yields and titres.

Chapter 6

Conclusion and Outlook

6. Conclusion and Outlook

In this this chapter we reflect upon the goals and questions that were initially outlined and how we are closer to the much-desired answers regarding the role and influence of gas-to-liquid mass transfer in syngas fermentation bioreactors performance. Furthermore, we reflect and on the meaning of this for the future of syngas fermentation development and industrialization.

6.1. Performance of Hollow Fibre Membrane bioreactors for syngas permeation and fermentation

Despite the limited number of experimental studies on bubbleless Hollow Fibre Membrane (HFM) bioreactors in syngas fermentation, and thereby the lack of experimental data and understanding that could be deployed for optimization, the large number of abiotic studies on this topic suggested that HFM bioreactors have the potential to largely surpass the gas-to-liquid mass transfer performance of the industrially standard bubbled reactors. This led us to question: Which membrane bioreactor configuration is most suitable for improvement of syngas mass fermentation mass transfer and volumetric productivity?

Our research suggests that hollow fibre membrane bioreactors with dense or asymmetric membranes, containing polydimethylsiloxane (PDMS) or polymethylpentene (PMP) are the most suitable configuration to achieve enhanced mass transfer in syngas fermentation. These configurations offer substantial advantages due to their high interfacial area, high permeability, mechanical stability (durability), and resistance to biofouling. The suitability of hollow fibre membrane (HFM) modules is further emphasized by their potential ability to support biofilm formation, which aids in cell retention and can enhance reactor performance by increasing the biomass concentration. Furthermore, flow configurations such as co-current or counter-current within these modules (gas in fibre lumen and liquid in membrane shell), along with adequate liquid recirculation rates, are crucial to maximizing mass transfer rates while preventing biofouling. The systematic study of gas feed configurations (open-/closed-end) and liquid flow patterns (co-/counter-/cross-current), fibre spacing, and process characteristics such as biofilm density and thickness, is still needed to further explore the full potential of this technology. This led to the next research question: Which operational conditions for such a syngas fermentation membrane bioreactor maximize volumetric productivity?

6.2. Mathematical model as a tool to design and optimize HFM bioreactors for gas fermentation

We used a model-based approach that allows to systematically design and optimize HFM bioreactors and to gain an understanding of each variable's contribution to the overall process performance.

The results indicate that, provided adequate gas pressures, high K_La values can be achieved, and the reaction rate will be the limiting factor up to a certain biomass concentration. Therefore, biofilm configurations are predicted to enhance productivities compared to suspended biomass configurations. Biofilm thickness, biomass concentration, and diffusion coefficients are key biofilm variables which still need to be experimentally determined and validated for accurate model predictions. This means that, currently, the model is most suitable for predicting trends and trade-off relations between process variables rather than exact quantitative predictions. As George Box (175) famously stated, "*All models are wrong, but some are useful"* we highlight the practical utility of the model despite its limitations in precise quantitative predictions.

The hydraulic retention time (HRT) was identified as a critical operational parameter, governing the trade-off between high ethanol concentration and high volumetric production rate: longer HRTs may increase ethanol concentrations but at the cost of lower production rates. To determine the exact trade-off HRT, a better understanding and validation of microbial stoichiometry and kinetics for CO consumption and ethanol formation is necessary. Incorporating biokinetic models that are more accurate or have more details such as described by Almeida Benalcazar (176) will improve predictions of ethanol concentrations and productivity. This includes better descriptions of microbial growth rates, substrate uptake rates, and product formation kinetics. The HFM bioreactor model described in this thesis serves as a valuable tool for evaluating and optimizing HFM bioreactor for syngas fermentation. By simulating various operational scenarios, the model can guide experimental designs and help identify the most effective strategies for enhancing mass transfer and productivity. Although the model currently focuses on syngas fermentation and ethanol production, its structure is adaptable to other gas substrates and products. This flexibility allows for broader applications in bioprocessing, enabling the optimization of HFM bioreactors for production of a range of biofuels and biochemicals. Adaptation of the model to other gas fermentation processes requires implementing a different gas composition and respective substrate properties (diffusion coefficients and solubilities in membrane and liquid phase, etc.). Furthermore, the HFM bioreactor setup can be modified to include a different membrane material (hence different diffusivity and solubility),

fibre spacing and length, etc. If a different mass transfer model applies (such as in the case of a microporous membrane material), the mass transfer model needs to be adjusted and can be even simplified according to mass transfer models discussed in Chapter 2. Further extension of the model to include permeation of volatile products (such as ethanol produced by syngas fermentation) to the feed gas will enable evaluation of new promising designs for *in-situ* product removal (ISPR).

6.3. HFM bioreactors for *in-situ* solventogenic product removal in syngas fermentation

In-situ product removal (ISPR) techniques in fermentation processes aim to alleviate product toxicity/inhibition and, consequently, increase liquid volumetric productivity (34, 177). HFM bioreactors for syngas fermentation can have this added valuable functionality which becomes especially interesting for volatile inhibiting products such as ethanol, as these can be removed by the feed gas. A dense membrane such as PDMS, which is already used in the field of syngas permeation and fermentation, is highly selective for ethanol and allows for its transfer to the gas phase, hence for its pervaporation (Chapter 2). In a study of such a design (177), as an extension of our previous model (Chapter 3) on analysis of ethanol production from CO in a HFM bioreactor, ethanol pervaporation proved to be a selective step and to have a significant impact on ethanol volumetric productivity. The gas phase velocity was demonstrated to increase ethanol's *in-situ* pervaporation rate. Through ethanol permeation and removal via the gas phase, the amount of dissolved ethanol in the liquid phase decreases and, consequently, the assumed inhibitory effect of the product decreases as well. Thus, overall volumetric productivity increases. In model calculations (177), we found a 52% increase of the productivity when comparing the optimal operational parameters defined for the previous model study case (Chapter 3). Moreover, at high gas flow rates, almost 90% of the produced ethanol was removed via the gas stream. An industrial scale process that recovers the product both from the liquid phase and gas phase can be designed – Figure 6.1.

The industrial scale approach for HFM bioreactos combines both scale-up and scale-out (scaling by numbering up). In the proposed process (Figure 6.1), commercial industrial modules of HFM are used (Oxymem, 4.5 m^3) and an annual production of 50 000 ton of ethanol per year is considered. The process has been simulated and evaluated in Comsol Multiphysics® 5.5 and AspenPlus® V8.8; the gross mass balances and the majority of data storage were compiled with spreadsheet software, and a techno-economic analysis was also performed. The detailed equipment list and settings for the ethanol recovery process and techno-economic feasibility calculations are reported by Beatriz (177). The model simulation of the scaled-up syngas fermentation process highlights that the low volume per individual industrial

membrane module requires the use of a high number of parallel reactor units to achieve the desired production scale.

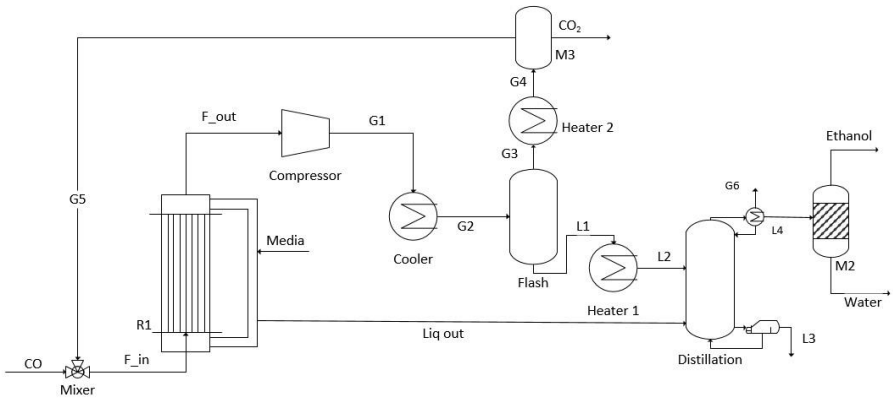

Figure 6.1 Conceptual industrial scale process flow design for syngas fermentation in a dense HFM bioreactor, with ethanol recovery from liquid and gas streams. R1 indicates modules of HFM, M2 is the molecular sieve for ethanol dehydration and M3 is the MEA-based CO2 capture unit (177).

Furthermore, key operational variables identified include packing density, gas inflow velocity, and hydraulic retention time. Careful tuning of these variables is essential for optimizing the overall process performance and determining the optimal number of HFM modules required. Additionally, the downstream processing strategy should incorporate a condensation step specifically for recovering ethanol from the gaseous stream, followed by distillation and dewatering steps to purify the final product. These findings provide a comprehensive framework for scaling up HFM-based syngas fermentation processes, ensuring both efficiency and economic viability. Finally, a techno-economic analysis was performed to evaluate the trade-offs between productivity, product concentration in the liquid and gaseous phases, costs, and other economic indicators. In this analysis, ethanol recovery scenarios were studied, and operational parameters were optimized to ensure maximum net present value (NPV) over 20 years of operation. It was concluded that HFM bioreactors are prohibitively expensive, accounting for 73% of equipment purchasing costs in the optimal scenario. Distillation and compression emerged as the costliest operations. The optimal ethanol recovery scenario involves simultaneous recovery from both the liquid and gas phases. There is a notable trade-off between productivity and costs; the least expensive operational set-up does not correspond to the highest achievable volumetric productivity. Consequently, this analysis suggests that the process of ethanol production from CO fermentation using HFM bioreactors is currently not profitable.

6.4. Bubbleless vs. bubbled syngas fermentation bioreactors

Now that we assessed the technical and economic performance of HFM bioreactors for syngas fermentation and permeation at an industrial scale, we can reflect on how this bubbleless configuration compares with a typical bubbled bioreactor configuration.

To perform a fair comparison between HFM bioreactors and bubble column (BC) reactors for syngas fermentation, we utilized a model initially developed by Almeida Benalcázar *et al.* (2020) for a syngas fermentation to ethanol in a bubble column bioreactor. This model was adapted to align reaction kinetics and process conditions with those used in the HFM bioreactor study (177), including modifications to incorporate the same ethanol inhibition model and adjustments to stoichiometry due to differences in biomass composition. Both processes were designed for a production scale of 50 000 ton of ethanol per year. This analysis (177) reveals that the volumetric productivity of the BC reactor is approximately 4.7 times higher than that of the HFM reactor. According to the models, this is the case since we can reach higher biomass concentration per volume of liquid phase in bubble column reactors (10 g/L) than in the HFM bioreactor configuration (3.65 g/L). Consequently, the volume required to achieve the same ethanol production is significantly smaller for the BC reactor, requiring only three bioreactors compared to the extensive number required for HFM reactors (1955 units). This is further emphasized by the scaling factor, which is lower for the BC (scale up) reactor versus the HFM reactor (scale out), indicating a more efficient economy of scale for the BC configuration.

Capital investment costs are markedly lower for the BC reactor scenario, with an estimated cost of 82 M€ compared to 502 M€ for the HFM bioreactor setup. This substantial difference is primarily attributed to the high purchasing costs associated with the large number of HFM reactor units needed (~1,955). Although the BC process includes an additional biomass filter not required in the HFM reactor process, this does not offset the overall cost advantage. Operational costs present a mixed scenario: while utilities are cheaper for the HFM bioreactor due to higher ethanol concentrations achieved in both the off-gas and liquid streams (21 M€/year for HFM reactor versus 34 M€/year for BC), total operational expenses are greater for the HFM bioreactor. This is largely due to the significant maintenance and depreciation costs associated with the numerous reactor units, requiring process control and maintenance. The net present value (NPV) analysis indicates that the BC reactor scenario is economically more viable. The capital investment in reactors has a profound impact on economic viability, with the high initial costs of HFM bioreactors making them less attractive despite their operational efficiency in terms of utility usage. In conclusion, the BC reactors come forward as the preferable

industrial bioreactors option for syngas fermentation due to their higher productivity, lower capital investment costs, and better overall economic performance.

6.5. The future of HFM bioreactors for syngas permeation and fermentation

We could then raise the questions of what would be needed to turn HFM bioreactors feasible for syngas fermentations and if that is realistically achievable. Our analysis underscores the need for further optimization and cost reduction strategies to make the HFM-based syngas fermentation process to ethanol economically viable.

The model results assessment assumed a conservative biomass density in the biofilm (of 15 g/L) (98, 177) whereas typical anaerobic biofilm-based bioreactors can reach around biomass densities in the biofilm of 50 g/L (178). Such biomass densities are achieved in typical biofilm-based bioreactors given the absence of gas mass transfer limitations. On the other hand, for syngas fermentation, one can reach either a high biomass density in the biofilm or a thick biofilm, but not both simultaneously. According to sensitivity analysis calculations (98), ethanol volumetric productivity and ethanol titres could roughly increase 2 to 3 times, for the latter biomass densities considering a constant biofilm thickness. This would result in a more favourable techno-economic assessment, although still insufficient to reach economic feasibility. This reinforces the critical need to experimentally validate those variables (biofilm thickness and biomass densities in biofilm) if a precise analysis and feasibility study is desired. Despite these uncertainties, our results (177) identify that HFM bioreactor costs account for the most of equipment investment costs, up to 88%, consisting of 15 % housing and 73% PDMS membrane fibres, for the conceptual process flow suggested in Figure 6.1. In general, to reach process economic feasibility, the membrane fibres costs would need to decrease substantially, which in practice difficult to achieve. A sensitivity analysis shows that a reduction of 20% in the HFM reactor cost would lead to a 17% reduction in CAPEX and a 19% improvement in NPV. Other strategies, although causing less impact, could include improvements in HFM module design, namely if bigger module volumes would become commercially available and higher packing densities could be used without hindering process performance. This would result in reduction in process control and housing costs. Our analysis for the product selling price shows a minimal ethanol selling price of 3345 €/ton for the proposed HFM bioreactor process flow, which is 3.6 times higher than market price considered (177). This suggests that HFM reactor could be more favourable for the production of other higher-value products (such hexanol, caproate, butyrate, etc.). These products require a much smaller production scale, and in in that case, perhaps HFM bioreactor could become more competitive with standard industrial bubbled bioreactors. This

could be particularly interesting for products which do not enhance mass transfer coefficient as much as solventogenic products (such as ethanol) do in bubbled bioreactors, and could be relevant to other types of gas fermentation processes (O_2, H_2, CH_4 or CO_2) - discussed in Chapter 4.

6.6. Performance of syngas fermentation in bubbled bioreactors

The aforementioned conclusions led us to redirect the research focus into the study of gas-to-liquid mass transfer behaviour and performance of bubbled bioreactors for syngas fermentation. Namely, it became relevant to investigate the influence of syngas fermentation broth properties (composition, viscosity, etc) on the gas-to-liquid mass transfer rate in bubbled bioreactors (such as bubble columns and stirred tank reactors, STRs) so that their operation is better understood and optimized.

The findings from Chapter 4 underscore the critical role of ethanol in enhancing gas mass transfer in syngas fermentation broths. Ethanol significantly increases the K_La by inhibiting bubble coalescence, which results in a smaller average bubble size. This is essential for improving the efficiency of syngas fermentations. This effect is particularly pronounced in concentrations up to 5 g L^{-1} of ethanol, beyond which K_La stabilizes. We also highlight the contribution of several other broth components and characteristics such as salinity, biomass, and surfactants (proteins, anti-foam, organic acids, other solventogenic products, etc.) to explain the dynamic nature of K_La in syngas fermentation processes. These components can either enhance or inhibit mass transfer depending on their specific interactions within the broth.

From an industrial perspective, our results suggest that syngas fermentation towards solventogenic products such as ethanol is advantageous in bubbled bioreactors because small bubble sizes are obtained, as required for fast gas-liquid mass transfer in the process. High K_La values (between 600 and 750 h^{-1} (16)) are predicted for industrial bubbled bioreactors during syngas fermentation to ethanol. Ethanol presence promotes these conditions by stabilizing smaller bubbles (0.2 to 1 mm), thereby increasing gas hold-up, and enhancing mass transfer. In contrast, gas-water systems with larger bubbles (5 to 7 mm) cannot achieve the same mass transfer performance. In fact, this is one of the reasons why empirical relations (derived from gas-water systems) fail to achieve correct K_La predictions for syngas fermentation broth.

This further endorses the suitability of bubbled bioreactors for industrial syngas fermentations. These reactors will achieve sufficient mass transfer rates. At very large scale, Bubble Columns are generally preferred to Stirred Tank Reactors (179, 180); therefore, Bubble Columns and the related Gas lift loop reactors currently come forward as competitive bioreactor configurations for industrial syngas

fermentation, but an in-depth discussion of this topic is outside the scope of this thesis.

Future research should continue to explore the interplay between different broth components and their impact on mass transfer characteristics. This will involve systematically studying the effects of various additives, such as salts, proteins, and other organic compounds, on K_La, bubble size, and gas hold-up. Developing more accurate predictive models that incorporate these variables is essential for optimizing fermentation processes (181). Additionally, investigating the scalability of these findings to larger industrial reactors and different types of gas fermentations will be crucial for translating laboratory successes to commercial applications.

To further optimize syngas fermentation in bubbled bioreactors regarding titres and volumetric productivities it is relevant to understand how the respective operational settings influence the fermentation performance. More specifically, it raises the question of what the influence of mass transfer rates, growth rates and the concentration of the co-products is on continuous syngas fermentation performance (titres and volumetric productivities)? Chapter 5 provides significant insights into how these factors influence CO metabolism in *Clostridium autoethanogenum*, in continuous fermentation, using a chemostat as a research device. We have identified that the concentration of undissociated acetic acid is one of the critical factors determining the ethanol yield and productivity; and that high concentrations inhibit microbial growth but shift the metabolism towards ethanol production. Consequently, controlling extracellular acetic acid levels through operational pH, dilution rate (hence growth rate in a chemostat), and exogenous acetate supplementation can optimize ethanol production. Furthermore, the growth rate affects product distribution, with higher growth rates impacting overall metabolic balance and acetate concentration without necessarily increasing ethanol production. These findings have substantial implications for industrial syngas fermentation processes aiming to maximize ethanol yields. By tuning variables such as agitation and gas supply rates, pH, and dilution rates, it is possible to control the concentration of undissociated acetic acid, thereby optimizing ethanol production.

Recovering and recycling acetate within the bioreactor could maintain high acetic acid concentrations, promoting ethanol production while managing microbial inhibition. An innovative downstream process could involve multiple distillation stages, with the initial separation occurring under reduced pressure (182). By operating under a vacuum and avoiding the use of extra chemicals, this method ensures that microorganisms remain intact and can be recycled back into the fermenter along with most of the water and acetic acid (182). The process

performance could be further optimized using advanced heat pumping and heat integration techniques, enhancing both economic and environmental outcomes (182). Consequently, this improved downstream process has potential to recover high-purity ethanol, prevents biomass loss, and boosts fermentation yield by enabling a closed-loop operation (182).

Our results could be further improved by integration of reconciled chemostat data across a wide range of conditions and the identification of knowledge gaps related to dissolved gas concentrations (104). This lack of knowledge on dissolved CO concentrations is caused by a lack of dissolved CO measurements. Although several methods have been developed for measurement of dissolved CO concentrations (156, 183, 184, 185), most are laborious and time consuming, expensive, or not compatible with certain experimental setups. Development of an affordable commercial sensor for dissolved CO measurements would be a significant advance in solving this limitation. Accurately linking dissolved gas concentrations and product inhibition to the kinetics of acetogens is key to solve one of the major research gaps in the field of syngas fermentation and to yield successful scale-up and industrialization of the technology.

Future research should indeed focus on further elucidating the mechanisms behind metabolic shifts and explore genetic modifications to enhance microbial tolerance to products and improve the efficiency of the Wood–Ljungdahl pathway. Understanding and manipulating these variables will be essential for advancing syngas fermentation technology and achieving sustainable biochemical production.

6.7. The future of syngas fermentation

Syngas fermentation industrialization has expanded globally. While industry leads the field by licensing their technology for various gas feedstocks and expanding their product portfolio, academic research groups and scientific work published on the topic is growing exponentially (186). Bubbled bioreactors, namely gas lift and bubble columns, emerge as a competitive bioreactor configuration for process industrialization and scale up. Understanding the impact of syngas fermentation broth composition on bubble stabilization and mass transfer enhancement is crucial for process modelling and design. Unravelling the microbial kinetics and their relation to dissolved gases and product concentration is key to drive the fermentation performance further and optimize process design. The same applies to expanding the knowledge on gas-to-liquid mass transfer behaviour and the contribution of other operational conditions. This progress is exciting and favourable to a future panorama where industry decarbonization and carbon

recycling technologies become the norm. A norm that is absolutely necessary to fight climate change, and for human species and planet preservation.

References

(1) Liew, F. M., Martin, M. E., Tappel, R. C., Heijstra, B. D., Mihalcea, C., & Köpke, M. (2016). Gas Fermentation—A Flexible Platform for Commercial Scale Production of Low-Carbon-Fuels and Chemicals from Waste and Renewable Feedstocks. *Frontiers in Microbiology*, *7*, 694.

(2) Schopf, J. W. (1983). *Earth's earliest biosphere : its origin and evolution*. Princeton University Press.

(3) Phillips, J., Huhnke, R., & Atiyeh, H. (2017). Syngas Fermentation: A Microbial Conversion Process of Gaseous Substrates to Various Products. *Fermentation*, *3*(2), 28.

(4) Bengelsdorf, F. R., Beck, M. H., Erz, C., Hoffmeister, S., Karl, M. M., Riegler, P., Wirth, S., Poehlein, A., Weuster-Botz, D., & Dürre, P. (2018). Bacterial Anaerobic Synthesis Gas (Syngas) and CO 2 + H 2 Fermentation. In S. Sariaslani & G. M. Gadd (Eds.), *Advances in applied microbiology* (Vol. 103, pp. 143–221). Academic Press.

(5) Köpke, M., & Simpson, S. D. (2020). Pollution to products: recycling of 'above ground' carbon by gas fermentation. *Current Opinion in Biotechnology*, *65*, 180–189.

(6) Redl, S., Diender, M., Jensen, T. Ø., Sousa, D. Z., & Nielsen, A. T. (2017). Exploiting the potential of gas fermentation. *Industrial Crops and Products*, *106*, 21–30.

(7) Bengelsdorf, F. R., & Dürre, P. (2017). Gas fermentation for commodity chemicals and fuels. *Microbial Biotechnology*, *10*(5), 1167–1170.

(8) Almeida Benalcázar, E., Deynoot, B. G., Noorman, H., Osseweijer, P., & Posada, J. A. (2017). Production of bulk chemicals from lignocellulosic biomass via thermochemical conversion and syngas fermentation: a comparative techno-economic and environmental assessment of different site-specific supply chain configurations. *Biofuels, Bioproducts and Biorefining*, *11*(5), 861–886.

(9) Almeida Benalcázar, E., Noorman, H., Maciel Filho, R., & Posada, J. A. (2020). Modeling ethanol production through gas fermentation: a biothermodynamics and mass transfer-based hybrid model for microbial growth in a large-scale bubble column bioreactor. *Biotechnology for Biofuels*, *13*(1), 59.

(10) Klasson, K. T., Ackerson, M. D., Clausen, E. C., & Gaddy, J. L. (1991). Bioreactor design for synthesis gas fermentations. *Fuel*, *70*(5), 605–614.

(11) Abubackar, H. N., Veiga, M. C., & Kennes Christian. (2011). Biological conversion of carbon monoxide: rich syngas or waste gases to bioethanol. *Biofuels, Bioproducts and Biorefining*, *5*(1), 93–114.

(12) Munasinghe, P. C., & Khanal, S. K. (2010). Biomass-derived syngas fermentation into biofuels: Opportunities and challenges. *Bioresource Technology*, *101*(13), 5013–5022.

(13) Yasin, M., Jang, N., Lee, M., Kang, H., Aslam, M., Bazmi, A. A., & Chang, I. S. (2019). Bioreactors, gas delivery systems and supporting technologies for microbial synthesis gas conversion process. *Bioresource Technology Reports*, *7*, 100207.

(14) Drioli, E., Criscuoli, A., & Curcio, E. (2006). *Membrane contactors: fundamentals, applications and potentialities* (Vol. 11). Elsevier.

(15) Reij, M. W., Keurentjes, J. T. ., & Hartmans, S. (1998). Membrane bioreactors for waste gas treatment. *Journal of Biotechnology*, *59*(3), 155–167.

(16) Puiman, L., Abrahamson, B., Lans, R. G. J. M. va. der, Haringa, C., Noorman, H. J., & Picioreanu, C. (2022). Alleviating mass transfer limitations in industrial external-loop syngas-to-ethanol fermentation. *Chemical Engineering Science*, *259*, 117770.

(17) Heijnen, J. J., & Van't Riet, K. (1984). Mass transfer, mixing and heat transfer phenomena in low viscosity bubble column reactors. *The Chemical Engineering Journal*, *28*(2), B21–B42.

(18) Zieminski, S. A., Caron, M. M., & Blackmore, R. B. (1967). Behavior of air bubbles in dilute aqueous solutions. *Industrial and Engineering Chemistry Fundamentals*, *6*(2),

233–242.

(19) Lessard, R. R., & Zieminski, S. A. (1971). Bubble Coalescence and Gas Transfer in Aqueous Electrolytic Solutions. *Industrial and Engineering Chemistry Fundamentals*, *10*(2), 260–269.

(20) Galaction, A. I., Cascaval, D., Oniscu, C., & Turnea, M. (2004). Prediction of oxygen mass transfer coefficients in stirred bioreactors for bacteria, yeasts and fungus broths. *Biochemical Engineering Journal*, *20*(1), 85–94.

(21) Prins, A., & van't Riet, K. (1987). Proteins and surface effects in fermentation: foam, antifoam and mass transfer. *Trends in Biotechnology*, *5*(11), 296–301.

(22) Neto, A. S., Wainaina, S., Chandolias, K., Piatek, P., & Taherzadeh, M. J. (2025). Exploring the Potential of Syngas Fermentation for Recovery of High-Value Resources: A Comprehensive Review. In *Current Pollution Reports* (Vol. 11, Issue 1, pp. 1–18). Springer.

(23) Asimakopoulos, K., Gavala, H. N., & Skiadas, I. V. (2018). Reactor systems for syngas fermentation processes: A review. *Chemical Engineering Journal*, *348*, 732–744.

(24) Yasin, M., Jeong, Y., Park, S., Jeong, J., Lee, E. Y., Lovitt, R. W., Kim, B. H., Lee, J., & Chang, I. S. (2015). Microbial synthesis gas utilization and ways to resolve kinetic and mass-transfer limitations. *Bioresource Technology*, *177*, 361–374.

(25) Daniell, J., Köpke, M., & Simpson, S. (2012). Commercial Biomass Syngas Fermentation. *Energies*, *5*(12), 5372.

(26) Takors, R., Kopf, M., Mampel, J., Bluemke, W., Blombach, B., Eikmanns, B., Bengelsdorf, F. R., Weuster-Botz, D., & Dürre, P. (2018). Using gas mixtures of CO, CO2 and H2 as microbial substrates: the do's and don'ts of successful technology transfer from laboratory to production scale. *Microbial Biotechnology*, *11*(4), 606–625.

(27) Köpke, M., Held, C., Hujer, S., Liesegang, H., Wiezer, A., Wollherr, A., Ehrenreich, A., Liebl, W., Gottschalk, G., & Dürre, P. (2010). Clostridium ljungdahlii represents a microbial production platform based on syngas. *Proceedings of the National Academy of Sciences*, *107*(29), 13087–13092.

(28) Straathof, A. J. J. (2014). Transformation of Biomass into Commodity Chemicals Using Enzymes or Cells. *Chemical Reviews*, *114*(3), 1871–1908.

(29) Munasinghe, P. C., & Khanal, S. K. (2010). Syngas fermentation to biofuel: Evaluation of carbon monoxide mass transfer coefficient (kLa) in different reactor configurations. *Biotechnology Progress*, *26*(6), 1616–1621.

(30) Orgill, J. J., Atiyeh, H. K., Devarapalli, M., Phillips, J. R., Lewis, R. S., & Huhnke, R. L. (2013). A comparison of mass transfer coefficients between trickle-bed, hollow fiber membrane and stirred tank reactors. *Bioresource Technology*, *133*, 340–346.

(31) Bredwell, M. D., Srivastava, P., & Worden, R. M. (1999). Reactor Design Issues for Synthesis-Gas Fermentations. *Biotechnology Progress*, *15*(5), 834–844.

(32) Munasinghe, P. C., & Khanal, S. K. (2012). Syngas fermentation to biofuel: Evaluation of carbon monoxide mass transfer and analytical modeling using a composite hollow fiber (CHF) membrane bioreactor. *Bioresource Technology*, *122*, 130–136.

(33) Ebrahimi, S., Kleerebezem, R., Kreutzer, M. T., Kapteijn, F., Moulijn, J. A., Heijnen, J. J., & van Loosdrecht, M. C. M. (2006). Potential application of monolith packed columns as bioreactors, control of biofilm formation. *Biotechnology and Bioengineering*, *93*(2), 238–245.

(34) Ylitervo, P., Akinbomi, J., & Taherzadeh, M. J. (2013). Membrane bioreactors' potential for ethanol and biogas production: a review. *Environmental Technology*, *34*(13–14), 1711–1723.

(35) Charcosset, C. (2006). Membrane processes in biotechnology: An overview. *Biotechnology Advances*, *24*(5), 482–492.

(36) Yang, M.-C., & Cussler, E. L. (1986). Designing hollow-fiber contactors. *AIChE Journal*, *32*(11), 1910–1916.

(37) Kartohardjono, S., & Chen, V. (2005). Mass transfer and fluid hydrodynamics in sealed end hydrophobic hollow fiber membrane gas-liquid contactors. *Journal of Applied Membrane Science & Technology*, *2*(1), 1–12.

(38) Kumar, A., Dewulf, J., & Van Langenhove, H. (2008). Membrane-based biological waste gas treatment. *Chemical Engineering Journal*, *136*(2), 82–91.

(39) Stanojević, M., Lazarević, B., & Radić, D. (2003). Review of membrane contactors designs and applications of different modules in industry. *FME Transactions*, *31*(2), 91–98.

(40) Shen, Y., Brown, R., & Wen, Z. (2014). Syngas fermentation of Clostridium carboxidivoran P7 in a hollow fiber membrane biofilm reactor: Evaluating the mass transfer coefficient and ethanol production performance. *Biochemical Engineering Journal*, *85*, 21–29.

(41) Ismail, A. F., Khulbe, K. C., & Matsuura, T. (2015). *Gas separation membranes* (Vol. 7). Springer.

(42) Zhou, H., & Jin, W. (2018). Membranes with Intrinsic Micro-Porosity: Structure, Solubility, and Applications. *Membranes*, *9*(1).

(43) Zhao, S., Feron, P. H. M., Deng, L., Favre, E., Chabanon, E., Yan, S., Hou, J., Chen, V., & Qi, H. (2016). Status and progress of membrane contactors in post-combustion carbon capture: A state-of-the-art review of new developments. *Journal of Membrane Science*, *511*, 180–206.

(44) Gabelman, A., & Hwang, S.-T. (1999). Hollow fiber membrane contactors. *Journal of Membrane Science*, *159*(1), 61–106.

(45) Feron, P. H. M., & Jansen, A. E. (2002). CO2 separation with polyolefin membrane contactors and dedicated absorption liquids: performances and prospects. *Separation and Purification Technology*, *27*(3), 231–242.

(46) Casey, E., Glennon, B., & Hamer, G. (1999). Review of membrane aerated biofilm reactors. *Resources, Conservation and Recycling*, *27*(1), 203–215.

(47) Mallevialle, J., Odendaal, P. E., Wiesner, M. R., American Water Works, A., Research, F., Lyonnaise des, E., & Water Research Commission of South, A. (1996). *Water treatment membrane processes*. McGraw-Hill.

(48) Sridhar, S., Smitha, B., & Aminabhavi, T. M. (2007). Separation of Carbon Dioxide from Natural Gas Mixtures through Polymeric Membranes—A Review. *Separation & Purification Reviews*, *36*(2), 113–174.

(49) Resnick, P. R., & Buck, W. H. (1999). Teflon® AF: A Family of Amorphous Fluoropolymers with Extraordinary Properties. In G. Hougham, P. E. Cassidy, K. Johns, & T. Davidson (Eds.), *Fluoropolymers 2: Properties* (pp. 25–33). Springer US.

(50) Merkel, T. C., Gupta, R. P., Turk, B. S., & Freeman, B. D. (2001). Mixed-gas permeation of syngas components in poly(dimethylsiloxane) and poly(1-trimethylsilyl-1-propyne) at elevated temperatures. *Journal of Membrane Science*, *191*(1), 85–94.

(51) Voss, M. A., Ahmed, T., & Semmens, M. J. (1999). Long-Term Performance of Parallel-Flow, Bubbleless, Hollow-Fiber-Membrane Aerators. *Water Environment Research*, *71*(1), 23–30.

(52) Ahmed, T., & Semmens, M. J. (1992). Use of sealed end hollow fibers for bubbleless membrane aeration: experimental studies. *Journal of Membrane Science*, *69*(1), 1–10.

(53) Wang, Z., Dong, S., Li, N., Cao, X., Sheng, M., Xu, R., Wang, B., Wu, H., Ma, C., Yuan, Y., Xu, H., Chen, F., & Zhao, S. (2018). Chapter 3 - CO2-Selective Membranes: How Easy Is Their Moving From Laboratory to Industrial Scale? In A. Basile & E. P. Favvas (Eds.), *Current Trends and Future Developments on (Bio-) Membranes* (pp. 75–102). Elsevier.

(54) Pinnau, I. (2000). MEMBRANE SEPARATIONS | Membrane Preparation. In I. D. Wilson (Ed.), *Encyclopedia of Separation Science* (pp. 1755–1764). Academic Press.

(55) Bazhenov, D. S., Bildyukevich, V. A., & Volkov, V. A. (2018). Gas-Liquid Hollow Fiber Membrane Contactors for Different Applications. *Fibers*, *6*(4).

(56) Wan, C. F., Yang, T., Lipscomb, G. G., Stookey, D. J., & Chung, T.-S. (2017). Design and fabrication of hollow fiber membrane modules. *Journal of Membrane Science*, *538*, 96–107.

(57) Orgill, J. J., Abboud, M. C., Atiyeh, H. K., Devarapalli, M., Sun, X., & Lewis, R. S. (2019). Measurement and prediction of mass transfer coefficients for syngas constituents

in a hollow fiber reactor. *Bioresource Technology*, *276*, 1–7.

(58) Yasin, M., Park, S., Jeong, Y., Lee, E. Y., Lee, J., & Chang, I. S. (2014). Effect of internal pressure and gas/liquid interface area on the CO mass transfer coefficient using hollow fibre membranes as a high mass transfer gas diffusing system for microbial syngas fermentation. *Bioresource Technology*, *169*, 637–643.

(59) Jang, N., Yasin, M., Kang, H., Lee, Y., Park, G. W., Park, S., & Chang, I. S. (2018). Bubble coalescence suppression driven carbon monoxide (CO)-water mass transfer increase by electrolyte addition in a hollow fiber membrane bioreactor (HFMBR) for microbial CO conversion to ethanol. *Bioresource Technology*, *263*, 375–384.

(60) Ferreira, B. S., Fernandes, H. L., Reis, A., & Mateus, M. (1998). Microporous hollow fibres for carbon dioxide absorption: Mass transfer model fitting and the supplying of carbon dioxide to microalgal cultures. *Journal of Chemical Technology & Biotechnology*, *71*(1), 61–70.

(61) Lee, P.-H., Ni, S.-Q., Chang, S.-Y., Sung, S., & Kim, S.-H. (2012). Enhancement of carbon monoxide mass transfer using an innovative external hollow fiber membrane (HFM) diffuser for syngas fermentation: Experimental studies and model development. *Chemical Engineering Journal*, *184*, 268–277.

(62) Zhao, Y., Haddad, M., Cimpoia, R., Liu, Z., & Guiot, S. R. (2013). Performance of a Carboxydothermus hydrogenoformans-immobilizing membrane reactor for syngas upgrading into hydrogen. *International Journal of Hydrogen Energy*, *38*(5), 2167–2175.

(63) Anggraini, I. D., Keryanti, M. T. A. P. K., Purwadi, R., Noda, R., Watanabe, T., & Setiadi, T. (2019). Bioethanol Production via Syngas Fermentation of Clostridium Ljungdahlii in a Hollow Fiber Membrane Supported Bioreactor. *International Journal of Technology*, *10*(3), 481–490.

(64) Zhang, F., Ding, J., Zhang, Y., Chen, M., Ding, Z.-W., van Loosdrecht, M. C. M., & Zeng, R. J. (2013). Fatty acids production from hydrogen and carbon dioxide by mixed culture in the membrane biofilm reactor. *Water Research*, *47*(16), 6122–6129.

(65) Zhang, F., Ding, J., Shen, N., Zhang, Y., Ding, Z., Dai, K., & Zeng, R. J. (2013). In situ hydrogen utilization for high fraction acetate production in mixed culture hollow-fiber membrane biofilm reactor. *Applied Microbiology and Biotechnology*, *97*(23), 10233–10240.

(66) Wang, H.-J., Dai, K., Xia, X.-Y., Wang, Y.-Q., Zeng, R. J., & Zhang, F. (2018). Tunable production of ethanol and acetate from synthesis gas by mesophilic mixed culture fermentation in a hollow fiber membrane biofilm reactor. *Journal of Cleaner Production*, *187*, 165–170.

(67) Shen, N., Dai, K., Xia, X.-Y., Zeng, R. J., & Zhang, F. (2018). Conversion of syngas (CO and H2) to biochemicals by mixed culture fermentation in mesophilic and thermophilic hollow-fiber membrane biofilm reactors. *Journal of Cleaner Production*, *202*, 536–542.

(68) Wang, Y.-Q., Yu, S.-J., Zhang, F., Xia, X.-Y., & Zeng, R. J. (2017). Enhancement of acetate productivity in a thermophilic (55 °C) hollow-fiber membrane biofilm reactor with mixed culture syngas (H2/CO2) fermentation. *Applied Microbiology and Biotechnology*, *101*(6), 2619–2627.

(69) Tsai, S.-P., Datta, R., Basu, R., & Yoon, S.-H. (2012). *Syngas conversion system using asymmetric membrane and anaerobic microorganism*. Synata Bio Inc.

(70) Luo, G., Wang, W., & Angelidaki, I. (2013). Anaerobic Digestion for Simultaneous Sewage Sludge Treatment and CO Biomethanation: Process Performance and Microbial Ecology. *Environmental Science & Technology*, *47*(18), 10685–10693.

(71) Perez-Calleja, P., Aybar, M., Picioreanu, C., Esteban-Garcia, A. L., Martin, K. J., & Nerenberg, R. (2017). Periodic venting of MABR lumen allows high removal rates and high gas-transfer efficiencies. *Water Research*, *121*, 349–360.

(72) Wang, C. Y., Mercer, E., Kamranvand, F., Williams, L., Kolios, A., Parker, A., Tyrrel, S., Cartmell, E., & McAdam, E. J. (2017). Tube-side mass transfer for hollow fibre membrane contactors operated in the low Graetz range. *Journal of Membrane Science*, *523*, 235–246.

(73) Semmens, M. J. (2008). Alternative MBR configurations: using membranes for gas transfer. *Desalination*, *231*(1), 236–242.

(74) Fang, Y., Novak, P. J., Hozalski, R. M., Cussler, E. L., & Semmens, M. J. (2004). Condensation studies in gas permeable membranes. *Journal of Membrane Science*, *231*(1), 47–55.

(75) Chen, H., Zhao, L., Hu, S., Yuan, Z., & Guo, J. (2018). High-Rate Production of Short-Chain Fatty Acids from Methane in a Mixed-Culture Membrane Biofilm Reactor. *Environmental Science & Technology Letters*, *5*(11), 662–667.

(76) Whiteley, M., Diggle, S. P., & Greenberg, E. P. (2017). Progress in and promise of bacterial quorum sensing research. *Nature*, *551*(7680), 313–320.

(77) Hickey, R., Datta, R., Tsai, S.-P., & Basu, R. (2014). *Membrane supported bioreactor for conversion of syngas components to liquid products*. Synata Bio Inc.

(78) Nerenberg, R. (2016). The membrane-biofilm reactor (MBfR) as a counter-diffusional biofilm process. *Current Opinion in Biotechnology*, *38*, 131–136.

(79) Zetty Arenas, A. M. (2019). Towards enhanced second-generation n-butanol production from sugarcane [Delft University of Technology]. In *Biotechnology*.

(80) Wang, Z.-W., & Chen, S. (2009). Potential of biofilm-based biofuel production. *Applied Microbiology and Biotechnology*, *83*(1), 1–18.

(81) Philips, J., Rabaey, K., Lovley, D. R., & Vargas, M. (2017). Biofilm Formation by Clostridium ljungdahlii Is Induced by Sodium Chloride Stress: Experimental Evaluation and Transcriptome Analysis. *PLOS ONE*, *12*(1), e0170406.

(82) Pantaléon, V., Bouttier, S., Soavelomandroso, A. P., Janoir, C., & Candela, T. (2014). Biofilms of Clostridium species. *Anaerobe*, *30*, 193–198.

(83) Khalid, H., Amin, F. R., Gao, L., Chen, L., Chen, W., Javed, S., & Li, D. (2023). Syngas conversion to biofuels and biochemicals: a review of process engineering and mechanisms. *Sustainable Energy & Fuels*, *8*(1), 9–28.

(84) Klasson, K. T., Ackerson, M. D., Clausen, E. C., & Gaddy, J. L. (1992). Bioconversion of synthesis gas into liquid or gaseous fuels. *Enzyme and Microbial Technology*, *14*(8), 602–608.

(85) Kavousi, F., Syron, E., Semmens, M., & Casey, E. (2016). Hydrodynamics and gas transfer performance of confined hollow fibre membrane modules with the aid of computational fluid dynamics. *Journal of Membrane Science*, *513*, 117–128.

(86) Atchariyawut, S., Jiraratananon, R., & Wang, R. (2008). Mass transfer study and modeling of gas–liquid membrane contacting process by multistage cascade model for CO2 absorption. *Separation and Purification Technology*, *63*(1), 15–22.

(87) Pavasant, P., dos Santos, L. M. F., Pistikopoulos, E. N., & Livingston, A. G. (2000). Prediction of optimal biofilm thickness for membrane-attached biofilms growing in an extractive membrane bioreactor. *Biotechnology and Bioengineering*, *52*(3), 373–386.

(88) Freitas Dos Santos, L. M., Pavasant, P., Strachan, L. F., Pistikopoulos, E. N., & Livingston, A. G. (1997). Membrane attached biofilms for waste treatment - Fundamentals and applications. *Pure and Applied Chemistry*, *69*(11), 2459–2469.

(89) Ahmadi Motlagh, A. R., Voller, V. R., & Semmens, M. J. (2006). Advective flow through membrane-aerated biofilms: Modeling results. *Journal of Membrane Science*, *273*(1), 143–151.

(90) Matsumoto, S., Terada, A., & Tsuneda, S. (2007). Modeling of membrane-aerated biofilm: Effects of C/N ratio, biofilm thickness and surface loading of oxygen on feasibility of simultaneous nitrification and denitrification. *Biochemical Engineering Journal*, *37*(1), 98–107.

(91) Martin, K. J., Picioreanu, C., & Nerenberg, R. (2015). Assessing microbial competition in a hydrogen-based membrane biofilm reactor (MBfR) using multidimensional modeling. *Biotechnology and Bioengineering*, *112*(9), 1843–1853.

(92) Martin, K. J., Picioreanu, C., & Nerenberg, R. (2013). Multidimensional modeling of biofilm development and fluid dynamics in a hydrogen-based, membrane biofilm

reactor (MBfR). *Water Research*, *47*(13), 4739–4751.

(93) Edel, M., Horn, H., & Gescher, J. (2019). Biofilm systems as tools in biotechnological production. *Applied Microbiology and Biotechnology*, *103*(13), 5095–5103.

(94) Quek, V. C., Shah, N., & Chachuat, B. (2018). Modeling for design and operation of high-pressure membrane contactors in natural gas sweetening. *Chemical Engineering Research and Design*, *132*, 1005–1019.

(95) Haddadi, B., Jordan, C., Miltner, M., & Harasek, M. (2018). Membrane modeling using CFD: Combined evaluation of mass transfer and geometrical influences in 1D and 3D. *Journal of Membrane Science*, *563*, 199–209.

(96) Krishna, R., & Wesselingh, J. A. (1997). The Maxwell-Stefan approach to mass transfer. *Chemical Engineering Science*, *52*(6), 861–911.

(97) COMSOL. (2018). *Chemical Reaction Engineering Module User's Guide (v. 5.4)*. COMSOL Multiphysics.

(98) Puiman, L. (2020). *Modelling syngas fermentation in hollow fibre membrane reactors, Master Thesis* [Delft University of Technology].

(99) Danckwerts, P. V. (1953). Continuous flow systems: Distribution of residence times. *Chemical Engineering Science*, *2*(1), 1–13.

(100) Mohammadi, M., Mohamed, A. R., Najafpour, G. D., Younesi, H., & Uzir, M. H. (2014). Kinetic Studies on Fermentative Production of Biofuel from Synthesis Gas Using *Clostridium ljungdahlii*. *The Scientific World Journal*, *2014*, 910590.

(101) Fernández-Naveira, Á., Abubackar, H. N., Veiga, M. C., & Kennes, C. (2016). Carbon monoxide bioconversion to butanol-ethanol by Clostridium carboxidivorans: kinetics and toxicity of alcohols. *Applied Microbiology and Biotechnology*, *100*(9), 4231–4240.

(102) Kleerebezem, R., & Van Loosdrecht, M. C. M. (2010). A Generalized Method for Thermodynamic State Analysis of Environmental Systems. *Critical Reviews in Environmental Science and Technology*, *40*(1), 1–54.

(103) Richter, H., Molitor, B., Wei, H., Chen, W., Aristilde, L., & Angenent, L. T. (2016). Ethanol production in syngas-fermenting Clostridium ljungdahlii is controlled by thermodynamics rather than by enzyme expression. *Energy & Environmental Science*, *9*(7), 2392–2399.

(104) Kerkhof, I., Puiman, L., & Straathof, A. J. J. (2024). Understanding microbial syngas fermentation rates. *Applied Microbiology and Biotechnology*, *108*(1), 1–15.

(105) Häusler, E. B. G., van der Wielen, L. A. M., & Straathof, A. J. J. (2016). Evaluation of gas supply configurations for microbial product formation involving multiple gaseous substrates. *Bioresources and Bioprocessing*, *3*(1), 1–12.

(106) Teixeira, L. V., Moutinho, L. F., & Romão-Dumaresq, A. S. (2018). Gas fermentation of C1 feedstocks: commercialization status and future prospects. *Biofuels, Bioproducts and Biorefining*, *12*(6), 1103–1117.

(107) Jourdin, L., & Burdyny, T. (2021). Microbial Electrosynthesis: Where Do We Go from Here? *Trends in Biotechnology*, *39*(4), 359–369.

(108) Elisiário, M. P., De Wever, H., Van Hecke, W., Noorman, H., & Straathof, A. J. J. (2021). Membrane bioreactors for syngas permeation and fermentation. *Critical Reviews in Biotechnology*, 1–17.

(109) Cabau-Peinado, O., Straathof, A. J. J., & Jourdin, L. (2021). A General Model for Biofilm-Driven Microbial Electrosynthesis of Carboxylates From CO2. *Frontiers in Microbiology*, *12*, 1405.

(110) Stone, K. A., Hilliard, M. V., He, Q. P., & Wang, J. (2017). A mini review on bioreactor configurations and gas transfer enhancements for biochemical methane conversion. *Biochemical Engineering Journal*, *128*, 83–92.

(111) Garcia-Ochoa, F., & Gomez, E. (2009). Bioreactor scale-up and oxygen transfer rate in microbial processes: An overview. *Biotechnology Advances*, *27*(2), 153–176.

(112) Zlokarnik, M. (1980). Koaleszenzphänomene im System gasförmig/flüssig und deren Einfluß auf den O2-Eintrag bei der biologischen Abwasserreinigung.

Korrespondenz Abwasser, *27*(11), 728–734.

(113) Keitel, G., & Onken, U. (1982). Inhibition of bubble coalescence by solutes in air/water dispersions. *Chemical Engineering Science*, *37*(11), 1635–1638.

(114) Jamialahmadi, M., & Müller-Steinhagen, H. (1992). Effect of alcohol, organic acid and potassium chloride concentration on bubble size, bubble rise velocity and gas hold-up in bubble columns. *The Chemical Engineering Journal*, *50*(1), 47–56.

(115) Zlokarnik, M. (1981). Verfahrenstechnische Grundlagen der Reaktorgestaltung. *Acta Biotechnologica*, *1*(4), 311–325.

(116) Shchukarev, S. A., & Tolmacheva, T. A. (1968). Solubility of oxygen in ethanol — Water mixtures. *Journal of Structural Chemistry 1968 9:1*, *9*(1), 16–21.

(117) Cussler, E. L. (2011). *Diffusion: mass transfer in fluid systems* (3rd ed.). Cambridge University Press.

(118) Akita, K., & Yoshida, F. (1973). Gas Holdup and Volumetric Mass Transfer Coefficient in Bubble Columns. Effects of Liquid Properties. *Industrial and Engineering Chemistry Process Design and Development*, *12*(1), 76–80.

(119) Kawase, Y., Halard, B., & Moo-Young, M. (1987). Theoretical prediction of volumetric mass transfer coefficients in bubble columns for Newtonian and non-Newtonian fluids. *Chemical Engineering Science*, *42*(7), 1609–1617.

(120) Nakanoh, M., & Yoshida, F. (1980). Gas Absorption by Newtonian and Non-Newtonian Liquids in a Bubble Column. *Industrial and Engineering Chemistry Process Design and Development*, *19*(1), 190–195.

(121) Uchida, S., Tsuyutani, S., & Seno, T. (1989). Flow regimes and mass transfer in counter-current bubble columns. *The Canadian Journal of Chemical Engineering*, *67*(5), 866–869.

(122) Vatai, G. Y., & Tekić, M. N. (1989). Gas hold-up and mass transfer in bubble columns with pseudoplastic liquids. *Chemical Engineering Science*, *44*(10), 2402–2407.

(123) Lizardi-Jiménez, M. A., López-Ordáz, P., González-Brambila, M. M., Linares-Morales, A., & Melgarejo-Torres, R. (2018). Effect of Biomass Concentration on Oxygen Mass Transfer, Power Consumption, Interfacial Tension and Hydrodynamics in a Multiphase Partitioning Bioreactor. *International Journal of Chemical Reactor Engineering*, *16*(10).

(124) Rosso, D., Larson, L. E., & Stenstrom, M. K. (2008). Aeration of large-scale municipal wastewater treatment plants: state of the art. *Water Science and Technology*, *57*(7), 973–978.

(125) Fackler, N., Heijstra, B. D., Rasor, B. J., Brown, H., Martin, J., Ni, Z., Shebek, K. M., Rosin, R. R., Simpson, S. D., Tyo, K. E., Giannone, R. J., Hettich, R. L., Tschaplinski, T. J., Leang, C., Brown, S. D., Jewett, M. C., & Köpke, M. (2021). Stepping on the Gas to a Circular Economy: Accelerating Development of Carbon-Negative Chemical Production from Gas Fermentation. *Annual Review of Chemical and Biomolecular Engineering*, *12*, 439–470.

(126) Köpke, M., Mihalcea, C., Bromley, J. C., & Simpson, S. D. (2011). Fermentative production of ethanol from carbon monoxide. *Current Opinion in Biotechnology*, *22*(3), 320–325.

(127) Besagni, G., Inzoli, F., De Guido, G., & Pellegrini, L. A. (2016). Experimental investigation on the influence of ethanol on bubble column hydrodynamics. *Chemical Engineering Research and Design*, *112*, 1–15.

(128) APHA/AWWA/WEF. (1999). Standard methods for the examination of water and wastewater. In *Standard Methods* (20th ed.).

(129) Jackson, M. L., & Shen, C. -C. (1978). Aeration and mixing in deep tank fermentation systems. *AIChE Journal*, *24*(1), 63–71.

(130) Reid, R. C., Prausnitz, J. M., & Poling, B. E. (1987). *The properties of gases and liquids* (4th ed.). McGraw-Hill.

(131) Bi, Y. H., Hill, G. A., & Sumner, R. J. (2001). Enhancement of the overall volumetric oxygen transfer coefficient in a stirred tank bioreactor using ethanol. *The Canadian Journal of Chemical Engineering*, *79*(3), 463–467.

(132) Bin, A. K., & Smith, J. M. (1982). CHEMICAL ENGINEERING COMMUNICATIONS MASS TRANSFER IN A PLUNGING LIQUID JET ABSORBER. *CHEMICAL ENGINEERING COMMUNICATIONS*, *15*, 367–383.

(133) Miyahara, T., & Nagatani, N. (2009). Influence of alcohol addition on liquid-phase volumetric mass transfer coefficient in an external-loop airlift reactor with a porous plate. *Journal of Chemical Engineering of Japan*, *42*(10), 713–719.

(134) Sun, X., Atiyeh, H. K., Huhnke, R. L., & Tanner, R. S. (2019). Syngas fermentation process development for production of biofuels and chemicals: A review. In *Bioresource Technology Reports*.

(135) Heffernan, J. K., Valgepea, K., de Souza Pinto Lemgruber, R., Casini, I., Plan, M., Tappel, R., Simpson, S. D., Köpke, M., Nielsen, L. K., & Marcellin, E. (2020). Enhancing CO2-Valorization Using Clostridium autoethanogenum for Sustainable Fuel and Chemicals Production. *Frontiers in Bioengineering and Biotechnology*, *8*.

(136) De Kok, S., Meijer, J., Van Loosdrecht, M. C. M., & Kleerebezem, R. (2013). Impact of dissolved hydrogen partial pressure on mixed culture fermentations. *Applied Microbiology and Biotechnology*, *97*(6), 2617–2625.

(137) Oels, U., Schügerl, K., & Todt, J. (1976). Gasanteil, Stofftransportgeschwindigkeitskoeffizient und spezifische Phasengrenzfläche in Gleichstrom-Blasensäulen. *Chemie Ingenieur Technik*, *48*(1), 73–73.

(138) Krishna, R., Urseanu, M. I., & Dreher, A. J. (2000). Gas hold-up in bubble columns: influence of alcohol addition versus operation at elevated pressures. *Chemical Engineering and Processing: Process Intensification*, *39*(4), 371–378.

(139) Lamont, J. C., & Scott, D. S. (1970). An eddy cell model of mass transfer into the surface of a turbulent liquid. *AIChE Journal*, *16*(4), 513–519.

(140) McClure, D. D., Lamy, M., Black, L., Kavanagh, J. M., & Barton, G. W. (2017). An experimental investigation into the behaviour of antifoaming agents. *Chemical Engineering Science*, *160*, 269–274.

(141) Schumpe, A., Saxena, A. K., & Fang, L. K. (1987). Gas/liquid mass transfer in a slurry bubble column. *Chemical Engineering Science*, *42*(7), 1787–1796.

(142) Bandyopadhyay, B., Humphrey, A. E., & Taguchi, H. (1967). Dynamic measurement of the volumetric oxygen transfer coefficient in fermentation systems. *Biotechnology and Bioengineering*, *9*(4), 533–544.

(143) Linek, V., Sinkule, J., & Beneš, P. (1991). Critical assessment of gassing-in methods for measuring kla in fermentors. *Biotechnology and Bioengineering*, *38*(4), 323–330.

(144) Wilkinson, P. M., Spek, A. P., & van Dierendonck, L. L. (1992). Design parameters estimation for scale-up of high-pressure bubble columns. *AIChE Journal*, *38*(4), 544–554.

(145) Burgard, A., Burk, M. J., Osterhout, R., Van Dien, S., & Yim, H. (2016). Development of a commercial scale process for production of 1,4-butanediol from sugar. *Current Opinion in Biotechnology*, *42*, 118–125.

(146) Abrini, J., Naveau, H., & Nyns, E.-J. (1994). Clostridium autoethanogenum, sp. nov., an anaerobic bacterium that produces ethanol from carbon monoxide. *Archives of Microbiology*, *161*(4), 345–351.

(147) Elisiário, M. P., De Wever, H., Van Hecke, W., Noorman, H., & Straathof, A. J. J. (2022). Membrane bioreactors for syngas permeation and fermentation. *Critical Reviews in Biotechnology*, *42*(6).

(148) de Lima, L. A., Ingelman, H., Brahmbhatt, K., Reinmets, K., Barry, C., Harris, A., Marcellin, E., Köpke, M., & Valgepea, K. (2022). Faster Growth Enhances Low Carbon Fuel and Chemical Production Through Gas Fermentation. *Frontiers in Bioengineering and Biotechnology*, *10*.

(149) Mock, J., Zheng, Y., Mueller, A. P., Ly, S., Tran, L., Segovia, S., Nagaraju, S., Köpke, M., Dürre, P., & Thauer, R. K. (2015). Energy Conservation Associated with Ethanol Formation from H 2 and CO 2 in Clostridium autoethanogenum Involving Electron Bifurcation. *Journal of Bacteriology*, *197*(18), 2965–2980.

(150) Valgepea, K., de Souza Pinto Lemgruber, R., Meaghan, K., Palfreyman, R. W., Abdalla, T., Heijstra, B. D., Behrendorff, J. B., Tappel, R., Köpke, M., Simpson, S. D., Nielsen, L. K., & Marcellin, E. (2017). Maintenance of ATP Homeostasis Triggers Metabolic Shifts in Gas-Fermenting Acetogens. *Cell Systems*, *4*(5), 505-515.e5.

(151) Liew, F., Henstra, A. M., Köpke, M., Winzer, K., Simpson, S. D., & Minton, N. P. (2017). Metabolic engineering of Clostridium autoethanogenum for selective alcohol production. *Metabolic Engineering*, *40*, 104–114.

(152) Diender, M., Parera Olm, I., Gelderloos, M., Koehorst, J. J., Schaap, P. J., Stams, A. J. M., & Sousa, D. Z. (2019). Metabolic shift induced by synthetic co-cultivation promotes high yield of chain elongated acids from syngas. *Scientific Reports*, *9*(1), 18081.

(153) Clesceri, L. S., Greenberg, A., & Eaton, A. D. (1999). *Standard methods for the examination of water and wastewater* (20th ed.). American Public Health Association, American Water Work Association, Water Environment Federation.

(154) Heijnen, J. J., & Kleerebezem, R. (2010). Bioenergetics of Microbial Growth. In M. C. Flickinger (Ed.), *Encyclopedia of Industrial Biotechnology* (pp. 1–66).

(155) Allaart, M. T., Diender, M., Sousa, D. Z., & Kleerebezem, R. (2023). Overflow metabolism at the thermodynamic limit of life: How carboxydotrophic acetogens mitigate carbon monoxide toxicity. *Microbial Biotechnology*, *16*(4), 697–705.

(156) Mann, M., Miebach, K., & Büchs, J. (2021). Online measurement of dissolved carbon monoxide concentrations reveals critical operating conditions in gas fermentation experiments. *Biotechnology and Bioengineering*, *118*(1), 253–264.

(157) Bertsch, J., & Müller, V. (2015). Bioenergetic constraints for conversion of syngas to biofuels in acetogenic bacteria. *Biotechnology for Biofuels*, *8*(1), 1–12.

(158) Diender, M. (2019). *Exploration of microbial systems as biocatalysts for conversion of synthesis gas to bio-based chemicals* [Wageningen University and Research].

(159) Schulz, S., Molitor, B., & Angenent, L. T. (2023). Acetate augmentation boosts the ethanol production rate and specificity by Clostridium ljungdahlii during gas fermentation with pure carbon monoxide. *Bioresource Technology*, *369*, 128387.

(160) Gaddy, J., Arora, D., Ko, C.-W., Phillips, J., Basu, R., Wikstrom, C., & Clausen, E. (2003). *Methods for increasing the production of ethanol from microbial fermentation* (2003/0211585 A1).

(161) Kwon, S. J., Lee, J., & Lee, H. S. (2022). Acetate-assisted carbon monoxide fermentation of Clostridium sp. AWRP. *Process Biochemistry*, *113*, 47–54.

(162) Xu, H., Liang, C., Chen, X., Xu, J., Yu, Q., Zhang, Y., & Yuan, Z. (2020). Impact of exogenous acetate on ethanol formation and gene transcription for key enzymes in Clostridium autoethanogenum grown on CO. *Biochemical Engineering Journal*, *155*, 107470.

(163) Basen, M., Schut, G. J., Nguyen, D. M., Lipscomb, G. L., Benn, R. A., Prybol, C. J., Vaccaro, B. J., Poole, F. L., Kelly, R. M., & Adams, M. W. W. (2014). Single gene insertion drives bioalcohol production by a thermophilic archaeon. *Proceedings of the National Academy of Sciences of the United States of America*, *111*(49), 17618–17623.

(164) Straathof, A. J. J. (2023). Modelling of end-product inhibition in fermentation. *Biochemical Engineering Journal*, *191*, 108796.

(165) Stoll, I. K., Boukis, N., & Sauer, J. (2019). Syngas fermentation at elevated pressure - experimental results. *Proceedings of the 27th European Biomass Conference and Exhibition*, 1255–1261.

(166) Oswald, F., Stoll, I. K., Zwick, M., Herbig, S., Sauer, J., Boukis, N., & Neumann, A. (2018). Formic Acid Formation by Clostridium ljungdahlii at Elevated Pressures of Carbon Dioxide and Hydrogen. *Frontiers in Bioengineering and Biotechnology*, *6*.

(167) Peters, V., Janssen, P. H., & Conrad, R. (1999). Transient Production of Formate During Chemolithotrophic Growth of Anaerobic Microorganisms on Hydrogen. *Current Microbiology*, *38*(5), 285–289.

(168) Kantzow, C., & Weuster-Botz, D. (2016). Effects of hydrogen partial pressure on autotrophic growth and product formation of Acetobacterium woodii. *Bioprocess and Biosystems Engineering*, *39*(8), 1325–1330.

(169) Techtmann, S. M., Colman, A. S., Murphy, M. B., Schackwitz, W. S., Goodwin, L. A., & Robb, F. T. (2011). Regulation of multiple carbon monoxide consumption pathways in anaerobic bacteria. *Frontiers in Microbiology*, *2*(JULY), 147.

(170) Valgepea, K., de Souza Pinto Lemgruber, R., Abdalla, T., Binos, S., Takemori, N., Takemori, A., Tanaka, Y., Tappel, R., Köpke, M., Simpson, S. D., Nielsen, L. K., & Marcellin, E. (2018). H2 drives metabolic rearrangements in gas-fermenting Clostridium autoethanogenum. *Biotechnology for Biofuels*, *11*(1), 55.

(171) Chen, J., Daniell, J., Griffin, D., Li, X., & Henson, M. A. (2018). Experimental testing of a spatiotemporal metabolic model for carbon monoxide fermentation with Clostridium autoethanogenum. *Biochemical Engineering Journal*, *129*, 64–73.

(172) Barik, S., Prieto, S., Harrison, S. B., Clausen, E. C., & Gaddy, J. L. (1988). Biological production of alcohols from coal through indirect liquefaction. *Applied Biochemistry and Biotechnology*, *18*(1), 363–378.

(173) Diender, M., Stams, A. J. M., & Sousa, D. Z. (2016). Production of medium-chain fatty acids and higher alcohols by a synthetic co-culture grown on carbon monoxide or syngas. *Biotechnology for Biofuels*, *9*(1), 82.

(174) Vega, J. L., Prieto, S., Elmore, B. B., Clausen, E. C., & Gaddy, J. L. (1989). The Biological production of ethanol from synthesis gas. *Applied Biochemistry and Biotechnology*, *20–21*(1), 781–797.

(175) Box, G. E. P. (1976). Science and statistics. *Journal of the American Statistical Association*, *71*(356), 791–799.

(176) Almeida Benalcazar, E. F. (2023). *Modeling the anaerobic fermentation of CO, H2 and CO2 mixtures at large and micro-scales* [Delft University of Technology].

(177) Beatriz, M. G. S. B. (2020). *In-situ ethanol removal in a hollow fiber membrane bioreactor for syngas fermentation, Master Thesis* [University of Lisbon].

(178) van den Berg, L., Pronk, M., van Loosdrecht, M. C. M., & de Kreuk, M. K. (2023). Density measurements of aerobic granular sludge. *Environmental Technology*, *44*(13), 1985–1995.

(179) Crater, J., Galleher, C., & Lievense, J. (2017). *Consultancy on large-scale submerged aerobic cultivation process design - Final technical report* (Issue May).

(180) Noorman, H. J., Van Winden, W., Heijnen, J. J., & Van Der Lans, R. G. J. M. (2018). Intensified Fermentation Processes and Equipment. *RSC Green Chemistry*, *2018-January*(55), 1–41.

(181) Volger, R., Puiman, L., & Haringa, C. (2024). Bubbles and Broth: A review on the impact of broth composition on bubble column bioreactor hydrodynamics. *Biochemical Engineering Journal*, *201*, 109124.

(182) Janković, T., Straathof, A. J. J., & Kiss, A. A. (2023). Advanced downstream processing of bioethanol from syngas fermentation. *Separation and Purification Technology*, *322*, 124320.

(183) Munasinghe, P. C., & Khanal, S. K. (2014). Evaluation of hydrogen and carbon monoxide mass transfer and a correlation between the myoglobin-protein bioassay and gas chromatography method for carbon monoxide determination. *RSC Advances*, *4*(71), 37575–37581.

(184) Ungerman, A. J., & Heindel, T. J. (2007). Carbon Monoxide Mass Transfer for Syngas Fermentation in a Stirred Tank Reactor with Dual Impeller Configurations. *Biotechnology Progress*, *23*(3), 613–620.

(185) Whang, K., Shin, Y., Baek, W., Jo, Y., Hwang, J. H., Min, J., Kim, D., & Kang, T. (2022). Direct and precise determination of volumetric mass transfer coefficient of carbon monoxide for miniaturized gas-liquid reactors via sensitive probing of raman transitions. *Chemical Engineering Journal*, *429*, 132260.

(186) Calvo, D. C., Luna, H. J., Arango, J. A., Torres, C. I., & Rittmann, B. E. (2022). Determining global trends in syngas fermentation research through a bibliometric analysis. *Journal of Environmental Management*, *307*, 114522.

Acknowledgements

"It's not what we have in our life, but who we have in our life that counts"
J. M. Laurence

If there is something that I appreciate even more than science and fermentation, it is the group of people (family, friends and colleagues) whom I had the privilege to have by my side during my PhD. So I have to admit that this is my favourite section of the thesis, because it makes me look back at my PhD journey with tremendous gratitude. You taught me several lessons and helped shape the person and scientist that I became.

Adrie, thank you for taking on the responsibility and leading the supervision of this project. Your never-ending technical knowledge in bioprocess engineering will always impress me and is clearly reflected in the scientific quality of our papers. During times of adversity, you taught me to seek solutions rather than dwelling on the problem; after all: "*It is what it is!".* Thank you for the countless rounds of corrections and for teaching me how to write better (and more concise) sentences. Thank you for advising and guiding me through the thesis while allowing me the freedom to explore my scientific creativity. And, of course, for all your patience through the consecutive extended deadlines.

Henk, it has been a privilege to have you as my co-promotor. Two of your major lessons continue to resonate with me: *"Always start with the end in mind"* and *"The perfect is the enemy of the good."* Your consistently high-level, constructive, and challenging feedback has helped me grow as a scientist. It has also elevated our research to be pertinent, always with industry in mind.

Heleen, thank you for welcoming me into VITO, always with such kindness and hospitality. Your vast expertise in membrane bioprocesses made this project possible. Learning from you and your team, in the lab, in Mol, was a fantastic and fun start to the project. I truly appreciate your constructive and encouraging feedback over the years.

Wouter, your enthusiasm about gas permeation in membrane bioreactors was contagious and instrumental to the project (and the review!). *Alé!* Beyond our meetings, I truly enjoyed our conference dinners and drinks.

Developing and navigating this project while continuously coordinating the feedback of four (very) different supervisors was perhaps the greatest "Project management" traineeship I could have asked for. Thank you!

To my paranymphs, I am so lucky to have you by my side.

Mariana, you are the most caring, protective and supportive best friend and paranymph I could wish for. Also, a natural leader and brilliant project manager: all our trips and social events were organised to perfection. You make life happier, funnier and more entertaining. I cannot imagine my PhD without you. *"You are the Scully to my Hitchcock."* Thank you! Obrigada por estares sempre lá: seja para me trazer almoço e me fazer sair da cama em dias difíceis; para proteger as minhas experiências de "perigos" indesejáveis; para me trazer medicamentos "premium" quando estou a arder com febre; ou para ler as minhas proposições e aceitares com orgulho ser minha paranymph.

Zeynep, our friendship started before I even dreamt about doing a PhD. You are in all my favourite memories about Delft, about friendship, about festivals, about sunsets, and about simple pleasures in life. You are sunshine in the form of a person. You have always been there with a huge heart, uplifting words and unconditional support. And now you are there as my paranymph as well, what a dream! Thank you!

To everyone in Applied Sciences, which made this journey possible, bearable and fun:

Lars, you were my first MSc student, but you set the bar so high that, soon after, you became a colleague and close friend. I am so happy you were inspired to join the world of syngas fermentation for your own PhD, and I am incredibly grateful to have someone as brilliant as you along the journey. This collaboration has yielded joint papers and projects, endless deep scientific discussions, conferences, and so many fun trips and drinks (in Delft, Nottingham, Düsseldorf, you name it). Thank you for being so supportive and such an honest critic when I needed it. A real partner in crime!

Madalena, foi uma honra supervisionar o teu projeto e a tua magnífica tese de mestrado, mesmo tendo que nos adaptar à pandemia e gerir tudo remotamente. As tuas capacidades, ética de trabalho, resiliência e determinação são impressionantes e ensinaram-me imenso. **Floor,** you helped me run the first CO fermentations in the lab and to face all the problems and frustrations that came along with it. You taught me to be a better mentor, thank you! **Liselot,** you were a fast learner and wrote a splendid BSc thesis. **Lilo,** you brilliantly picked up that work and elevated it to the next level. Thank you! What started as a fun side project ended up being a published paper and a valuable chapter of this thesis. I believe I have learnt as much with you as (I hope) you have learnt with me.

Marijn, you are the materialization of what I think academia and science should be: a prime example of integrity, curiosity and dedication. You inspire me to keep

standing for my beliefs and values (even when it comes at a personal cost). And as if this is not enough, you are also the kindest friend and person in the world. **Oriol**, you have tremendous creative and scientific talent! Thank you for all the uplifting doodle post-it notes over the years, they truly made my day, every single time. That, and the *delicacies* of Catalunya, of course! Thank you both, for adopting me in your office, for all the pep-talks and interventions, scientific discussions, and for being the best listeners during my venting sessions! You taught me to be resilient.

Tiago, nem vou tentar estar ao nível dos teus agradecimentos porque, honestamente, aquilo está lindo e fez-me chorar. Que sorte ter-te reencontrado depois do Técnico, no meu douturamento. O teu sentido de humor (ainda que básico, como o meu) tornou os meus dias tão mais alegres e divertidos. És das pessoas mais determinadas que conheço, e isso é inspirador! Admiro tanto a tua amizade, o teu coração gigante e todos os teus valores inabaláveis. Estás sempre lá com os melhores conselhos, e vou ter sempre saudades de te ter a ti à Mariana no escritório ao lado, como os melhores confidentes!

Song, you taught me that *"everything will be alright in the end, so if it's not alright, then it's not the end*". I think this says a lot about your incredible technical talent. You never gave up on any piece of lab equipment or failed experiment. You went above and beyond to find solutions and troubleshoot our problems in the lab, always with the utmost dedication, passion, and supportive attitude. You kept me sane through the freakout moments and the long working days in the lab. All our experimental work would have not been possible without you! A tremendous thank you! On top of that, I am so happy that I also got to know you as a friend and appreciate your unfiltered sense of humour over the years.

David, *primo*, I feel so lucky to have started the PhD journey at the same time as you. You make life more fun! From teaching fermentation lab practicals to coffee breaks, to dinners, trips or any event really! Meeting you means laughing uncontrollably until our bellies hurt; it means comfort and delicious meals (Ay, la paella!); it means heartfelt serious and silly conversations. I really admire your scientific and creative talent as well. Thank you for helping me design the cover of this thesis.

Joan, I am so happy to have shared the office with you over the years. You have a brilliant mind (even though you're very humble about it). I really admire your eagerness and passion to discuss science. Together with **Daniela,** you guys have the talent to lighten up and entertain every room.

Daphne, thank you for jumping on board with my crazy ideas and co-organizing what was set to be an epic BPE study trip for the whole section (very sadly sabotaged

by the pandemic). I am so happy that you are also living in Copenhagen. **Tim,** hanging out with you is always instantaneously fun, whether in the office, over a beer, or while teaching you Portuguese over a conference dinner. **Maarten,** I love standing next to you, with our half-meter height difference, yet still feel that we are very alike in our passion for fermentation and sports. **Roxana,** thank you for always being so kind, understanding, and supportive. **Zulhaj**, your hardworking attitude was inspiring! **Mona,** thank you for being so outspoken and supportive. **Eduardo,** thank you for all the brilliant discussions we had over the years, whether about syngas fermentation or about life.

To the BPE members who welcomed me at the start of my PhD, thank you for all the wise and experienced advice (and fun karaoke sessions). **Debby**, I had a blast with you at BioPro. **Joana,** tens sempre um abraçinho reconfortante para dar. **Rita**, partilhámos tantos dos mesmos desafios e frustrações! **Marcelo** and **Silvia**, you never failed in bringing interesting scientific discussion topics into our coffee breaks. **Bianca,** tens sempre uma palavra carinhosa para partilhar. **Chema,** your energy and impromptu musical jam sessions in the office made my day. **Mónica,** we became friends during our master's, but I was also lucky to do the PhD next to you. Thank you for all the annual Super Bowl nights and your good advice.

To the new members of BPE, **Tamara, Marika, Mariana, Miki, Brenda, Héctor, Rik** and **Ramon,** thank you for keeping up the legacy. I wish you also build a memorable time during your PhDs.

To the extraordinary BPE staff: **Marcel, Marieke, Ludo, Cees, Christiaan, Marieke, Stef** and **Max,** thank you for your invaluable input and contributions over the years. Your passion and work have been instrumental in maintaining the scientific excellence of our group to inspire us and drive us forward. **Kawieta,** your professionalism, efficiency and dedication keep the section up and running. Your encouragement and support have been invaluable over the years!

Maria, you are one of the reasons I decided to do this PhD project in the first place. Your leadership and mentoring skills are beyond inspirational. **Cristian,** you are one of the reasons why I am passionate about bioprocesses modeling and why Chapter 3 exists. You are a brilliant and inspiring teacher. "Processes & Separation" teaching assistance, together with **Francesc**, was one of the most fun and rewarding activities of my PhD. Thank you for the opportunity and trust!

Mark, you supervised my MSc thesis, and now you are once again present on my committee. What a wholesome full circle this is. It has been a privilege to work with you and your research group. To everyone in EBT who welcomed me in the lab -

Dimitri, **Dirk**, **Rob**, **Zita**, and **Ben** - thank you. You are the reason why my experiments with carbon monoxide were possible and safe. **Maxim**, your determination and passion for science are inspiring. Thank you for all the exciting discussions about syngas fermentation metabolism, and a great partnership in the lab. Thank you for always providing entertaining and fun times in EBT, **Simon**, **Marta**, **Ingrid**, **Sam**, **Timmy**, **Rodoula** & **Angelos**, **Nina**, **Lemin**, **Ali**, and **Stefan**.

To the best PhD committee: **Alexandra**, **Sergio**, **Maxime**, **Aafke** and **Maxime**. I had a blast organizing the symposium with you and all the social activities that made the pandemic a bit more bearable. **Ale**, you are a force of nature, and I deeply admire your resilience and creativity.

To my PDEng squad, thank you for "adopting me" as one of your own, **Paco**, **Emma**, **James**, **Tommaso**, **Miguel S.**, **Sara**, **Miguel A.**, **Marichu**, **Diogo** and **Joana**. Thank you for the memorable times we shared in the Botanical Garden Friday nights, in De Gist, and on our *tripmminies*. **Paco**, I know I can always count on you for the most brutally honest advice or deep scientific discussions, and that was very much needed during my PhD (and life), thank you. **Emma**, you make life sweeter and more bearable. **James**, my gentle giant, I dearly miss our talks, long walks in nature, and spontaneous weekend meetups.

Gustavo and **Vidhvath**, you are my rock. Ten years and counting of unwavering support and heartfelt friendship, through highs and lows. Through graduations, internships, jobs, challenges and heartaches. Countless coffee breaks, assignments, cards and döner kebab dinners, *t' Kelderje* drinks, board games, and pizza Valentina nights; you are also part of my favourite memories in the Netherlands and one of the reasons I survived my PhD. I'm so grateful to have you in my life.

Outside of the faculty there were also friendships forged for life.

Carla, you moved back from Delft too soon and left us broken-hearted. But being the beautiful soul that you are, you left an extraordinary legacy. **Zeynep**, when I first met you in the epic *Ananas house*, I thought *"I want this girl to be my friend".* Little did I know that one day I would get to ask you to be my paranymph. **Miguel**, it was during one of our deep (or silly) conversations in *Smeerboel*, that I came up with the most profound realization about my PhD. In all honesty, that conviction hasn't changed. Thank you for being the kick-starter of crazy and epic adventures over the years and for always being so caring in helping me navigate through life's highs and lows. **Kiko**, when I faced a difficult decision between staying in my bubble of comfort or jumping into the unknown you encouraged me to reflect on what I would regret most not doing. And that's a life advice I still follow today, 100%. Thank you! **Marc**, I am so

lucky I had the chance to redeem your first impression of me and that, since then, we shared so many memorable moments together. I miss our parties, your kind words, but also our intellectual conversations and your advice (especially on investments). **Lidia,** my strong and independent, adventurous force of nature. I want to be like you when I grow up. Thank you for encouraging me to look at life with a positive attitude and leave my pessimistic side behind. **Joan,** five minutes after we met, we were already wearing matching t-shirts. That says a lot about our friendship, and I think that's beautiful. Thank you for everything, but especially for your big heart which you relentlessly try to mask with your sense of humour [insert "The Office" reference here]. **Pau,** I miss your beautiful and kind smile. **Sergio,** thank you for so many years of entertaining coffee breaks, beers, nights outs, festivals and crazy adventures. But also, thank you for all the pep-talks, support and for being a true partner in crime since the start of the PhD. The dog of that photo would indeed be proud of us. I hope you all know that your friendship has rebuilt my self-confidence in moments of vulnerability and hopelessness, and it brings me tremendous happiness in life.

Aos portugueses na Holanda, **Chuck, Raquel, Lenny, Ticha, Parreira, Domingos, Diva, Zé, Tiago, Hugo, Catarina** e **Mafalda**, obrigada por terem feito da Holanda um bocadinho mais casa durante a pandemia e o meu doutoramento. **Parreira,** por partilhares sempre as tuas especiarias comigo, ainda que demasiado potentes. **Domingos,** por todos os avacalhos, partidas e abraços apertados. **Ticha,** pelo teu coração gigante e atitude irreverente. **Lenny,** por todas as conversas impertinentes e desafiantes. **Raquel,** por todos os jantares e atividades, passeios e bons conselhos. **Chuck,** por mereceres um parágrafo inteiro. **Diva,** por seres uma buddy incrível e por incentivares e por alinhares nas mais loucas aventuras. **Catarina,** por todo o companheirismo e compreensão. **Mafalda,** pelo que me ensinaste e apoiaste em quatro meses valer por uma vida inteira.

Às minhas amigas de sempre e para sempre, **Isabel** e **Maria,** obrigada por estarem sempre incondicionalmente presentes. **Alexandra**, *bela*, melhor amuleto da sorte que as nossas danças de casa de banho, é a tua amizade.

À minha família, não há agradecimentos que *tenham avondo*.

Aos meus macaquinhos, **João Carlos, Sílvia, Henrique** e **Mariana,** por me acolherem na vossa família (*no colégio dos miúdos, até hoje, ainda pensam que eu sou bastarda*) e me encorajarem e apoiarem incondicionalmente. Que sorte em vos ter! Primas **Ana** e **Mafalda**, por me alegrarem e serem casa na Holanda. **Tios** e **Tias, Primos** e **Primas**, por todo o amor.

Mana, obrigada por me completares. Por seres a minha maior fã e cúmplice desde sempre. És um exemplo de força e superação e, por isso, uma inspiração. **Mãe,** obrigada por me ensinares que não há desafio que não se supere com paixão e dedicação. Por seres sempre um exemplo a seguir, quer em ambição, em valores ou criatividade. Por nunca esconderes o orgulho. Pelos melhores conselhos. Por, em conjunto com o pai, serem o meu porto de abrigo. **Pai,** obrigado por me ensinares honestidade e humildade (*"tiveste 19? Só?"*). Na verdade, obrigado por me ensinares tudo, e mais alguma coisa. Estou convencida de que o meu interesse por engenharia começou logo em pequenina, por te admirar. Mas a melhor lição que me ensinaste não foi de engenharia; foi que o nosso maior legado são as relações que construímos e é *"daqueles, que por obras valerosas, se vão da lei da morte libertando"*. **Avó,** obrigada por te preocupares sempre comigo, com o meu trabalho (e meus *"bichinhos"*) mas também com que me divirta e aproveite a vida. Obrigada por me deixares sempre de coração cheio quando falamos. Tens um superpoder para me confortar e acalmar todos os medos e incertezas. És um exemplo de trabalho árduo, resiliência, e uma verdadeira inspiração. Ensinaste-me que o amor é cuidar, é tolerância e cumplicidade (e a nunca aceitar menos do que isso). Obrigada por, assim como *o avô*, me apoiares incondicionalmente, desde sempre! Graças a ti, o passarinho continua a voar de pouso em pouso.

Mãe, **Pai,** **Mana** e **Avó**, a palavra saudade ganhou outro significado quando passei a morar a mais de 2000 km de vocês. Principalmente à distância, o vosso apoio incondicional nas mais loucas decisões e aventuras da *caganita de coelho* e nos momentos mais desafiantes, foi completamente decisivo para o meu sucesso. Por isso, este grau também é vosso. Obrigada por tudo!

List of publications

Full papers

Elisiário, M. P., Puiman, L., Van Hecke, W., De Wever, H., Noorman, H., Picioreanu, C., & Straathof, A. J. J. Syngas fermentation in a hollow fibre membrane bioreactor: a predictive model. *Manuscript in preparation*

Timmer, M. J., Vaz, M. I., De Paepe, J., De Corte, I. J., Elisiário., M. P., Straathof, A. J. J., Van Winckel, T., Vlaeminck, S. E. Combined membrane aeration and filtration for energy and space efficient COD removal in water re-use. *Water Research X, 27, 100344.*

Elisiário, M. P., Van Hecke, W., De Wever, H., Noorman, H., & Straathof, A. J. J.(2023). Acetic acid, growth rate, and mass transfer govern shifts in CO metabolism of *Clostridium autoethanogenum*. *Applied Microbiology and Biotechnology*, *107*(17), 5329-5340.

Puiman, L*., Elisiário, M. P.*, Crasborn, L. M., Wagenaar, L. E., Straathof, A. J. J., & Haringa, C. (2022). Gas mass transfer in syngas fermentation broths is enhanced by ethanol. *Biochemical Engineering Journal*, *185*, 108505.

Elisiário, M. P., De Wever, H., Van Hecke, W., Noorman, H., & Straathof, A. J. (2022). Membrane bioreactors for syngas permeation and fermentation. *Critical Reviews in Biotechnology*, *42*(6), 856-872.

* These authors contributed equally to this work.

Conference contributions

(presenting author is underlined)

Puiman, L., Elisiário, M.P., Straathof, A.J.J., Picioreanu, C., Noorman, H.J., & Haringa, C. Relieving mass transfer limitations in industrial syngas-to-ethanol fermentation processes. *14th ECCE and 7th ECAB* (September 2023), Berlin, Germany. Oral presentation.

Elisiário, M. P., Van Hecke, W., De Wever, H., Noorman, H.J., Straathof, A.J.J. Acetic acid, dilution rate, and mass transfer rate jointly shift CO metabolism towards ethanol. *Himmelfahrtstagung on Bioprocess Engineering* (May 2023) Weimar, Germany. Poster presentation

Elisiário, M. P., Puiman, L., Noorman, H.J., Picioreanu, C. & Straathof, A.J.J. A modelling tool for gas fermentation in Hollow Fibre Membrane Bioreactors. *Recent*

Advances in Fermentation Technology (November 2022), Orlando, USA. Poster presentation.

Elisiário, M. P., De Wever, H., Van Hecke, W., Noorman, H.J., Straathof, A.J.J., Syngas fermentation bioreactors. *VITO Clean Vision Summit* (June 2022), Ghent, BE. Poster presentation.

Puiman, L., Elisiário, M.P., Straathof, A.J.J., Haringa, C., Noorman, H.J., & Picioreanu, C. Relieving mass transfer limitations in industrial syngas-to-ethanol fermentation processes. *European Federation of Biotechnology - Spring conference* (May 2022), online. Oral presentation.

Elisiário, M. P., Puiman, L., De Wever, H., Van Hecke, W., Noorman, H.J., Picioreanu, C. & Straathof, A.J.J., Modelling syngas fermentation in a membrane bioreactor. *ESBES Symposium* (May 2021), online. Oral presentation

Elisiário, M. P., Puiman, L., De Wever, H., Van Hecke, W., Noorman, H.J., Picioreanu, C. & Straathof, A.J.J., Modelling syngas fermentation in hollow fibre membrane bioreactors. *The Carbon Recycling Network conference* (February 2020), Nottingham, UK. Oral presentation.

Elisiário, M. P., De Wever, H., Van Hecke, W., Noorman, H.J., Straathof, A.J.J., Syngas Mass Transfer in a Membrane Bioreactor. *12th ECCE and 5th ECAB* (September 2019), Florence, IT. Oral presentation

Curriculum Vitae

Marina was born on 14th August, 1993, in Serpa, a picturesque town in the southeastern corner of the Alentejo, Portugal. She grew up and completed her secondary education there in an environment that sparked her curiosity about nature, biology, and chemistry. This led her to pursue a Bachelor of Science (BSc) in Biological Engineering at Instituto Superior Técnico, Lisbon, Portugal, which she completed in 2014. This degree cemented a strong theoretical foundation in mathematics, chemistry, physics, and biotechnology.

Afterwards, she embarked on an exchange year abroad in the Applied Sciences Faculty at the Technical University of Delft, Netherlands, under the Erasmus programme. This experience inspired her to pursue a Master of Science (MSc) in Life Sciences and Technology, Biochemical Engineering track, also at TU Delft. There, she further developed her competences and knowledge in bioprocess modelling, transport phenomena, separation technologies, and fermentation technology. She completed this degree in 2017 with a research project on environmental biotechnology, studying the "competition between denitrification and dissimilatory nitrate reduction to ammonium."

Subsequently, Marina kickstarted her career as a bioprocess engineer at the biotech startup Delft Advanced Biorenewables (DAB) in Delft, where she developed and scaled-up fermentation processes for the production and *in-situ* product recovery of a flavour and fragrance substance. Determined to focus on fermentation technologies, she returned to TU Delft in 2018 to pursue a PhD in syngas fermentation under the guidance of Dr. ir. Adrie J. J. Straathof and Prof. dr. ir. Henk J. Noorman, leading to this dissertation.

In 2023, Marina joined Novonesis (Novozymes legacy) in Copenhagen, Denmark, as a fermentation scientist, where she is responsible for the development and scale-up of fermentation processes to industrial scale. Her experiences and accomplishments reflect her commitment to advancing scientific knowledge and contributing to the development of environmentally friendly technologies. Her academic and professional path showcases her dedication to harnessing the power of biotechnology for a sustainable future.